PNNL-28478

Snohomish Public Utility District MESA 2

An Assessment of Battery Technical Performance

March 2019

A Crawford
V Viswanathan
J Alam
P Balducci
D Wu
C. Vartanian
K Mongird

U.S. DEPARTMENT OF ENERGY

DISCLAIMER

This report was prepared as an account of work sponsored by an agency of the United States Government. Neither the United States Government nor any agency thereof, nor Battelle Memorial Institute, nor any of their employees, makes **any warranty, express or implied, or assumes any legal liability or responsibility for the accuracy, completeness, or usefulness of any information, apparatus, product, or process disclosed, or represents that its use would not infringe privately owned rights**. Reference herein to any specific commercial product, process, or service by trade name, trademark, manufacturer, or otherwise does not necessarily constitute or imply its endorsement, recommendation, or favoring by the United States Government or any agency thereof, or Battelle Memorial Institute. The views and opinions of authors expressed herein do not necessarily state or reflect those of the United States Government or any agency thereof.

PACIFIC NORTHWEST NATIONAL LABORATORY
operated by
BATTELLE
for the
UNITED STATES DEPARTMENT OF ENERGY
under Contract DE-AC05-76RL01830

Printed in the United States of America

Available to DOE and DOE contractors from the
Office of Scientific and Technical Information,
P.O. Box 62, Oak Ridge, TN 37831-0062;
ph: (865) 576-8401
fax: (865) 576-5728
email: reports@adonis.osti.gov

Available to the public from the National Technical Information Service
5301 Shawnee Rd., Alexandria, VA 22312
ph: (800) 553-NTIS (6847)
email: orders@ntis.gov <http://www.ntis.gov/about/form.aspx>
Online ordering: http://www.ntis.gov

This document was printed on recycled paper.
(8/2010)

PNNL-28478

Snohomish Public Utility District MESA 2

An Assessment of Flow Battery Energy Storage System Technical Performance

A Crawford
V Viswanathan
J Alam
P Balducci
D Wu
C Vartanian
K Mongird

March 2019

Prepared for
the U.S. Department of Energy
under Contract DE-AC05-76RL01830

Pacific Northwest National Laboratory
Richland, Washington 99352

Executive Summary

Energy storage integration into the U.S. electrical grid has been gathering momentum, especially with the increasing penetration of power generated by renewable resources. Several states have storage procurement targets to deal with a variety of issues such as afternoon ramping requirements, frequency regulation/control, utility grid support, and time shifting of renewable energy generation. In this work, we investigated the technical attributes of energy storage to provide benefits to stakeholders, comprised of multiple utilities and their customers. The work was funded jointly by the Washington Clean Energy Fund (CEF) and the U.S. Department of Energy Office of Electricity Delivery and Energy Reliability (DOE-OE).

Motivation for this Work

As part of Washington CEF 1, a $4.4 million grid modernization grant was awarded to the Snohomish Public Utility District (SnoPUD) to purchase and evaluate a Flow Battery Energy Storage System (FBESS) named the Modular Energy Storage Architecture (MESA) 2 by SnoPUD. The grant supported exploration of energy storage applications and associated benefits for the following use-cases:

- Energy Shifting
- Provide Grid Flexibility
- Improve Distribution Systems Efficiency.

These use-cases or services were identified as applicable for MESA 2 and were defined based on utility- and site-specific characteristics. Because FBESSs are quite diverse in their characteristics, it was important to first characterize performance over time using a DOE-OE standardized baseline test procedure for energy storage. The DOE-OE procedure includes representative generic duty cycle profiles, test procedure guidance, and calculation guidance for determining key FBESS characteristics, including energy capacity, response time, internal resistance, and efficiency. Normalizing FBESS performance to this standardized baseline also facilitates evaluation of FBESS against other electro-chemistries evaluated for similar use-cases. After conducting baseline tests to evaluate the FBESS's general characteristics, we tested the FBESS for the three energy storage use-cases listed above. During testing, we collected data to evaluate key FBESS performance metrics relative to the use-cases. Outcomes of these analyses will be beneficial to SnoPUD in terms of understanding how to operate MESA 2 but will also be beneficial to industry in terms of enhancing our understanding of the performance of FBESSs.

Summary of Work Performed

This report documents the results of our study of the technical performance of the 2.2 MW, 8 MWh MESA 2 advanced vanadium FBESS, consisting of four 0.55-MW, 2-MWh strings. System performance was based on a number of baseline and use-case tests. The FBESS is located at the SnoPUD-owned substation located in Everett, Washington. The FBESS was procured by SnoPUD with matching funds provided by the Washington CEF.

Baseline tests were intended to assess the general technical capability of the FBESS (e.g., stored energy capacity, ramp rate performance, ability to track varying charge/discharge commands, direct current [DC] battery internal resistance, etc.). Use-case tests were utilized to examine the FBESS performance while engaged in specific grid services (e.g., arbitrage, power factor correction, etc.). The project measured and/or calculated parameters that are important for understanding FBESS performance when subjected to

actual field operation for achieving economic benefits, such as round-trip efficiency (RTE)[1] with and without rest, with and without auxiliary loads, auxiliary power consumption, signal command tracking, temperature trends during operation, parasitic power loss unaccounted by auxiliary load during rest, and state of charge (SOC) excursions. We used recorded test results to analyze these baseline and use-case parameters. Because the assessment methodology would be the same, the results and lessons presented in this report also could be beneficially applied to any assessment of FBESSs based on technical specifications and/or field deployment results. The performance assessment methodology developed and used for this report generalizes to additional FBESS chemistries.

Key Questions Addressed

We based our analysis of FBESS performance on metrics developed using the DOE-OE Energy Storage Performance Protocol and additional metrics identified in this project. In combination, these general and project-specific metrics allowed structured evaluation of questions that are key for ultimately determining the cost effectiveness of FBESSs used for grid energy storage applications.

The following questions were addressed:

1. How does the FBESS perform during baseline and use-case testing for various duty cycles? For example, what is the RTE of the FBESS?
2. How does the FBESS perform for high ramp rate duty cycles? For example, what is the FBESS response time and ramp rate?
3. What percent of time was the FBESS not available?
4. What are some of the issues identified in this project that are not very obvious?

Key Outcomes

The MESA 2 FBESS was subjected to reference performance tests (RPT), including measurements of energy capacity at various rates of charge and discharge, ability to track volatile signals, internal resistance, and response time/ramp rate. The RPTs conducted before use case testing are referred to as baseline tests in this report.

In addition, duty cycles were developed for various use cases to be performed for this project, and FBESS use case performance was tested and analyzed accordingly. The following sections summarize key outcomes for both baseline and use case performance testing.

Outcome 1

Outcome 1 revealed findings related to discharge capacity and RTE. The FBESS SOC was allowed to go as high as the battery management system would allow, while the discharge time was estimated to ensure the entire constant power region was included.

1. Discharge energy varied non-linearly with SOC due to the sloping nature of the open circuit voltage as f(SOC) and coupled mass transport-kinetics related losses at low SOCs.
2. The energy provided was normalized for four strings because all four strings were rarely available at one time.

[1] The RTE is simply the ratio of discharge energy to charge energy, ensuring the FBESS SOC is brought back to the initial state of charge.

Discharge Energy Capacity

The range of discharge energy capacity for all RPTs and C-rates ranged from 3,435 to 6,345 kWh.

RPTs were done at various discharge rates at a fixed charge rate of 1,200 kW and at various charge rates at a fixed discharge rate of 1,150 kW. The range of discharge energy capacity for all tested cycles at constant discharge power and C-rates ranged from 3,080 to 5,545 kWh. The discharge energy capacity did not change much as the charge power was varied.

Round-Trip Efficiency

Inclusive of all loss sources, the range of RTEs (with and without auxiliary consumption) for all tests performed was 33 to 75%.

For baseline reference performance capacity tests, RTE was 54 to 63%, increasing to 68 to 75% when auxiliary consumption was excluded. As expected, the gain in RTE when auxiliary consumption was excluded was greater at lower power levels. The RTE for the baseline reference performance frequency regulation test was in the 48 to 52% range, increasing to 55 to 60% when auxiliary consumption was excluded.

The RTE varied from 33 to 54% for the various use-cases. The high rest percentages and low power levels lowered the RTE because auxiliary consumption was a higher percentage of total charge and discharge energy. Excluding auxiliary consumption, the RTE increased as power decreased to ~300 kW average power, below which the power conversion system (PCS) efficiency dropped, thus lowering the RTE. As expected, the increase in RTE when auxiliary consumption was excluded peaked when power levels were low and rest periods were high. The DC-DC RTE peaked at lower power levels compared to the alternating current (AC)-AC RTE because PCS efficiency declines significantly at low power levels for the latter.

Figure ES.1 shows charge/discharge energies and RTEs results from the baseline tests.

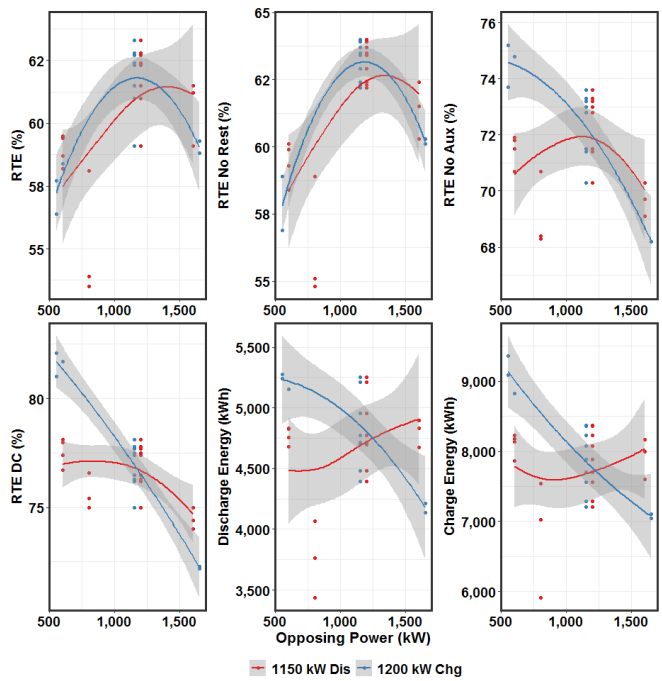

Figure ES.1. Baseline Performance Test for Energy Capacity – Charge, Discharge Energy, and RTE at Various Power Levels

The RTE for volatile signals such as frequency regulation was in the 48 to 52% range at an average power of 1,200 kW for RPT, while the regulation services RTE was around 50% at an average power of 450 kW. The low power levels used for regulation services compared to RPT led to the SOC remaining above 60%, contributing to higher RTE, balanced by higher auxiliary and PCS losses at lower power level contributing to lower RTE. Figure ES.2 shows the frequency regulation duty cycle for the baseline tests. The charge, discharge energy and RTE is shown in Figure ES.2 for the RPT.

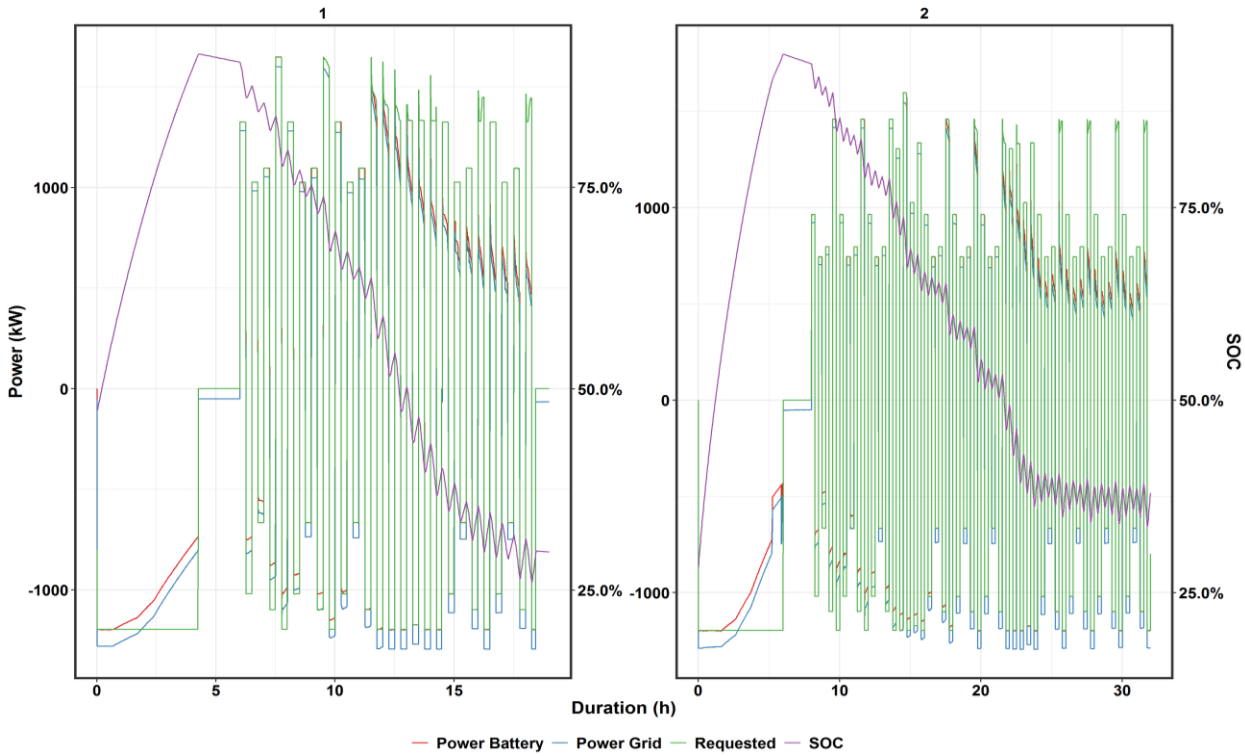

Figure ES.2. Reference Performance Test for Frequency Regulation

Outcome 2

Outcome 2 reports findings related to response time and internal resistance.

Response Time

The response time of the FBESS ranged from 2 to 4 seconds for the range of test cycles performed.

The response time of the FBESS hardware was 2 to 4 seconds, corresponding to ramp rates of 25 to 50% of rated power per second. This included a communication lag of <1 second and a hardware lag of <1 second. Note that only two strings were active during this test.

FBESS Internal Resistance

The FBESS charge and discharge resistance, corrected for four strings, was in a tight range of 0.04 to 0.05 ohms in the SOC range investigated, with the outlier being 0.1 ohms at 12% SOC during charge. This also corresponds to a low ramp rate of 500 kW/s, possibly because the battery management system restricted ramp rates due to higher resistance at low SOCs. The in situ resistance for all strings (normalized to the four-string value) is shown to be in line with the results for the RPT. In general, the charge and discharge resistance increase slightly when the SOC is less than 40%. Overall, there is no trend with increasing test duration.

Outcome 3

Outcome 3 reports findings on system availability.

The total test duration was 173 days, out of which 78 days (45%) were lost for various reasons. Fifty days (29%) of the test duration was lost due to string-related issues, which include stack SOC mismatch, stack leak, and PCS disconnection. While PCS disconnection is arguably an independent issue, for these tests, PCS disconnections mainly were due to string-related issues. For example, leakage of electrolyte compromised PCS electronics for String 1. Pump-related issues contributed to 10 lost days or 6% of the test duration. Miscellaneous, communications, maintenance, and human intervention issues contributed to 7, 6, 3, and 2 days, respectively, or 4, 3, 2, and 1%. Note that string-related issues contributed to 64% of the 78 days lost followed by pump-related issues at 13% of the lost days. Details are shown in Figure ES.3. There were a total of 38 work stoppages, out of which string-related stoppages accounted for 63%, which is in line with the contribution towards the percentage of days lost. It is important to note that Pacific Northwest National Laboratory (PNNL) was unable to complete the entire test program because the FBESS experienced operational failure and was taken offline.

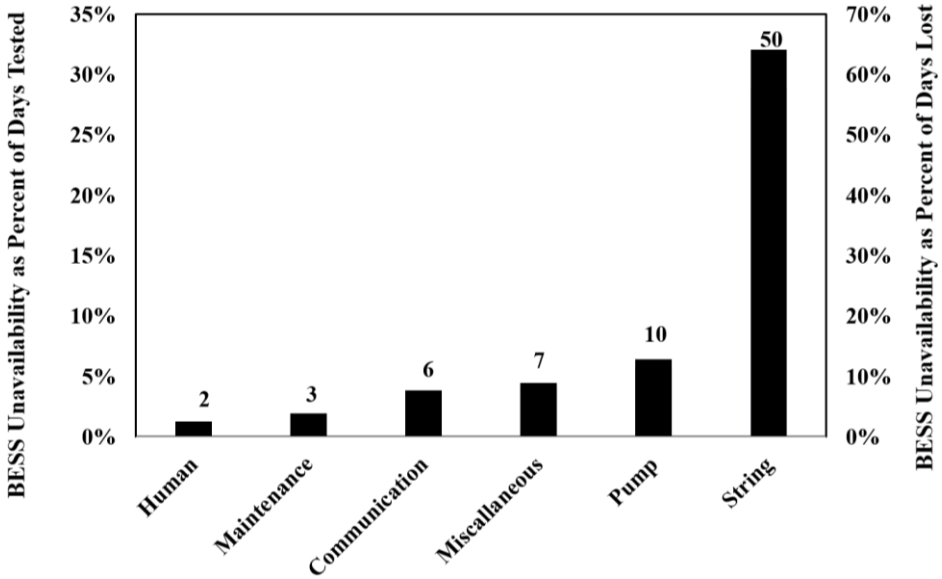

Figure ES.3. Contribution to Lost Time from Various Categories

Outcome 4

Outcome 4 includes findings for issues that surfaced during testing that were outside of specific structured objectives (e.g., testing to measure and report RTEs).

Issues identified during testing that were neither obvious nor necessarily anticipated leading up to testing are described in detail in Appendix A and briefly described below.

1. The data tag list provided by SnoPUD had several duplicate tags.
2. Auxiliary power consumption was not monitored because this tag was not part of the MESA tag list for FBESS. Auxiliary consumption for each string or for the FBESS cannot be determined separately. It was calculated by the difference between feeder meter power and the sum of all four PCS power levels. This difference also includes one-way transformer losses that were not available.

3. Power distribution among strings depended on the deviation of the string SOC from the FBESS SOC. It is hypothesized that discharge power is limited primarily by string minimum SOC, and charge power is limited primarily by string maximum SOC.
4. Available power did not reliably decrease when a string dropped out during discharge. The available power was reduced by 550 kW (one string) only when the string SOC reached zero or when a subsequent charge command was issued and the string could not accept charge.
5. During discharge and charge, available power simply depended on the number of active strings. During rest, when a string was subjected to pulse charge to maintain its SOC above a critical level, the available power decreased by the amount corresponding to the pulse charge.
6. Charging was endothermic, with a decrease in temperature occurring during charging.
7. Auxiliary energy consumption increased with increasing temperature and was less for charge compared to discharge at the same power levels. Considering charging is endothermic, this is a surprising outcome. A possible explanation is that when charging, the electrolyte flow rate per unit power is higher.
8. Thermal management consisted of cooling load based on positive deviation from a set point of 35°C for extended operation or 40°C in each string.

Acknowledgments

We are grateful to Mr. Bob Kirchmeier, Senior Energy Policy Specialist at the Washington Department of Commerce for providing his guidance during this project. We are also grateful to Dr. Imre Gyuk, who is the Energy Storage Program Manager in the Office of Electricity Delivery and Energy Reliability at the U.S. Department of Energy, for providing financial support and leadership on this and other related work at Pacific Northwest National Laboratory. We wish to acknowledge Philip Craig from BlackByte Cyber Security and team members from the Snohomish Public Utility District, including Kelly Wallace, Bob Anderson, Kevin Lanum, Brian Foley, Arturas Floria, and Kevin Lavering. Finally, we wish to acknowledge Jason Yedniak from Doosan GridTech.

Acronyms and Abbreviations

A	amperes
AC	alternating current
ACE	area control error
Ah	ampere-hours
BMS	battery management system
BMU	battery management unit
BSET	Battery Storage Evaluation Tool
CEF	Clean Energy Fund
DC	direct current
DERO	Distributed Energy Resources Optimizer
DG	Doosan GridTech
DG-IC	Doosan GridTech-Intelligent Controller
DOD	depth of discharge
DOE-OE	U.S. Department of Energy Office of Electricity Delivery and Energy Reliability
ESS	energy storage system
FBESS	battery energy storage system(s)
kV	kilovolts
kVA	kilovolt-ampere
kW	kilowatts
kWh	kilowatt-hours
MESA	Modular Energy Storage Architecture
MW	megawatt(s)
MWh	megawatt hour(s)
PCS	power conversion system
PNNL	Pacific Northwest National Laboratory
RPT	reference performance tests
RTE	round-trip efficiency
SnoPUD	Snohomish Public Utility District
SOC	state of charge
V	volts
VAR	volt-ampere reactive
W	watt
Wh	watt hour(s)

Contents

Executive Summary iii
Acknowledgments xi
Acronyms and Abbreviations xiii
1.0 Introduction 1
2.0 MESA 2 Battery 3
2.1 Battery Energy Storage System Layout 3
2.2 Battery Technical Specifications 5
2.3 Battery Management System 6
2.4 Balancing Procedure 10
2.5 Energy Throughput 10
2.6 PCS One-Way and Round-Trip Efficiency 14
2.7 Thermal Management 15
2.8 Power Distribution among Strings 17
2.9 DC Round-Trip Efficiency 17
2.10 SOC Drop during Rest 20
3.0 Battery Performance Test Results 23
3.1 Baseline Test Results 24
3.2 Response Time/Ramp Rate Test 29
3.3 Frequency Regulation Test 31
3.4 Use-Case 1: Energy Arbitrage 34
3.4.1 Duty Cycle Summary 34
3.4.2 Test Results 34
3.5 Use-Case 2: System Capacity 35
3.5.1 Duty Cycle Summary 35
3.6 Use-Case 3: Regulation 38
3.6.1 Duty Cycle Summary 38
3.6.2 Test Results 38
3.7 Use-Case 4: Real-World Flexibility 40
3.7.1 Duty Cycle Summary 40
3.7.2 Test Results 40
3.8 Use-Case 5: Load Shaping 41
3.8.1 Duty Cycle Summary 41
3.8.2 Test Results 41
3.9 Use-Case 6: Power Factor Correction 43
3.9.1 Duty Cycle Summary 43
3.9.2 Test Results 43

3.10 Use-Case 7: Optimal Utilization of Energy Storage 44
4.0 Lessons Learned 45
4.1 Lessons Learned from Test Results 45
4.2 Lessons Learned in Design of Data Transfer 46
4.3 Lessons Learned in Design of Test Set Up 47
4.4 Lessons Learned from Site-Related Issues 47
5.0 Novel Findings 49
5.1 State-of-Charge Model 49
6.0 Conclusions 52
7.0 References 56
Appendix A − Supplemental Information A.1

Figures

1 Main Components of the Use-Case Analysis Project 1
2 MESA 2 2-MW, 8-MWh FBESS 3
3 Everett Substation One-Line Diagram of 2-MW, 8-MWh FBESS (Drawing S-32-E1A) 4
4 Example of String 4 Dropping Off before the SOC of the Module Decreases to Zero 8
5 2018-03-02 String 4 Drops out – Reaches -100% SOC 9
6 2018-03-07 Strings 1 and 3 Subjected to Pulse Charge during Rest to Keep SOC above ~3% 10
7 FBESS Cumulative Individual String Performance at the Grid 11
8 DC Battery Cumulative Performance 12
9 Cumulative FBESS Performance with and without Rest and Auxiliary Consumption 13
10 PCS Conversion Power Losses (left) and One-Way Efficiency (right) 14
11 PCS Conversion Individual String Power Losses (left) and One-Way Efficiency (right) 15
12 Auxiliary Power Consumption during Charge, Discharge, and Rest as a Function of Deviation from Various Temperatures 16
13 Auxiliary Consumption at Various Charge and Discharge Power Levels 17
14 Dependence of Power Distribution among Strings on SOC Deviation from the Mean during Charge and Discharge 18
15 DC RTE for Baseline Capacity Tests 19
16 Progressive Decay of String 4 Performance during 800 kW Charge/1150 kW Discharge 20
17 Effect of PCS State and Reactive Power on DC Power Consumption during Rest 21
18 MESA Standard Architecture (left) and Electrical Schematic (Right) 21
19 MESA2 Power Flow Schematic 23
20 FBESS Performance Curves from Baseline Tests 27
21 Energy Charged or Discharged at the Grid and PCS Level as a Function of FBESS SOC 28
22 attery Temperature Profile during Reference Performance Capacity Tests 29
23 FBESS Response Along with Signal Request – Reference Performance Test 30
24 Response Time and Ramp Rate Reference Performance Test Results 31
25 In Situ Charge and Discharge Resistance for Each String- Resistance Normalized to Four-String Basis 32
26 Results from Frequency Regulation DOE Protocol Tests 32
27 Results Showing Strings 3 and 4 are Weaker than String 4 during Frequency Regulation Test Run 1 (left) and Run 2 (right) 33
28 Energy Arbitrage Results 34
29 Energy Arbitrage Results for Each Day 36
30 Weak Strings 3 and 4 during Arbitrage Test 37
31 System Capacity Test Results 37
32 Regulation Test Results 39
33 Real-World Flexibility Test Results 40

34 Load Shaping Test Results 42
35 Power Factor Correction Test Results 43
36 DERO Performance Evaluation Methodology 44
37 Taper Power as a Function of SOC during Charge and Discharge 49
38 Validation of FBESS Performance Model 50
39 Temperature Change for the Various Baseline Capacity Tests for Charge, Rest and Discharge. 51

Tables

1 Use-Cases for CEF Projects 2
2 Technical Specifications for the 600 kW, 2200 kWh UET FBESS String 6
3 Regression of PCS Losses 14
4 Auxiliary Power Regression 16
5 Baseline Reference Performance Capacity Test Results 26
6 Frequency Regulation Test Results 33
7 Energy Arbitrage Test Results 35
8 System Capacity Test Results 38
9 Regulation Results 39
10 Real-World Flexibility Test Results 41
11 Load Shaping Test Results 42
12 Power Factor Correction Results 44
13 Regression Results for Rate of Temperature Change as a Function of Power, Power2, and the Difference between FBESS and Ambient Temperature. 51

1.0 Introduction

Pacific Northwest National Laboratory (PNNL) was chosen to provide analytical support under the Use-Case Analysis Project. This project is designed to facilitate efforts to integrate flow battery energy storage systems (FBESS) into the electrical grid by providing a framework for evaluating the technical and financial benefits of the energy storage system (ESS) and exploring the role of energy storage in delivering value to utilities and the citizens they serve. This framework and the tools used to implement it will evaluate a number of use-cases as applied to energy storage projects deployed by the participating utilities under the Clean Energy Fund (CEF) Program. The methodologies that emerge from this project for evaluating multiple storage benefits, and the detailed operational results from utility operation of energy storage, will have broad national relevance and applicability. There are three main components related to use-case testing and evaluation, as outlined in Figure 1.

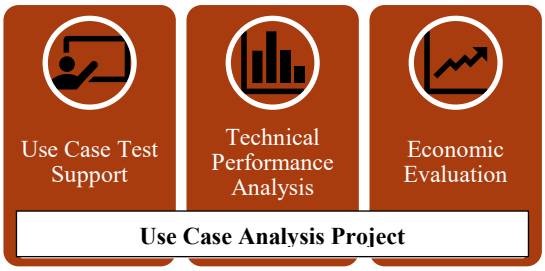

Figure 1. Main Components of the Use-Case Analysis Project

This report documents baseline and use-case technical performance of the Snohomish Public Utility District (SnoPUD) Modular Energy Storage Architecture 2 (MESA 2) FBESS, based on the framework and approaches defined by PNNL in the test plan report, and lessons learned during execution of the project. The technical support provided by PNNL included:

1. Develop protocols and duty cycles to test the ability of the FBESS to safely and effectively be used for the project's tested use-cases.
2. Identify performance metrics (e.g., ramp rate, round-trip efficiency [RTE], internal resistance) to be evaluated.
3. Analyze test results against a predefined set of performance metrics to determine the effectiveness of storage for each use-case.
4. Conduct baseline testing using cycles intended to quantify basic FBESS characteristics, including power and energy capacities, ramp rate/response time and internal resistance. Reference performance tests (RPT) for this project's FBESS used several duty cycles defined and described in the U.S. Department of Energy (DOE) Energy Storage Protocol and were performed at the beginning of the project (baseline tests). Because of string failure, the RPTs could not be repeated after use-case testing.
5. This project designed and tested three use-cases. These use-cases combined several energy storage applications as follows:
   - Use-Case 1 – Energy shifting consists of energy arbitrage and system capacity.
   - Use-Case 2 – Providing grid flexibility consists of regulation, load following, and real-world flexibility.

- Use-Case 3 – Outage management of critical loads, consists of Volt/VAR control with local and/or remote information and load shaping.
- Use-Case 7 – Optimal utilization of the FBESS across Use-Cases 1 through 3. This use-case could not be conducted as testing was stopped due to string failure.

These use-cases were selected from the full set being evaluated across several CEF battery energy storage projects (including FBESS and other technologies such as Li-ion batteries). Information in Table 1 describes the full range of use-cases under investigation and the ones that are relevant to this project.

Table 1. Use-Cases for CEF Projects

Use Case and application as described in PNNL Catalog	Avista	PSE	Sno – MESA1	Sno – MESA2	Sno - Controls Integration
UC1: Energy Shifting					
Energy shifting from peak to off-peak on a daily basis	Y	Y	Y	Y	
System capacity to meet adequacy requirements	Y	Y	Y	Y	
UC2: Provide Grid Flexibility					
Regulation services	Y	Y		Y*	
Load following services	Y	Y		Y*	
Real-world flexibility operation	Y	Y		Y*	
UC3: Improving Distribution Systems Efficiency					
Volt/Var control with local and/or remote information	Y		Y	Y	
Load-shaping service	Y	Y	Y	Y	
Deferment of distribution system upgrade	Y	Y			
UC4: Outage Management of Critical Loads		Y			
UC5: Enhanced Voltage Control					
Volt/Var control with local and/or remote information and during enhanced CVR events	Y				
UC6: Grid-connected and islanded micro-grid operations					
Black Start operation	Y				
Micro-grid operation while grid-connected	Y				
Micro-grid operation in islanded mode	Y				
UC7: Optimal Utilization of Energy Storage	Y	Y			Y

This project developed the composite cycle profiles and used these for testing the project's FBESS for the chosen use-case scenarios. The duty cycles and associated test results are described and discussed in the body of the report.

As the baseline and use-case tests were conducted, PNNL analyzed test results against a predefined set of performance metrics such as ramp rate, RTE, and internal resistance to determine the effectiveness of storage for each use-case.

Understanding the technical features and limitations is essential and provides much of the input data used to perform the economic evaluation of the use-cases to which a FBESS is subjected. Therefore, technical information on the MESA 2 FBESS is provided in the following section.

2.0 MESA 2 Battery

2.1 Battery Energy Storage System Layout

The project's 2.2-MW, 8-MWh vanadium redox FBESS consists of four strings, each rated at 0.55 MW and 2 MWh (see Figure 2). Vanadium redox is the safest chemistry used in batteries (SnoPUD Undated). The stack consists of only a small percentage of the total electrolyte content (ESA 2019). Hence, short circuit conditions do not result in thermal runaway. The amount of hydrochloric and sulfuric acid needed is less than 10%, which is a factor of 3 lower than that used in lead acid batteries. Each battery container has three 50 kW stacks connected in series.

Figure 2. MESA 2 2-MW, 8-MWh FBESS

Each string consists of five containers, with four battery containers housing the stacks and electrolyte and the fifth container housing the power conversion system (PCS) and associated controls. The strings are connected in parallel at the PCS level to the grid.

The arrangement of the four strings is also shown in Figure 3. Each string is labeled FBESS-1, -2, -3, and -4. Each string is connected to the direct current (DC) side of the bi-directional power inverter by a DC disconnect switch rated at 1000 volt (V) DC and 1,200 amperes (A) and a motorized DC circuit breaker rated at 1,000 V DC and 1,200 A. Each string is connected to the 15 k VAC grid via bolted pressure switches rated at 1,600 A and a Cooper Power 750 kVA 15,000YG/283Y transformer T1-X (X=1-4). Note that for this project, the overcurrent protection function of the bolted pressure switches was not used.

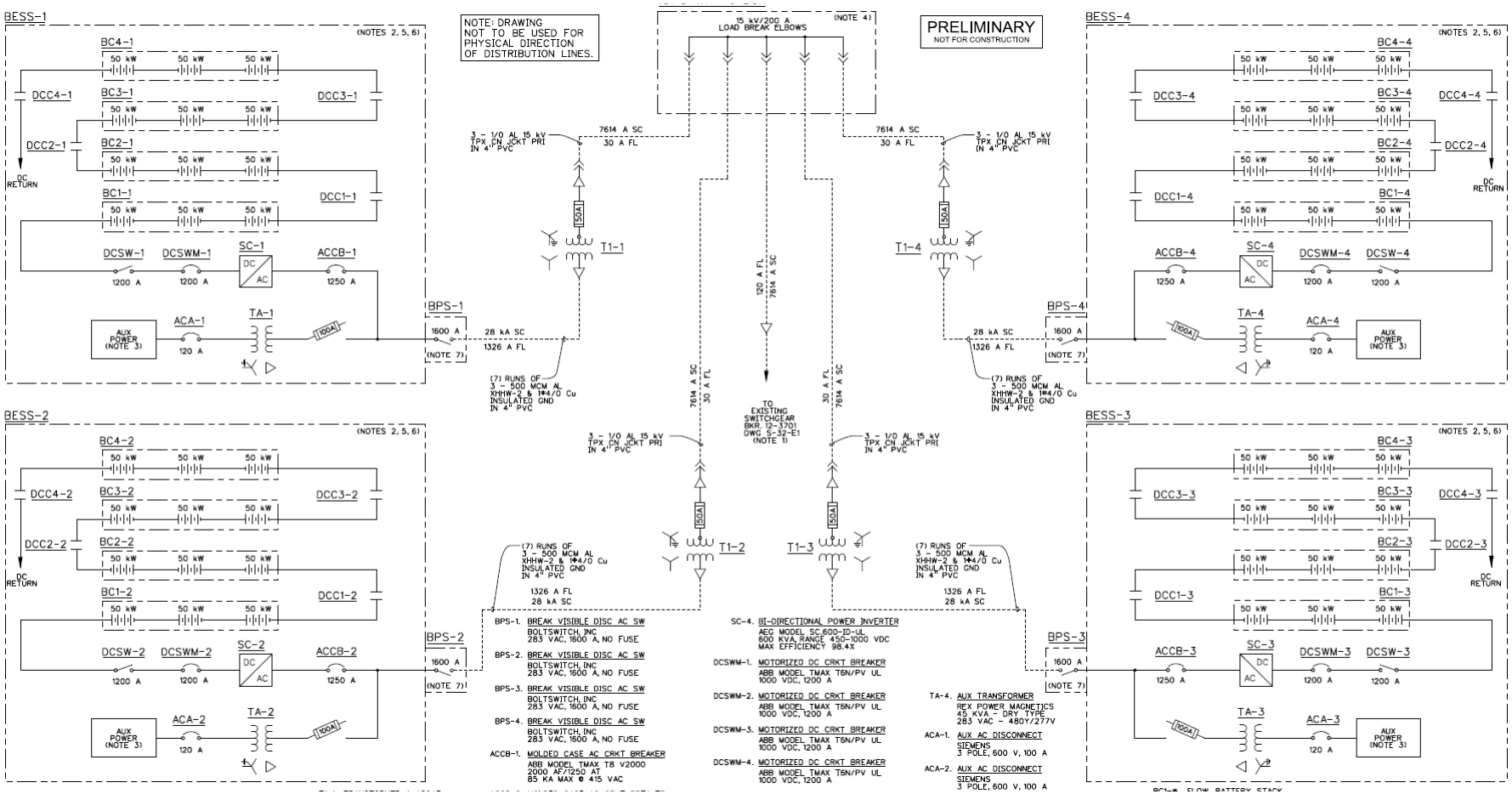

Figure 3. Everett Substation One-Line Diagram of 2-MW, 8-MWh FBESS (Drawing S-32-E1A)

Within each container during charge, the auxiliary power flows via REX Power Magnetics 45 kVA Dry Type 283 VAC – 480Y/277V transformers TA-X (X=1-4) to the auxiliary load via AC disconnect switches ACA-X (X=1-4) for cooling and pumping needs. The remaining power is directed to the AC side of bi-directional AEG Power Solutions inverters SC-X (X=1-4), each rated at 600 kVA, with a DC range of 450-1000 VDC, and a maximum efficiency of 98.4%. During discharge, the DC battery powers the auxiliary load by sending power through bi-directional inverters SC-X to TA-X.

There are no meters to measure auxiliary power flow. Additionally, there are no meters to measure power exchanges with the grid at the 283 V side of transformers T1-X. Power exchange with the grid is measured only at the 15-kV level. Hence, estimation of auxiliary load includes losses related to the transformer T1-X one-way efficiency.

Appendix A has additional details on the site layout and the FBESS one-line and three-line diagrams.

2.2 Battery Technical Specifications

According to the UniEnergy Technologies (UET) Product Sheet, the DC FBESS consists of four strings, each rated at 600 kW AC and 2.2 MWh AC. Each string has four 150 kW battery modules connected in series by DC contactors rated at 1000 VDC, 1200A. Each 150-kW module has three 50 kW power stacks[1] connected in series. Each string has five containers, with four containing stacks within each 150-kW battery module and electrolyte tanks and the fifth container housing the PCS. For the containers housing stacks and tanks, there is a built-in secondary containment. While the electrolyte is reusable, it is not clear if there is infrastructure in place to recycle and/or reuse stack components. The containers are rated to transport and seismic codes.

The technical specifications for each string are given in Table 2 (UET Undated). It is assumed that the kilowatt-hour energy at various AC power levels takes into account auxiliary load consumption. Note that the actual energy obtained during project execution was 52 to 55% of the values reported in Table 2. The FBESS was de-rated to 2.2 MW, 8 MWh after "extended contract negotiations" per input from UET, with the 8 MWh rated to be available at a power of 1 MW.

[1] In the rest of the document, "stacks" has been used to refer to "power stacks"

Table 2. Technical Specifications for the 600 kW, 2200 kWh UET FBESS String

Parameter	Value
Peak Power (kW AC)	600
Maximum Energy (kWh AC)	2,200
Energy (kWh AC) at 600 kW AC	1,200
Energy (kWh AC) at 500 kW AC	2,000
Energy (kWh AC) at 275 kW AC	2,200
AC RTE	70%
AC Voltage, kV	12.47
Response time (ms)[2]	<100
Reactive Power (kVAR)	+/- 450
Humidity	95% noncondensing
Footprint, m^2	76
Envelop (m)	12.5W × 6.1D × 2.9H
Volume (m3)	221.125
Weight (kg)	170000
Wh/L	9.9
W/L	2.7
Wh/kg	12.9
W/kg	3.5
Cycle life	Unlimited over the 20-year design life
Ambient Temperature °C	-40 to 50
Self-discharge rate[3]	Maximum of 2% of stored energy

2.3 Battery Management System

The battery management system (BMS) distributes power among the four strings according to a proprietary algorithm. Both the BMS and Doosan GridTech-Intelligent Controller (DG-IC) ensure that the maximum power rating of the string of 550 kW during discharge and 400 kW during charge is not exceeded. This provides a dual layer of safety.

Each string operates independently of the other. If one string fails, the other strings continue performing grid services and provide or absorb the required power, subject to the discharge and charge power limits.

Each string has five containers, four containing one battery module each and the fifth consisting of the bi-directional power inverter with BMS. Each battery module has three 50-kW stacks connected in series, with each stack consisting of 50 series-connected cells with open circuit voltage limits of 1.25 V on the low end to 1.49 V on the high end. The 1.25 V/cell is denoted as 0% SOC, while 1.49 V/cell is denoted as 100% SOC. Linear extrapolation results in an SOC of -100%at 1.00 V/cell. Open circuit voltage is measured for each battery module separately by placing reference electrodes in the flow path of the

[2] The response time is not defined in the technical specifications. This report uses the definition as stated in the DOE-OE Protocol

[3] The self-discharge rate is not defined in the technical specifications. This work reports the rate of decrease of SOC during rest as the self-discharge rate.

catholyte and anolyte and measuring the potential difference. The behavioral trends for each string are described below, with the highlights listed below:

- Distribution of charge and discharge power levels among strings as a function of string SOC or state of health
- Modes of unanticipated end of discharge in spite of high string SOC
  - SOC drops to 0%, and string stops discharging and accepting charge
  - SOC drops to ~5%during rest, at which point it receives charge pulses to maintain SOC between ~5 and 25%
  - Availability of power
    - When string SOC drops to 0%, it is deemed unavailable.
    - During prior discharge, the string reaches the end of discharge, but the BMS does not remove its availability till its SOC reaches 0%.
    - When the string is subjected to charge pulses during rest, the available power is reduced by the magnitude of the charge pulses.
- A precursor to failure during rest is the larger rate of decrease of SOC during rest, as high as 3.8% per hour. If any module voltage within the four-module string reaches an average voltage of 1.00V/cell or -100% SOC, the string is automatically faulted and disconnected from the grid

At the start of discharge at 2018-01-23 11:10:00, the power distribution is as follows:

String 1:	Disconnected
String 2:	358 kW, 93.8% SOC
String 3:	305 kW, 91.6% SOC
String 4:	198 kW, 83.9% SOC
Total:	861 kW
System SOC:	90.0%

At 2018-01-23 13:15:00, the data shows:

String 1:	Disconnected
String 2:	323 kW, 65.6% SOC
String 3:	299 kW, 64.6% SOC
String 4:	241 kW, 61.8% SOC
Total:	862 kW
System SOC:	64.0percent

The above discharge power distribution was linearly proportional to the SOC for each string.

At 2018-01-23 14:00:00, String 4 power was zero, even though its SOC at 49% was only marginally lower than the SOC of remaining strings (see Figure 4). There is a high likelihood that the minimum SOC for a String 4 module had reached 0%. Hence, discharge was stopped for String 4. The BMS stops discharge when the SOC in any battery module reaches 0%. It would have been useful to have the maximum and minimum SOC for each module so that modeling could be done at the module level to reliably predict individual string performance. The end user also would be able to adjust the battery operating parameters based on this additional data. At a minimum, having the maximum and minimum SOC values for each string would provide the end user advance information prior to unanticipated string failure due to module mismatch within the string.

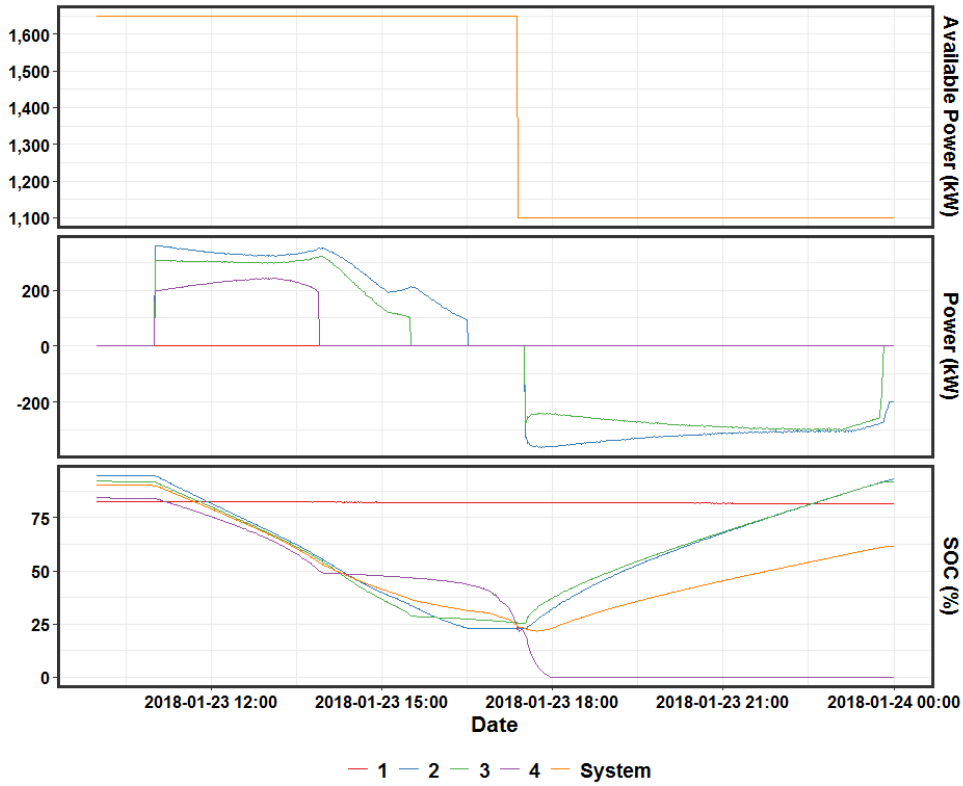

Figure 4. Example of String 4 Dropping Off before the SOC of the Module Decreases to Zero

The available power remained at 1,650 kW (three active strings) until 2018-01-23 17:20, even though String 4 discharge had terminated at 2018-01-23 14:00. At 2018-01-23 17:20, when a charge command was sent, the available power dropped to 1,100 kW, reflecting the fact that String 4 was not available. It appears it took a charge signal to be sent to the FBESS for the BMS to recognize that String 4 is not available. Ideally, once the end of discharge criterion for String 4 was reached at a high SOC of 49%, the BMS should have recognized that String 4 was no longer available.

At the start of charge, String 2 accepts 64% of power, even though the String 2 and 3 SOCs are nearly equal at the start of charge. This may be because the maximum SOC for a String 3 module may be higher than that for String 2. During charge, the BMS may be looking at the maximum SOC as criterion to distribute power. As a corollary, during discharge the BMS probably looks at the minimum SOC to distribute power. In both cases, less power probably goes to strings with wider gaps between maximum and minimum SOCs. Because the maximum and minimum SOC tags for each string were not available, this hypothesis could not be confirmed. The proposed BMS algorithm assuming maximum and minimum SOC tags for each string is provided in Appendix A.

When the average module voltage approaches a lower (unknown) limit, which is >1.00 V but very close to it, the string goes into a pulse charge mode in which it is subjected to charge pulses to ensure the module voltage stays above 1 V/cell. Figure 5 shows at 2018-03-02 16:25:00 at the start of discharge, 260 kW flows through each active String 1, 2 and 3, with SOC at 76%. After 1.5 hours, String 3 and 4 power levels are lower than with String 2 with SOC for all strings nearly equal. Close to two hours into the discharge, String 3 and 4 power reached zero, while the SOC for all strings was at ~30%. Once discharge ended, all strings were in rest mode. At 2018-03-02 20:20:00, the String 3 SOC reaches 7.3%, at which point it is subject to charge pulses. During the charge pulse, the available power drops by the magnitude of the charge pulse.

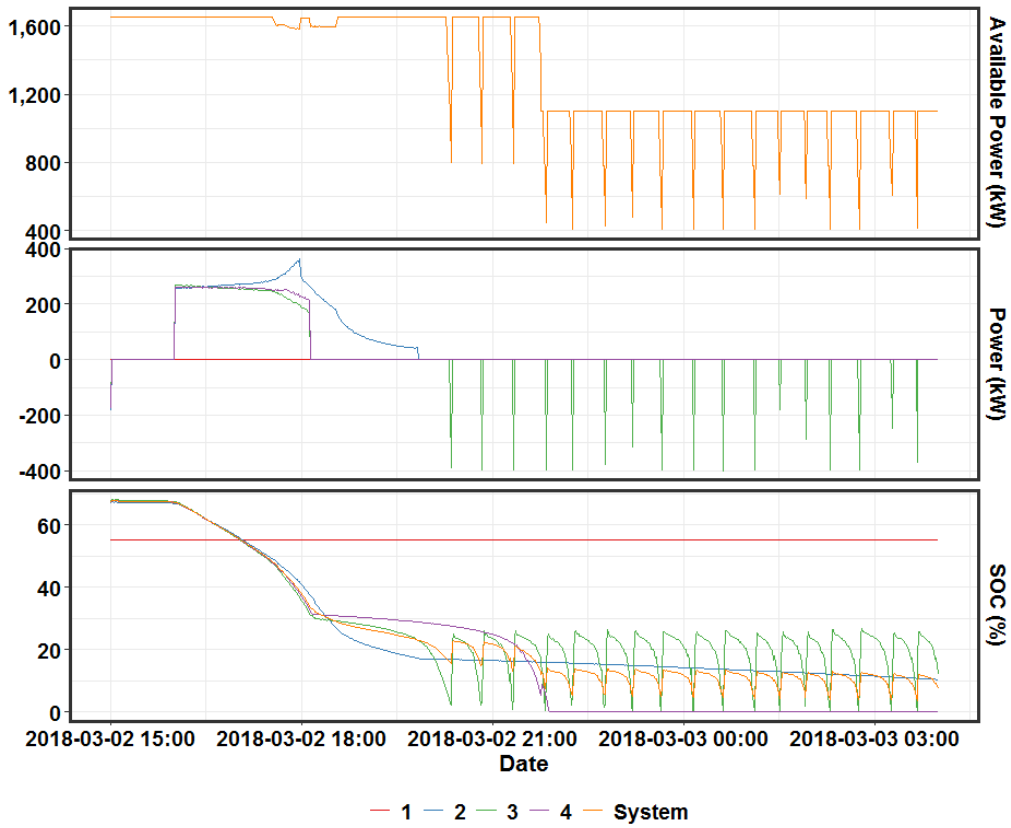

Figure 5. 2018-03-02 String 4 Drops out – Reaches -100% SOC

At 2018-03-02 22:00:00, with the FBESS still in rest mode, the String 4 SOC reaches 0%, and the available power drops by one string (550 kW). That is, even though String 4 had stopped discharging two hours into discharge, the available power algorithm removed its availability only when its SOC reached 0%, which corresponds to when one of the modules SOC has reached -100%. Note that 100% SOC corresponds to 1.49V/cell, 0% SOC corresponds to 1.25V/cell and -100% SOC corresponds to 1.00V/cell (Weber 2018). This indicates that for available power to drop by one string, the SOC has to reach 0%, or a charge or discharge command has to be sent to the string with a weak module.

Figure 6 shows that at 2018-03-07 12:20:00, String 1 and 3 SOC decrease during rest after charge from 30% and 45% SOC to 7.5% SOC in 6 hours and 19 hours, respectively. This rapid SOC drop may be caused by one weak module in each string that pulls down average string SOC. At this stage, pulse charging occurs to keep the SOC between 7.5% and 20% SOC for Strings 1 and 3. The available power during the charge pulse is reduced by the magnitude of the charge pulse. Note that the rate of SOC drop from 30 to 7.5% is nearly the same for Strings 1 and 3. This high rate of SOC drop can be considered to be a precursor to string failure.

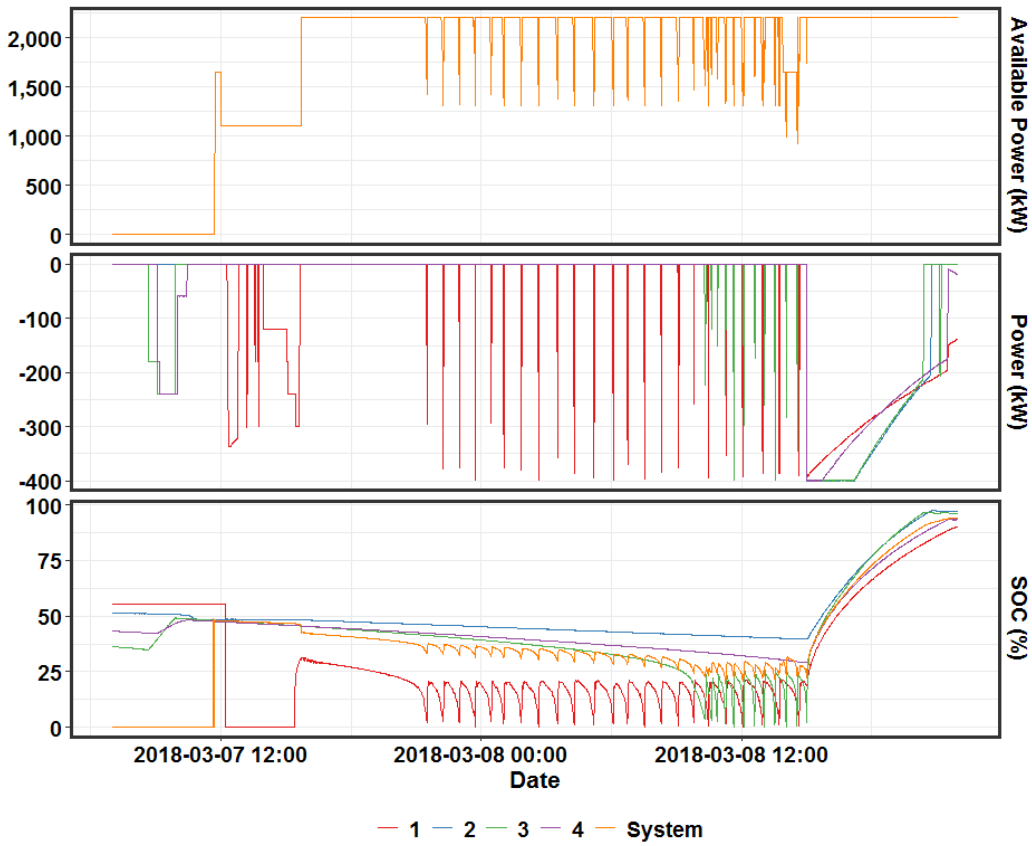

Figure 6. 2018-03-07 Strings 1 and 3 Subjected to Pulse Charge during Rest to Keep SOC above ~3%

2.4 Balancing Procedure

Strings fail for a variety of reasons, with one reason being a faulty, or "weak," stack within the string. Each string has four battery modules connected in series, with each module consisting of three 50 kW stacks. The SOC for each module is measured by open circuit voltage measurements using reference electrodes in the flow path of the catholyte and anolyte. If all stacks are uniform in terms of design and performance, the strings will remain well balanced after an initial balancing. However, for this project's FBESS, some of the stacks have high electrolyte crossover, resulting in a faster SOC drops during rest and discharge, and slower SOC increases during charge. This results in lower coulombic and energy efficiency. While the details of balancing procedure were not shared, faulty strings were placed in the local or maintenance mode. The SOC of the weak module was brought in line with the SOCs of the remaining modules within the string by charging at nominal rate. For strings with more than one weak module, the procedure is repeated for one module at a time. The string SOC is then brought to the desired SOC to match other strings by a suitable charge or discharge.

2.5 Energy Throughput

During testing, all four strings were available for only a fraction of the total available time allocated for this project's planned field demonstration and testing. The availability of the number of strings as a percentage of test time is given below.

No strings: 5%
One string: 8%
Two strings: 32%
Three strings: 27%
Four strings: 28%

The availability of each string is also provided below:

String 1: 23%
String 2: 39%
String 3: 45%
String 4: 38%

The cumulative performance of individual strings excluding all rest periods and auxiliary consumption is captured by Figure 7. At the start of testing, the RTE for all strings was low, as reflected by the higher rate of loss (cumulative discharge – cumulative charge/hours). Ignoring this initial portion, String 2 has the highest RTE, topping at 63% and ending at 54%. The RTE of String 4 was the lowest, peaking at 53% and ending at 45%. The RTE of String 3 peaked at 60% but finished at 45% as a result of pulse charging during rest when its SOC had reached low levels.

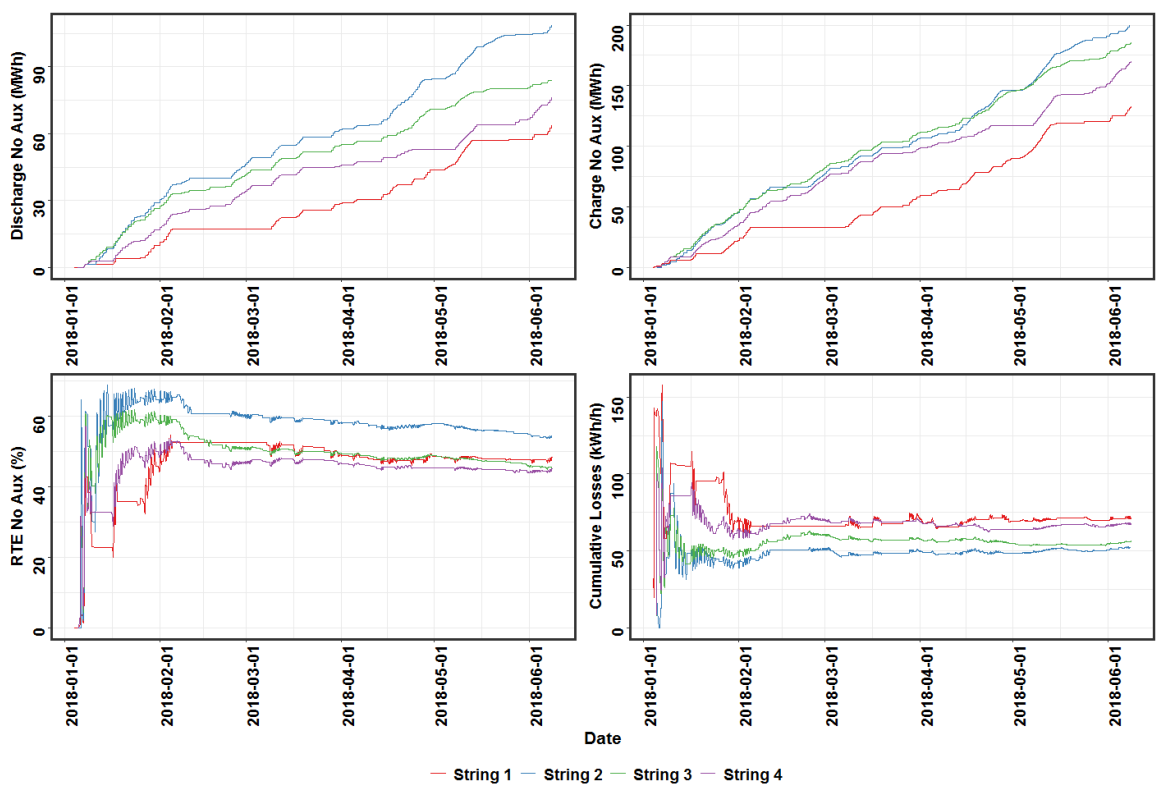

Figure 7. FBESS Cumulative Individual String Performance at the Grid

Due to multiple periods when String 1 was not available, mainly due to stack leaks leading to electronic malfunction, its charge and discharge throughputs were the lowest. The discharge energy throughputs corresponded to 52, 41, 38, and 32 full depth of discharge (DOD) cycles for Strings 2, 3, 4, and 1 respectively.

The battery modules are connected in series within each string. Because of electrolyte crossover within stacks with defective membranes during charge, additional charge is needed to compensate for this crossover. Because of a mismatch between SOCs of the four series-connected modules within each string, the healthy modules reach the high SOC limit while the modules with high crossover have lower SOCs. Hence, the average SOC of the string is lower at the end of charge. During discharge, the weaker modules reach their lower SOC limit, leading to premature ending of discharge. Adding up all power levels during non-rest periods with suitable unit adjustments, taking into account time difference between successive points, provides the cumulative kWh per hour loss rate. The cumulative RTE for all strings is consistent with the cumulative kWh per hour loss rate.

The String 1 RTE is lower than the String 2 RTE, possibly due to weaker stacks. As discussed later, Strings 1 and 3 fail in a different manner compared to String 4. All three strings have weak stacks that lead to SOC mismatches among their battery modules.

The discharge efficiency is higher at higher SOCs because the open circuit voltage increases linearly with increasing SOC. Hence, strings with balanced modules can be charged to higher SOCs, leading to better RTEs. The cumulative DC charge and discharge energy values follow the same trend.

The corresponding DC values, along with ampere-hours (Ah) throughput and coulombic efficiency are shown in Figure 8.

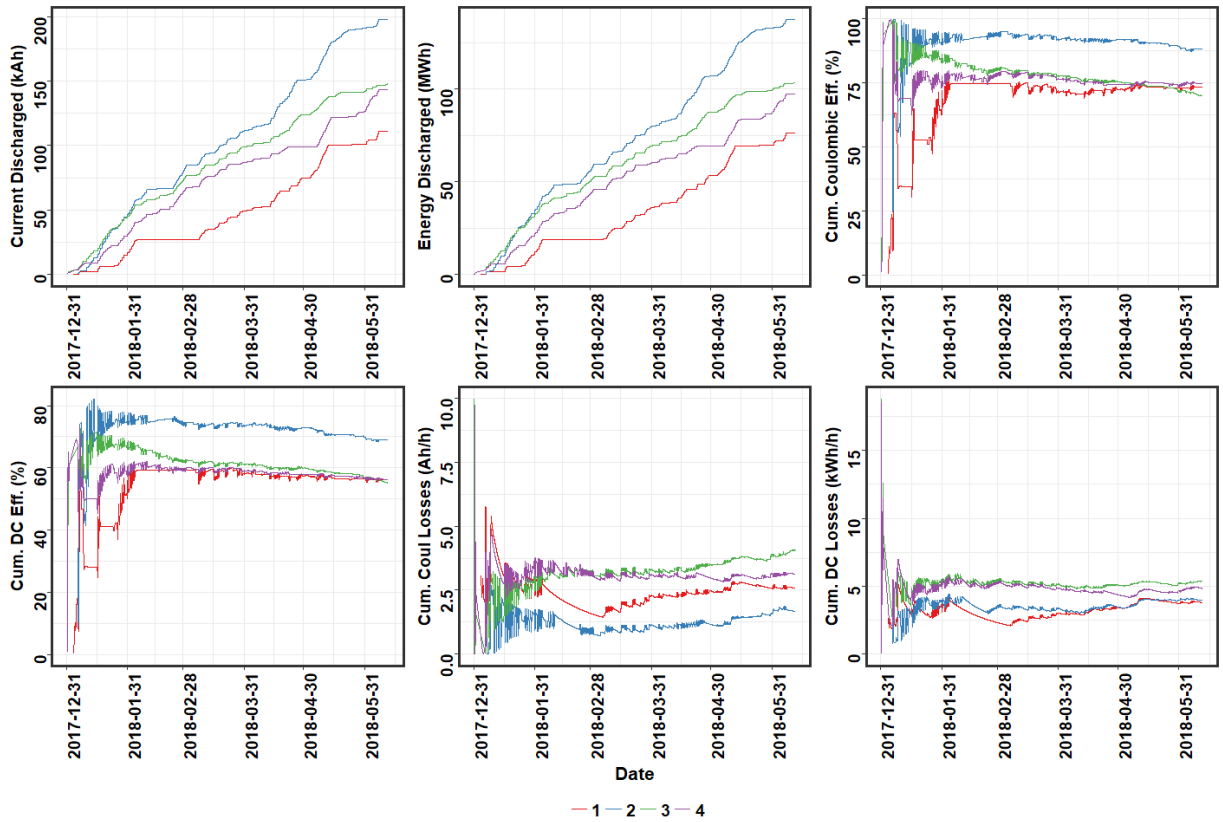

Figure 8. DC Battery Cumulative Performance

The coulombic and energy efficiency is lowest for Strings 1, 3, and 4. This finding is in line with the AC results for Strings 3 and 4. The DC kWh/h and Ah/h loss rates were calculated as described earlier for the AC kWh/h loss rate. String 2 has the lowest Ah/h loss rate, followed by String 1. As expected, because of

weak battery modules, Strings 3 and 4 had the highest Ah/h loss rates due to higher crossover levels. However, the coulombic efficiency was lowest for String 1, possibly because the cumulative Ah is lowest for this string. The cumulative DC RTE is also lowest for String 1, again because the cumulative Ah is lowest. Our analysis indicates the average power levels for String 1 were -202 kW during charge and 206 kW during discharge, while the corresponding power levels for other strings were 80% to 96% of these power levels. As seen in Figure 9 and Figure 10, the one-way PCS efficiency drops steeply when the absolute value of power is less than 200 kW. This probably explains the higher RTE for String 1 compared to Strings 3 and 4, in spite of its lower DC RTE. The DC-DC RTE was about 10% higher than the RTE without auxiliary consumption, showing the effect of PCS losses at the low average power levels during testing.

The cumulative discharge and charge energy for all strings combined, along with RTE is plotted in Figure 11. Excluding auxiliary consumption, 330,000 kWh were discharged by the FBESS, which corresponds to 51 full DOD cycles. The cumulative RTEs for the FBESS were 48, 42, and 34% with the last two numbers corresponding to excluding rest and excluding auxiliary consumption, respectively. The low RTE and the significant RTE reduction when rest and auxiliary consumption are included is reflective of the low average power levels for the test. The DC-DC RTE ends up at 60 to 70%, which shows that the low AC-AC RTE at the low power levels is mainly related to PCS losses and auxiliary consumption.

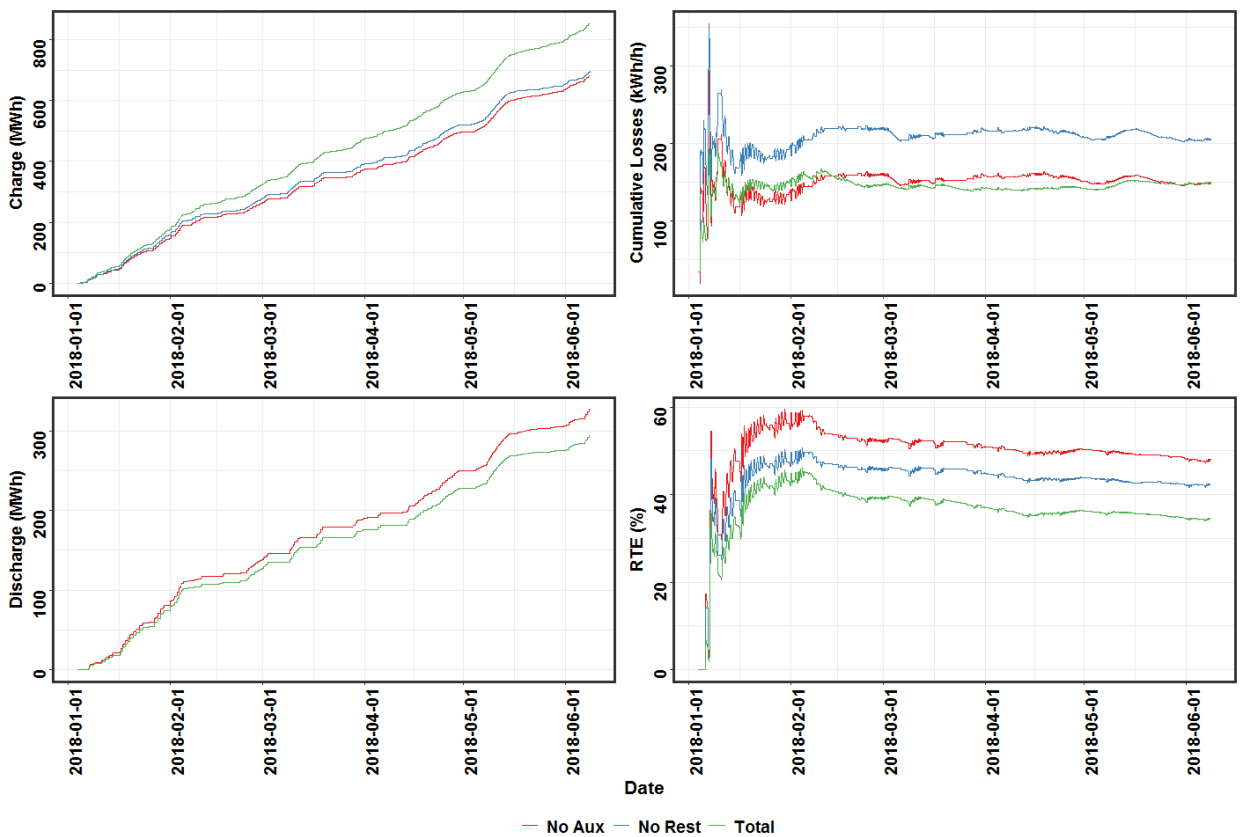

Figure 9. Cumulative FBESS Performance with and without Rest and Auxiliary Consumption

2.6 PCS One-Way and Round-Trip Efficiency

The ratio of PCS power to DC power is inverter one-way efficiency during discharge, while the ratio of DC power to PCS power during charge is one-way efficiency during charge. The difference between DC power and PCS power is plotted below in Figure 10. For a fixed power level, losses during charge are less than during discharge. Regression of the losses with respect to PCS power and number of active strings gives the coefficients in Table 3, with adjusted R^2 of 0.96. The PCS one-way efficiency is >0.95 at power levels <1,000 kW and >1,000 kW on a four-string basis. As expected, the efficiency at low percent of rated power decreases. At 500 kW discharge, the one-way efficiency is surprisingly low at 0.93. Charge efficiency is higher than discharge efficiency, with an average of the maximum for the four strings of 98% compared to 95% for discharge as seen from Figures 10 and 11.

Table 3. Regression of PCS Losses

Parameter	Coefficient	Standard Error	Units
Power (kW)	0.0129	4.28e-05	kW/kW
Power Squared (kW^2)	1.01e-05	5.84e-08	$kW/(kW^2)$
Number of Active Strings	6.14	0.0137	kW

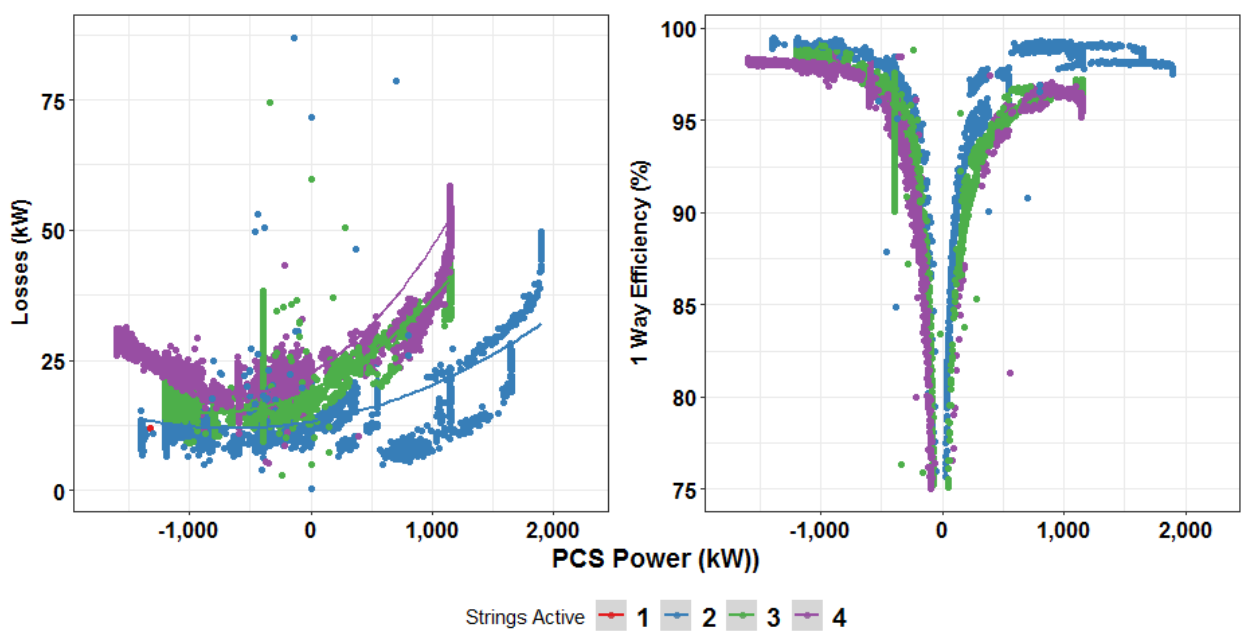

Figure 10. PCS Conversion Power Losses (left) and One-Way Efficiency (right)

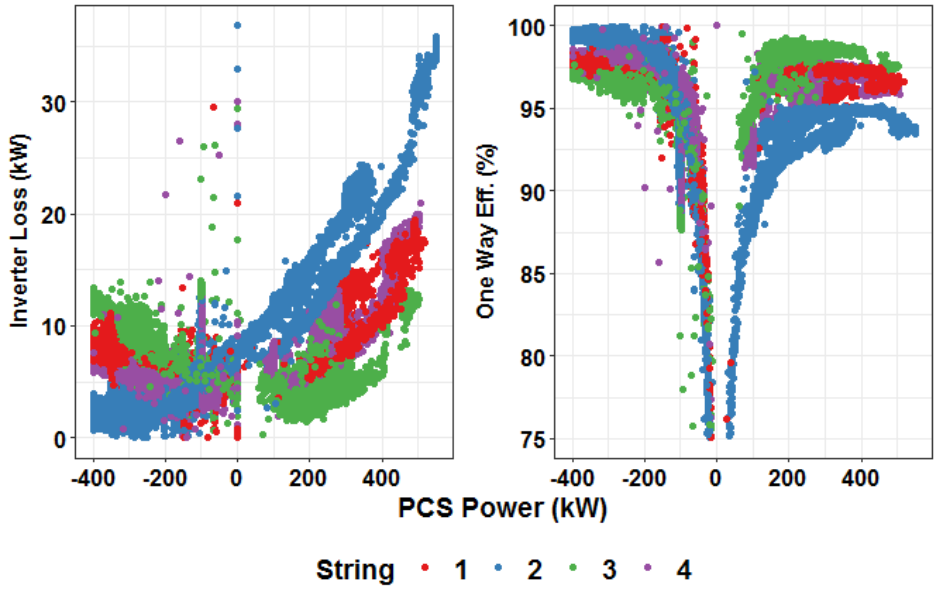

Figure 11. PCS Conversion Individual String Power Losses (left) and One-Way Efficiency (right)

Figure 11 shows data for each string across the power range investigated. At a fixed power, String 2 has the highest losses during discharge and lowest losses during charge. String 3 has the lowest losses during discharge and highest losses during charge, while String 2 and 4 losses are in between these extremes.

2.7 Thermal Management

Auxiliary consumption decreases as the battery and ambient temperatures decrease. This is consistent with the fact that thermal management consists of cooling only. Hence, low temperature corresponds to less auxiliary consumption. According to a UET engineer, the auxiliary consumption per string is 12 kW without cooling and 18 kW with cooling, with cooling activated for continuous power at >35°C and any time the temperature exceeds 40°C (Sun 2015). For a four-string system, this corresponds to 48 kW and 72 kW, respectively. Based on linear regression, the data show that auxiliary power consumption is in the 35 to 80 kW range (Figure 12), with auxiliary consumption increasing with ambient or FBESS temperature.

Embedded within this is the effect of temperature on auxiliary consumption. Surprisingly, auxiliary consumption at fixed power was higher for charge than for discharge, because charging has been shown to be endothermic for this flow battery (Figure 13). Per the technical specifications, the pumps have a variable speed drive, which implies the electrolyte flow rate varies as a function of operating parameters. Hence, auxiliary consumption without cooling load is expected to vary. A plausible explanation is that for fixed power, charging requires higher flow rate than discharging, resulting in higher auxiliary load during charging. Because of fixed overhead for some parts of the auxiliary load such as powering the BMS, communication, etc., the auxiliary power per string decreases as number of active strings decreases from four to two.

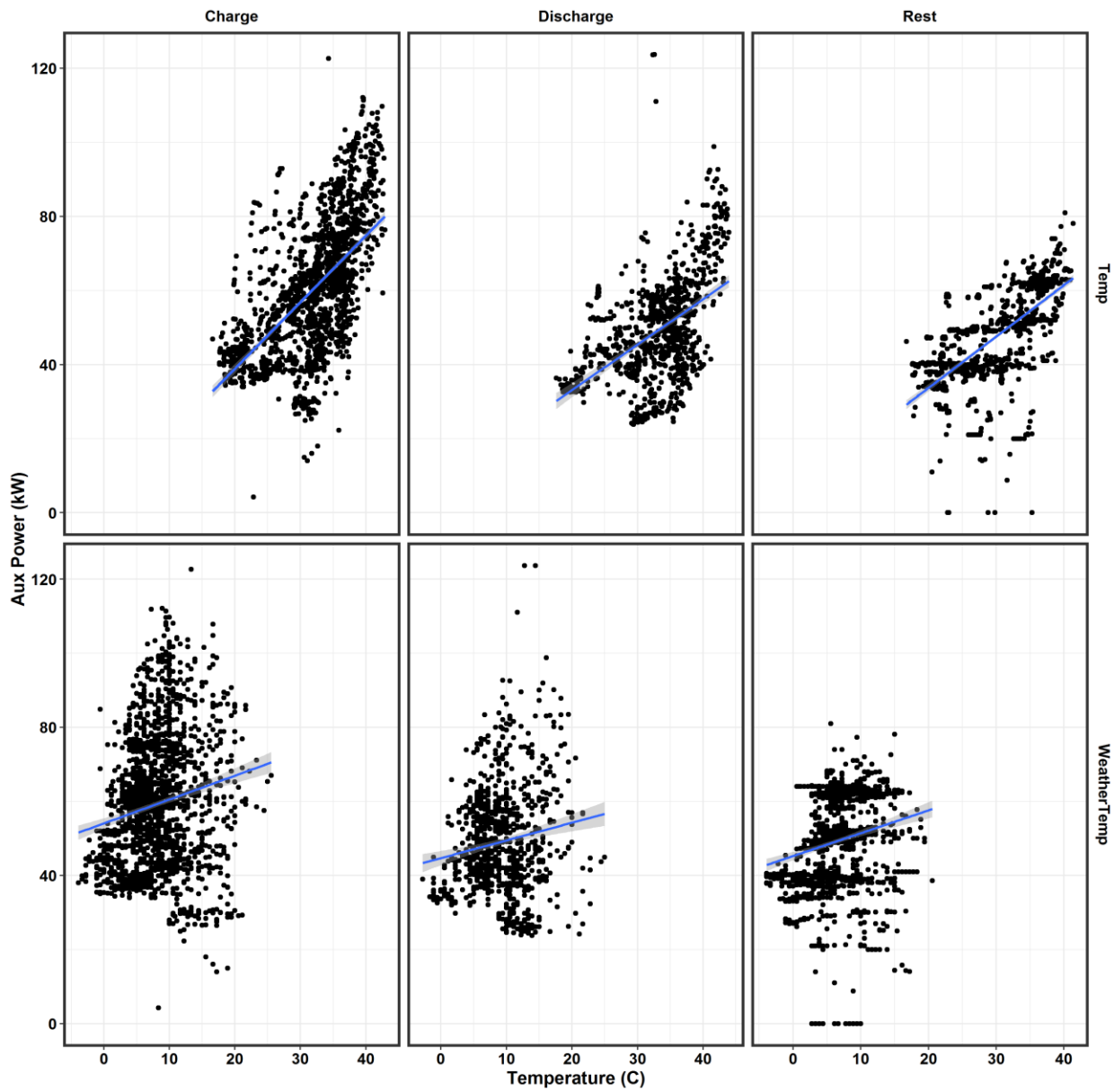

Figure 12. Auxiliary Power Consumption during Charge, Discharge, and Rest as a Function of Deviation from Various Temperatures

Auxiliary consumption was regressed vs. P, P^2, and number of strings as shown in Table 4 and Figure 13.

Table 4. Auxiliary Power Regression

Variable	State	Slope	R Squared
Temperature	Charge	1.73	0.07
Temperature	Rest	1.39	0.42
Temperature	Discharge	1.23	0.24
Weather Temperature	Charge	0.79	0.01
Weather Temperature	Rest	0.62	0.04
Weather Temperature	Discharge	0.48	0.02

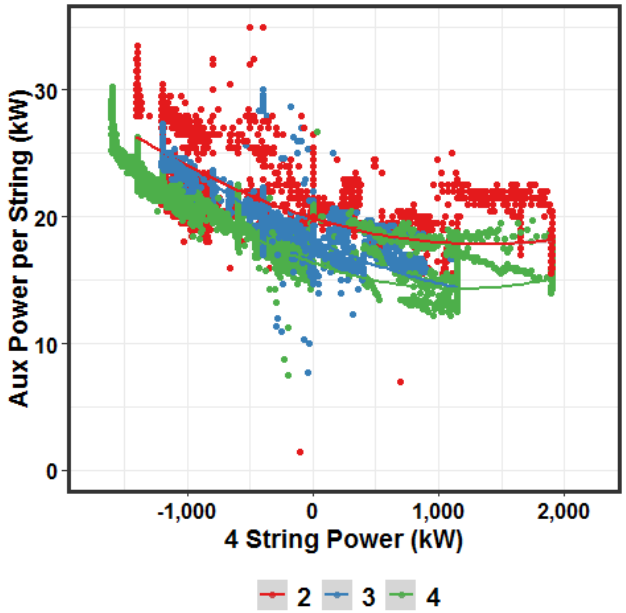

Figure 13. Auxiliary Consumption at Various Charge and Discharge Power Levels

2.8 Power Distribution among Strings

Using the available FBESS parameter tags[4] for SOC for each string, we carried out an analysis to determine power distribution among strings for charge and discharge as a function of string SOC deviations from the average FBESS SOC.

In Figure 14, the power distribution among strings is shown as a function of SOC difference from the mean. As expected, the discharge power increases linearly with increasing SOC deviations from the mean, while the reverse is true for charge. There are two linear regions for discharge. At high SOCs, the power distribution is more uniform, as would be expected.

The charge curve is $Y = x^{1/3}$, with string power increasing with greater negative SOC deviations from the mean. The cube root function probably is because maximum charge power of 1,600 kW is 72% of the maximum discharge of 2,200 kW, and possibly due to the fact that the BMS limits the ramp rate during charge based on SOC and ambient conditions. At high SOCs, even small deviations result in power tapering very steeply because power flow through fully charged strings decreases rapidly.

2.9 DC Round-Trip Efficiency

The DC RTE as a function of SOC was determined by taking the ratio of discharge to charge energy in the -5 to +5% SOC range for all baseline capacity tests (Figure 15). The taper portions are shown in blue. As expected, during charge, taper occurs at high SOC levels, and during discharge, taper occurs at low SOC levels.

[4] FBESS parameter tags are the names for each FBESS parameter that is being measured, recorded and passed to PNNL. In this report, the word "tags" is used to represent "FBESS parameter tags"

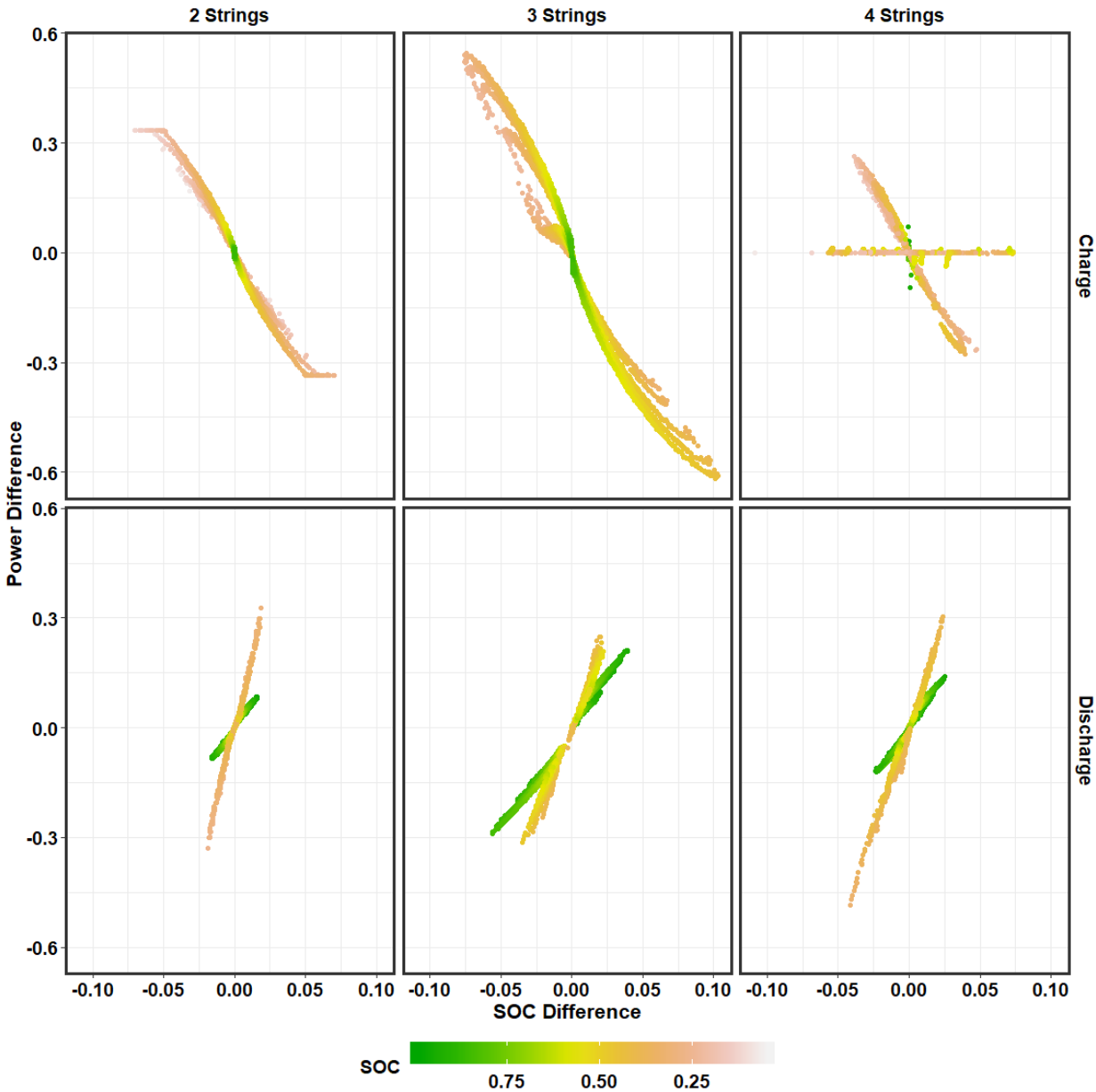

Figure 14. Dependence of Power Distribution among Strings on SOC Deviation from the Mean during Charge and Discharge

For a fixed charge power of 1200 kW, the RTE increased as discharge power decreased from 1,150 kW to 550 kW. For example, at 1,150 kW discharge, the RTE ranged from 80 to 85% in the 52 to 77% SOC range, while at 550 kW discharge, RTE ranged from 90 to 87% across the same SOC range. For a fixed discharge power of 1,150 kW, the RTE increased as charge power decreased. At a 1,200 kW charge, the RTE ranged from 80 to 85% in the 52 to 77% SOC range, while the corresponding numbers were 83 to 86% for the 600 kW charge.

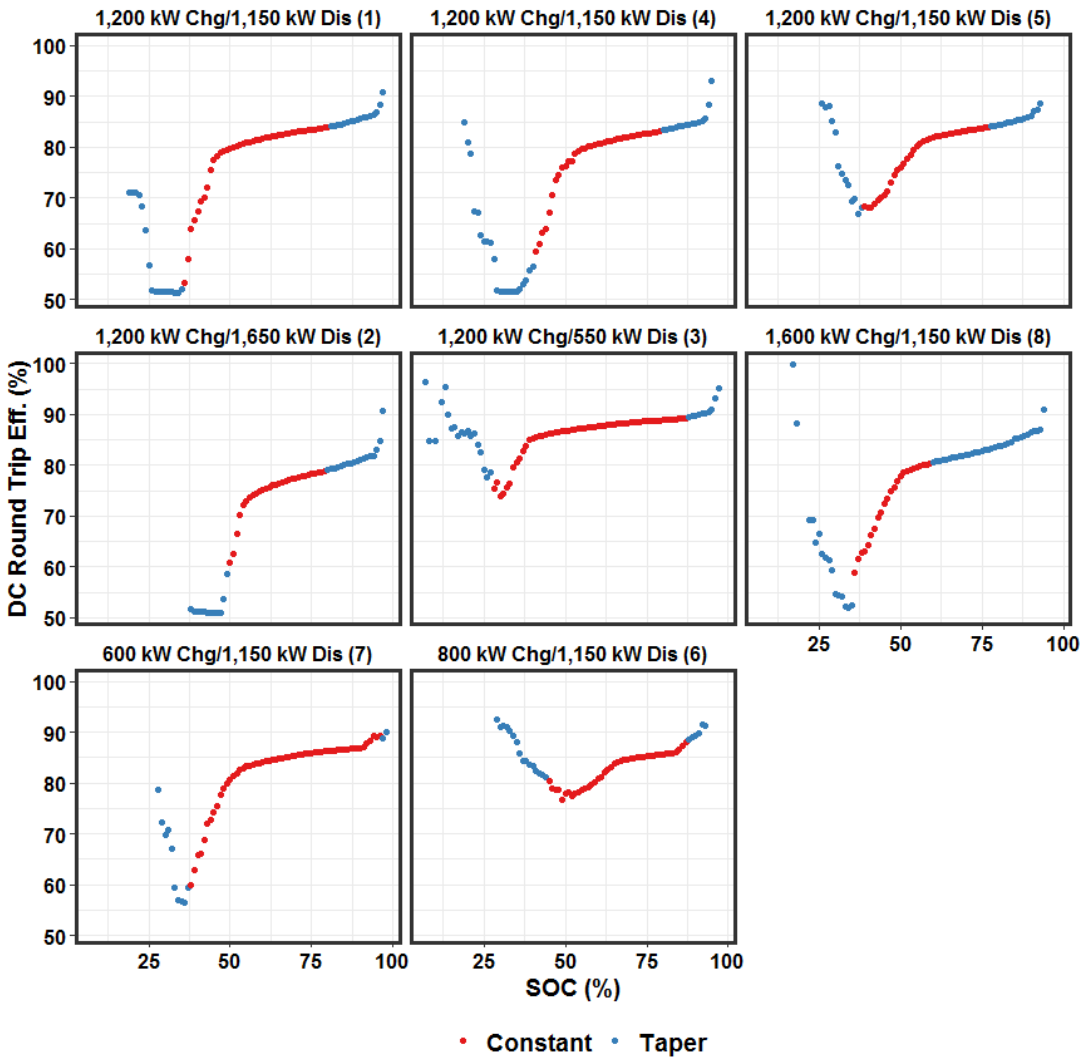

Figure 15. DC RTE for Baseline Capacity Tests

The RTE increased with increasing SOC at constant discharge power, as would be expected. The taper portion during charge increased as charge power increased, with taper starting at 57% SOC at 1,600 kW charge. During charge, as SOC increases in the taper portion, there is an upward spike in RTE, associated with steep reduction in charge current (and the associated higher electrochemical efficency). Prior to discharge taper, there is a slope change in the RTE as the rate of change of SOC during discharge increases as the SOC approaches the taper value. Because the ohmic resistance does not change much in the SOC range investigated, this increased rate of decrease of SOC is associated with depletion of reactants at the reaction zone, which leads to increased charge transfer resistance (Crawford et al. 2016). After the taper region, the RTE increases as expeced due to the decrease in power and associated current. As an outlier, the RTE for an 800 kW charge and 1,150 kW discharge run started to decrease rapidly at ~65% SOC, as opposed to this occurring in the 40 to 50% SOC for same discharge power and higher or lower charge power levels. The reason for the poor behavior for this run was that out of three starting strings, String 4 became progressively weaker and eventually dropped out after the fourth discharge cycle (Figure 16).

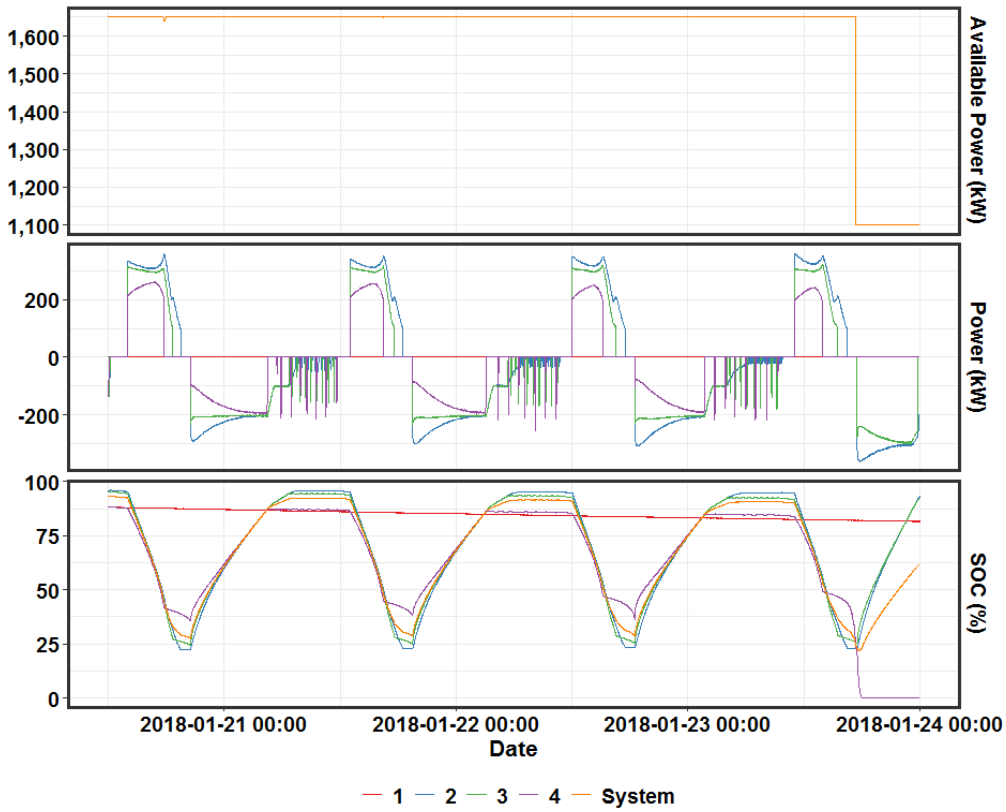

Figure 16. Progressive Decay of String 4 Performance during 800 kW Charge/1150 kW Discharge

2.10 SOC Drop during Rest

The SOC drop rate during rest is ~0.5% per hour under normal operation. However, when a string has weak stack modules, higher crossover in the weak stacks leads to rapid SOC drop at <30% string SOC, due to one of the battery modules reaching nearly 0% SOC. As seen earlier, for some instances, this results in SOC dropping to a very low level of ~3 to 5%, at which stage the string is subject to charge pulses. This occurs for Strings 1 and 3, and at times for String 2. For String 4, when one of the modules reaches -100% SOC (or a unit cell open circuit voltage of 1.00 V, at which point the string SOC is set to be 0%, and the string is disconnected. Hence, the SOC drop rate during rest is not predictable in a reliable manner because of the weak stack modules present in each string.

Approximately 1.7% of the time during rest the PCS is in a switching state. The DC discharge current and power during rest was nearly zero for high standard deviations of reactive power, while it ranged from zero to 22 A (0 to 18 kW) (on a per string basis) when the PCS was not switching. This appears to indicate that during rest, for 98% of the time the PCS does not switch; that is, it is disconnected from the grid. During these occasions, the DC battery provides system auxiliary needs. The DC power per string for the most part is 5 kW, indicating the electrolyte flow rate during rest is probably lower than during operation, thus consuming lower auxiliary power. It also indicates that during rest, the FBESS temperature is lower than the 35°C set point above which cooling would otherwise kick in. Figure 17 shows the effect of PCS state and reactive power on DC power consumption during rest.

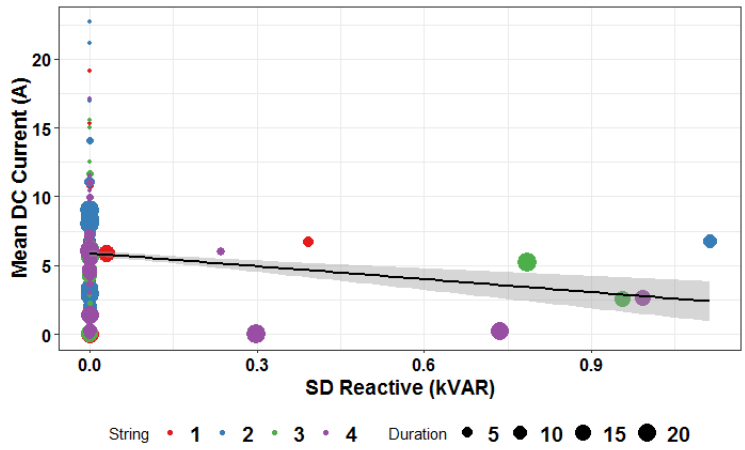

Figure 17. Effect of PCS State and Reactive Power on DC Power Consumption during Rest

Control system integration of the SnoPUD ESS is performed using MESA standards. At the planning stage, SnoPUD explored different standards for software and control system integration of ESS and experienced a lack of adequate open standards. Therefore, in collaboration with a number of partners, the MESA standard was developed (MESA 2016). The MESA standard is open, non-proprietary, and helps accelerate interoperability, scalability, safety, quality, and affordability in energy storage components and systems. Both battery energy storage units at SnoPUD MESA-1 are built on this standard. There are two major components of the MESA standard as shown in Figure 18. One is the MESA-Device that addresses how energy storage components within an ESS communicate with each other and other operational components and is built on the Modbus protocol. The other is the MESA-ESS that addresses ESS configuration management, ESS operational states, and the applicable ESS functions from the Institute of Electrical and Electronics Engineers 1815 Distributed Network Protocol 3 profile for advanced distributed energy resources functions.

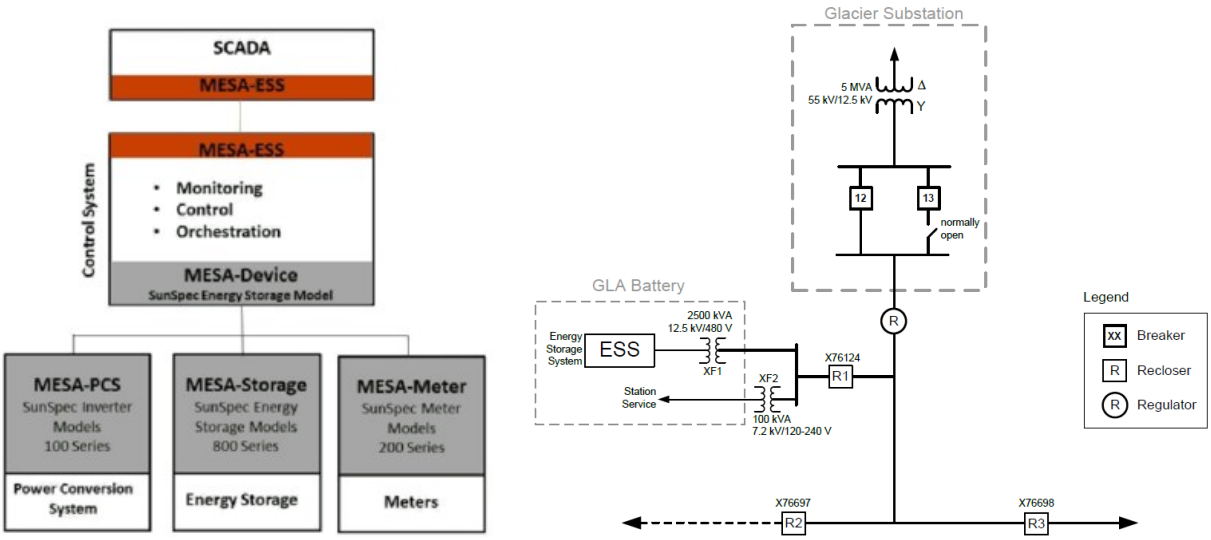

Figure 18. MESA Standard Architecture (left) and Electrical Schematic (Right)

Control is accomplished by the 1Energy-Intelligent Controller (1E-IC). Subsequent to project start, 1Energy was acquired by Doosan GridTech, and this product is now named DG-IC (Doosan 2016a). This control and communication platform for the ESS includes built-in operating modes that can be configured and fine-tuned to reach maximum economic benefits at changing grid and market conditions. Capabilities of DG-IC can also be extended by creating new operating modes through an Application Programming Interface. Built-in operating modes of DG-IC include Market-Based Charge/Discharge, Frequency Correction, Forecast Assurance, Power Following, Peak Power Limiting, Power Factor Correction, Volt/VAR, Volt/Watt, Power Smoothing, Islanding, State-of-Charge (SOC) Maintenance. Supervisory Control. Optimal control for different use-cases for MESA 2 ESS is performed by Doosan's Distributed Energy Resources Optimizer (DG-DERO) (Doosan 2016a), which is a management system for distributed energy resources that optimally aggregates economic values from fleets of ESS and other resources. The suite of bulk power applications that DERO considers in optimizing storage benefits includes energy arbitrage and avoiding certain market situations such as energy congestion, unfavorable purchase, and forecast error penalties (Doosan 2016b). Based on historical load and price data, local resource constraints, maintenance events and expected SOCs at the start of the day, day ahead schedules for optimal charging and discharging operations, typically looking ahead over the next 24 to 48 hours, are provided by DERO. Recommendations for schedule adjustments at different time horizons are made by DERO in response to changed conditions. Data tags for the energy storage were set based on the SunSpec Alliance Interoperability Specification (Miller Undated).

3.0 Battery Performance Test Results

During the first phase of tests, the FBESS was subjected to baseline testing as described in the U.S. Department of Energy Office of Electricity Delivery and Energy Reliability (DOE-OE) Performance Protocol (Viswanathan et al. 2014), with discharge at various C-rates for a constant C rate charge and at various charge rates for a constant rate discharge. Response time and ramp rate were measured at various SOCs, along with charge and discharge resistance. The results of these tests are presented in this chapter. The battery seemingly continued to discharge to provide the auxiliary power while at rest despite the PCS Meter not registering any power flow. Hence, we hypothesized the battery was set up as shown in Figure 19.

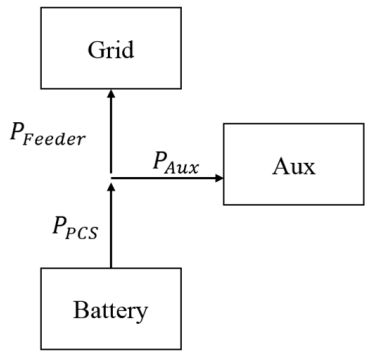

Figure 19. MESA2 Power Flow Schematic

For evaluating battery performance, we used the following definitions:

$$P_{grid} = P_{Feeder}$$

$$P_{batt} = P_{PCS}$$

$$P_{grid} = P_{batt} - P_{aux}$$

$$E_{Chg} = \int \left(P_{grid} < 0\right) P_{grid} dt$$

$$E_{Dis} = \int \left(P_{grid} > 0\right) P_{grid} dt$$

$$E_{Chgnorest} = \int \left(P_{req} < 0\right) P_{grid} dt$$

$$E_{Disnorest} = \int \left(P_{req} > 0\right) P_{grid} dt$$

$$E_{Chgnoaux} = \int \left(P_{req} < 0\right) P_{batt} dt$$

$$E_{Disnoaux} = \int \left(P_{req} > 0\right) P_{batt} dt$$

$$RTE = -\frac{E_{Dis}}{E_{Chg}}$$

$$RTE_{norest} = -\frac{E_{Disnorest}}{E_{Chgnorest}}$$

$$RTE_{noaux} = -\frac{E_{Disnoaux}}{E_{Chgnoaux}}$$

3.1 Baseline Test Results

The RTE ranged from 54 to 63% when rest and auxiliary consumption were included, increased to 55 to 64% when the rest period was excluded, and increased further to 68 to 75% when auxiliary consumption was excluded. Because rest periods varied within each repeating cycle to meet the requirement that each cycle duration needs to be an integer, rest times after each discharge for a repeating cycle varied from 1 to 1.75 hours. The RTE increase without auxiliary consumption ranged from 8 to 18%, with higher increases when charge or discharge power was less. When discharge power was halved from 1,150 kW, the increase in RTE was 18%, while when charge power was halved from 1,200 kW, the increase in RTE was only 13%. This finding is surprising because the results correspond to the charge power being allowed to taper while the discharge power remains constant. Also, the charge duration is set to be ~1 hour greater than predicted by the model to ensure the FBESS reaches the desired SOC at the end of charge. This results in about a 2-hour taper period during which auxiliary power consumption is a higher portion of total charge power input from the grid. Hence, the increase in RTE should be higher when auxiliary consumoption is excluded during charge. One explanation is that during discharge the auxiliary power is supported by the DC battery. Accounting for PCS losses and the losses in the 240-V/480-V AC transformer to support auxiliary consumption, the DC power draw is higher than the requested power. Because the DC power is obtained at a lower operating voltage during discharge, the current draw is high, resulting in greater SOC loss for a given auxiliary consumption. Whereas, during charge, the auxiliary power is directly suplied by the grid, bypassing the DC battery. Hence the gain in RTE is less when auxiliary consumption is excluded for a fixed charge power.

For constant power charge, RTE peaks at 1,100 kW discharge when auxiliary consumption is included. Note that PCS efficiency decreases rapidly at <300 kW, hence at lower power levels, the increasing RTE trend is expected to reverse. Excluding auxiliary consumption, the RTE increased with decreasing discharge power, thus reflecting higher DC efficiency at low power levels. Hence, the RTE at high charge power levels (1,600 kW charge, 1,150 kW discharge) is greater than the RTE at higher discharge power levels (1,800 kW discharge, 1,200 kW charge) both with and without auxiliary consumption. The gap decreases when DC-DC RTE is considered because PCS losses are excluded. At a fixed charge power, as discharge power decreases, the RTE without auxiliary consumption increases and starts to level off at 500 kW, while the DC-DC RTE continues to increase. For a fixed discharge power of 1,150 kW, the AC-AC RTE without auxiliary power consumption peaks at 1,200 kW charge, while the DC-DC RTE increases with decreasing power levels and flattens at 1,000 kW all the way to 500 kW.

For constant discharge power of 1,100 kW, the RTE increased with increasing charge power, whereas the RTE without auxiliary consumption peaked at 1,200 kW charge. This appears to indicate that at low charge power levels, the endothermic nature of charge leads to low temperature levels, which adversely affects charge and discharge efficiency. The lower auxiliary consumption at low charge power is overcome by higher electrochemical losses at low temperature. When auxiliary consumption is excluded, peak efficiency is obtained at 1,200 kW. This charge level appears to be optimal where the electrolyte temperature is maintained in the desired range without the need for cooling. At higher charge levels, electrochemical losses become a factor. Moreover, as seen in Figure 10, PCS losses are lower at high charge powers compared to high discharge power levels. This may be related to the DC operating voltage of the battery being at a more desirable value during charge compared to discharge.

In Appendix A, results for the entire SOC range investigated for all runs are presented. The maximum discharge energy with auxiliary consumption was 5,670 kWh at 1100 kW in the 97 to 18% SOC range, and was 6,300 kWh without auxiliary consumption at 550 kW in the 97 to 5% SOC range. Normalizing these numbers to 100% DOD yields energy levels of 7,180 and 6,845 kWh, respectively. Note that these numbers cannot be attained because the energy delivered by the FBESS per unit change in SOC decreases

sharply at low SOC. Hence, during these tests, the 8,000 kWh rated energy of the FBESS could not be obtained at any of the power levels tested.

As shown in Appendix A, the charge energy is reduced significantly when charge power is not allowed to taper. For example, at 1,200 kW charge, charge energy was limited to 5,350 kWh for one run, compared to 8,082 kWh when allowed to taper. This has two opposing effects on RTE—an increase in RTE due to reduced auxiliary consumption and a decrease in RTE due to lower SOC at the end of charge.

Table 5 and Figure 20 show the baseline reference performance capacity test results and FBESS performance curves from baseline tests.

Figure 21 shows cumulative discharge and charge energy as a function of SOC. The cumulative energy increases linearly with decreasing SOC until ~50% SOC. At lower SOC levels, the slope decreases, as less energy is obtained per unit change in SOC. The DC current increases at constant power with decrease in SOC, with an estimated 9% increase at 50% SOC and 17% increase at 10% SOC over the initial discharge current. The total discharge energy in the range investigated is 5,000 kWh, with highest energy available at 1150 kW discharge. Results are also plotted for energy discharged excluding auxiliary consumption. For this case, the maximum energy of ~5,700 kWh is obtained at a lower power level of 550 kW. The energy obtained during taper also is shown as dotted lines and is marginally higher for each discharge power level.

Charge energy increases linearly in the 40 to 90% range. At lower SOC, due to low operating voltage and associated greater current at fixed power, the charge energy needed for unit change in SOC is lower. As SOC increases, at 50% SOC, charge current decreases to ~93 percent of current at 10% SOC, and further decreases to ~85% at 100% SOC. The maximum charge energy is 7,600 kWh.

As seen in Figure 22, the battery temperature increases during discharge, stabilizes during rest, and decreases during charge. The rate of increase of temperature during discharge increases with discharge power, while rate of decrease of temperature during charge decreases with increasing charge power. Higher ambient temperature increases the rate of increase of temperature during discharge possibly because less heat is lost to ambient. Once the FBESS reaches the upper limit of 35°C for extended operation per UET technical specifications (Schenkman and Borneo 2015) and if it reaches 40°C per a UET engineer at which cooling kicks in, this trend may reverse.

Table 5. Baseline Reference Performance Capacity Test Results

Test	Cycle	Date	Duration (h)	Strings Active	Avg Discharge Power (kW)	Avg Charge Power (kW)	SOC Range	Charge Energy (kWh)	Discharge Energy (kWh)	RTE	Charge Energy No Rest (kWh)	RTE No Rest	Charge Energy No Aux (kWh)	Discharge Energy No Aux (kWh)	RTE No Aux	DC Charge Energy (kWh)	DC Discharge Energy (kWh)	RTE DC	Mean Temp (C)	Mean Amb Temp (C)
1	1	2017-12-22	21.0	2	1150	1200	43-97	8082	4776	59.1	7519	63.5	6956	5066	72.8	3394	2630	77.5	20.6	1.8
1	2	2017-12-22	17.0	2	1150	1200	40-98	7889	4955	62.8	7755	63.9	7185	5258	73.2	3497	2719	77.8	20.9	-0.4
1	3	2017-12-23	17.0	2	1150	1200	37-98	8357	5214	62.4	8218	63.4	7601	5545	73.0	3698	2862	77.4	20.0	-1.4
1	4	2017-12-24	17.0	2	1150	1200	36-97	8372	5251	62.7	8237	63.7	7614	5584	73.3	3705	2879	77.7	19.7	0.0
1	5	2017-12-25	15.0	2	1150	1200	36-97	8233	5211	63.3	8146	64.0	7531	5544	73.6	3665	2863	78.1	20.6	-0.3
1	Cumulative	NA	87.0	2	NA	NA	NA	40933	25407	62.1	39875	63.7	36887	26997	73.2	17959	13953	77.7	NA	NA
1	Mean	NA	17.4	2	1150	1200	38-97	8187	5081	62.1	7975	63.7	7377	5399	73.2	3592	2791	77.7	20.4	-0.1
2	1	2017-12-25	13.0	2	1650	1200	48-97	7043	4139	58.8	6866	60.3	6351	4332	68.2	3091	2233	72.2	20.8	0.2
2	2	2017-12-26	12.0	2	1650	1200	48-97	7101	4214	59.3	7012	60.1	6475	4417	68.2	3150	2276	72.3	20.8	1.6
2	Cumulative	NA	25.0	2	NA	NA	NA	14144	8353	59.1	13878	60.2	12826	8749	68.2	6241	4509	72.2	NA	NA
2	Mean	NA	12.5	2	1650	1200	48-97	7072	4176	59.0	6939	60.2	6413	4374	68.2	3120	2254	72.2	20.8	0.9
3	1	2018-01-11	27.0	2	550	1200	28-98	9359	5276	56.4	9277	56.9	8277	6102	73.7	4032	3264	81.0	29.2	6.5
3	2	2018-01-12	27.0	2	550	1200	28-97	9085	5244	57.7	8896	58.9	8084	6078	75.2	3966	3255	82.1	29.1	8.1
3	3	2018-01-13	24.0	2	550	1200	30-97	8829	5154	58.4	8829	58.4	7991	5974	74.8	3916	3200	81.7	29.3	6.9
3	Cumulative	NA	78.0	2	NA	NA	NA	27273	15674	57.5	27002	58.0	24352	18154	74.5	11914	9719	81.6	NA	NA
3	Mean	NA	26.0	2	550	1200	29-97	9091	5225	57.5	9001	58.1	8117	6051	74.6	3971	3240	81.6	29.2	7.2
4	1	2018-01-17	16.0	4	1150	1200	44-95	7206	4396	61.0	7061	62.3	6552	4607	70.3	6422	4817	75.0	32.9	10.1
4	2	2018-01-17	14.0	4	1150	1200	40-95	7564	4713	62.3	7490	62.9	6923	4951	71.5	6779	5185	76.5	35.9	7.5
4	Cumulative	NA	30.0	4	NA	NA	NA	14770	9109	61.7	14551	62.6	13475	9558	70.9	13201	10002	75.8	NA	NA
4	Mean	NA	15.0	4	1150	1200	42-95	7385	4554	61.6	7276	62.6	6738	4779	70.9	6600	5001	75.8	34.4	8.8
5	1	2018-01-19	16.0	3	1150	1200	37-94	7700	4699	61.0	7533	62.4	6932	4951	71.4	5097	3885	76.2	34.2	7.5
5	2	2018-01-19	13.0	3	1150	1200	40-93	7285	4481	61.5	7202	62.2	6618	4726	71.4	4866	3712	76.3	35.0	6.9
5	Cumulative	NA	29.0	3	NA	NA	NA	14985	9180	61.3	14735	62.3	13550	9677	71.4	9963	7597	76.3	NA	NA
5	Mean	NA	14.5	3	1150	1200	38-93	7492	4590	61.2	7368	62.3	6775	4838	71.4	4982	3798	76.2	34.6	7.2
6	1	2018-01-20	23.0	3	1150	800	45-93	7544	4068	53.9	7384	55.1	6275	4286	68.3	4493	3368	75.0	33.5	6.2
6	2	2018-01-21	23.0	3	1150	800	49-92	7028	3762	53.5	6869	54.8	5787	3961	68.4	4130	3114	75.4	32.8	5.7
6	3	2018-01-22	17.0	3	1150	800	51-91	5910	3435	58.1	5835	58.9	5116	3617	70.7	3711	2844	76.6	32.8	5.8
6	Cumulative	NA	63.0	3	NA	NA	NA	20482	11265	55.0	20088	56.1	17178	11864	69.1	12334	9326	75.6	NA	NA
6	Mean	NA	21.0	3	1150	800	48-92	6827	3755	55.2	6696	56.3	5726	3955	69.1	4111	3109	75.7	33.0	5.9
7	1	2018-01-27	22.0	4	1150	600	43-98	8178	4759	58.2	8022	59.3	7054	4987	70.7	6799	5214	76.7	33.6	6.9
7	2	2018-01-28	22.0	4	1150	600	41-97	8135	4832	59.4	8043	60.1	7049	5067	71.9	6790	5299	78.0	35.2	10.2
7	3	2018-01-29	22.0	4	1150	600	38-95	8225	4826	58.7	8061	59.9	7054	5066	71.8	6793	5302	78.1	36.7	7.6
7	4	2018-01-30	19.0	4	1150	600	37-94	7866	4682	59.5	7790	60.1	6873	4912	71.5	6643	5139	77.4	37.1	7.2
7	Cumulative	NA	85.0	4	NA	NA	NA	32404	19099	58.9	31916	59.8	28030	20032	71.5	27025	20954	77.5	NA	NA
7	Mean	NA	21.2	4	1150	600	40-96	8101	4775	59.0	7979	59.9	7008	5008	71.5	6756	5238	77.5	35.7	8.0
8	1	2018-02-03	15.0	4	1150	1600	36-95	8000	4894	61.2	7842	62.4	7328	5155	70.3	7188	5394	75.0	38.5	9.3
8	2	2018-02-03	15.0	4	1150	1600	35-94	8167	4830	59.1	8015	60.3	7390	5103	69.1	7217	5339	74.0	38.7	9.2
8	3	2018-02-04	12.0	4	1150	1600	36-93	7606	4676	61.5	7606	61.5	7080	4934	69.7	6944	5163	74.4	39.0	9.7
8	Cumulative	NA	42.0	4	NA	NA	NA	23773	14400	60.6	23463	61.4	21798	15192	69.7	21349	15896	74.5	NA	NA
8	Mean	NA	14.0	4	1150	1600	36-94	7924	4800	60.6	7821	61.4	7266	5064	69.7	7116	5299	74.5	38.7	9.4

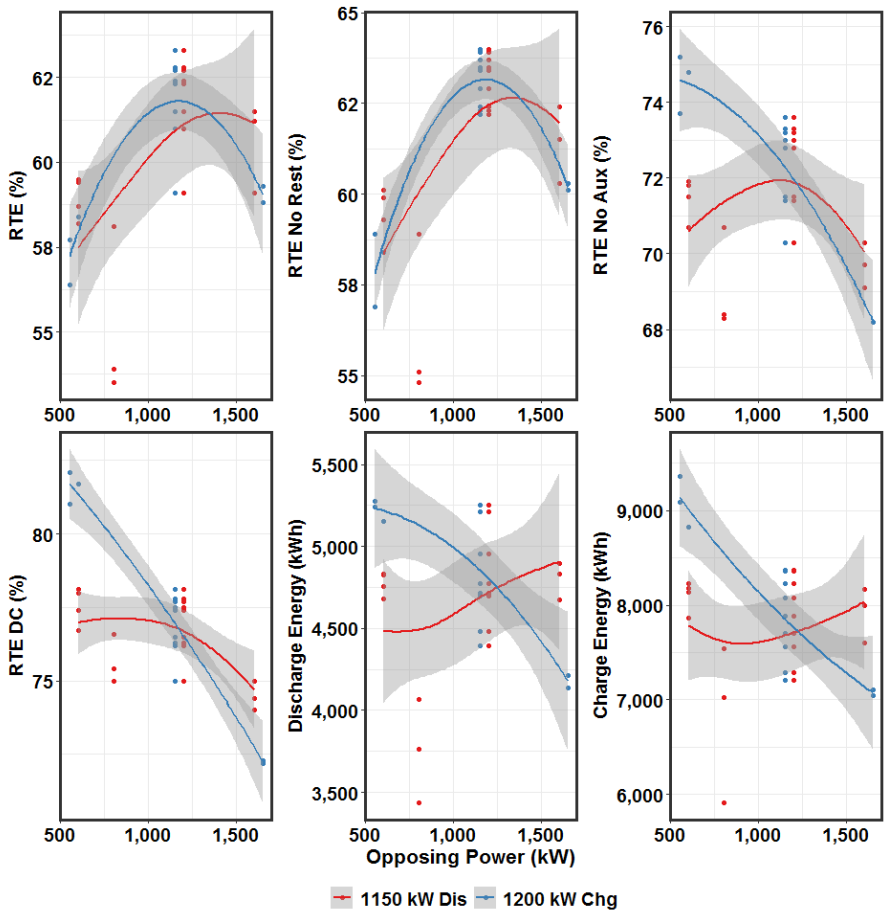

Figure 20. FBESS Performance Curves from Baseline Tests

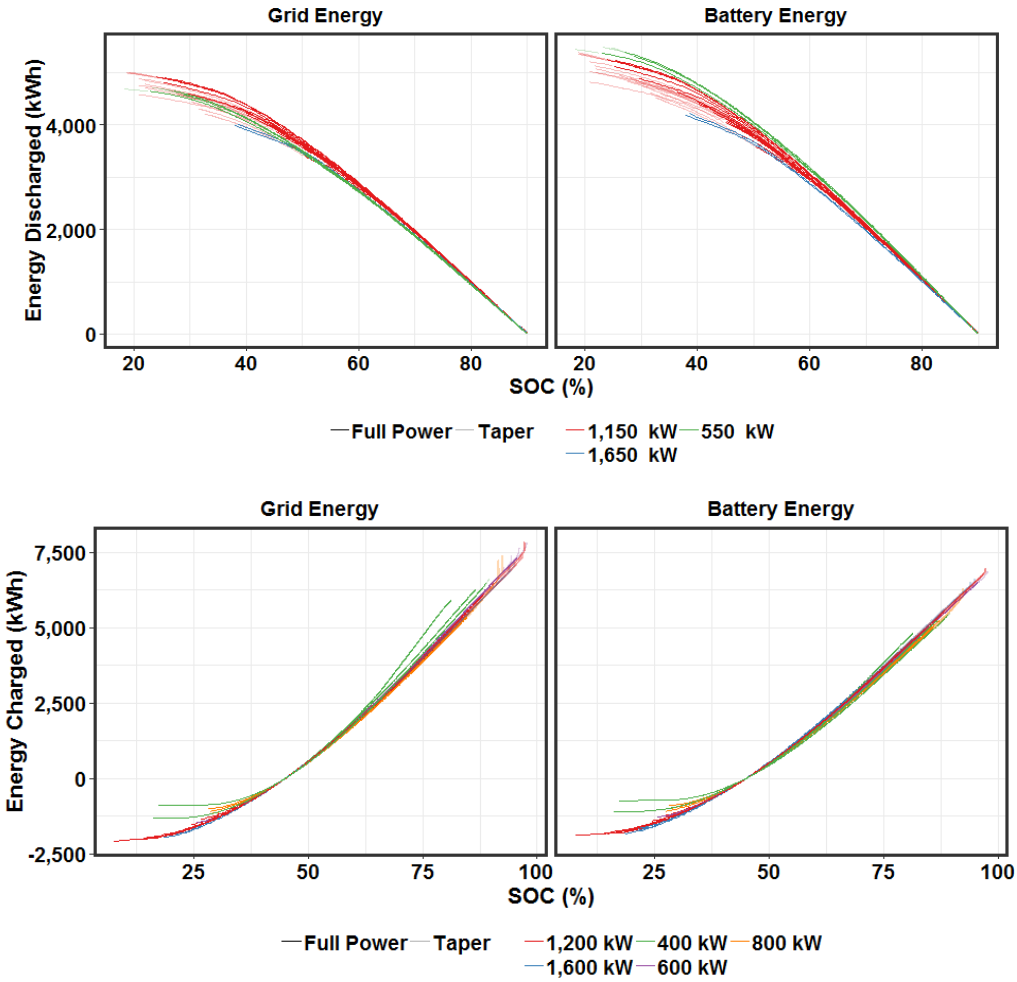

Figure 21. Energy Charged or Discharged at the Grid and PCS Level as a Function of FBESS SOC

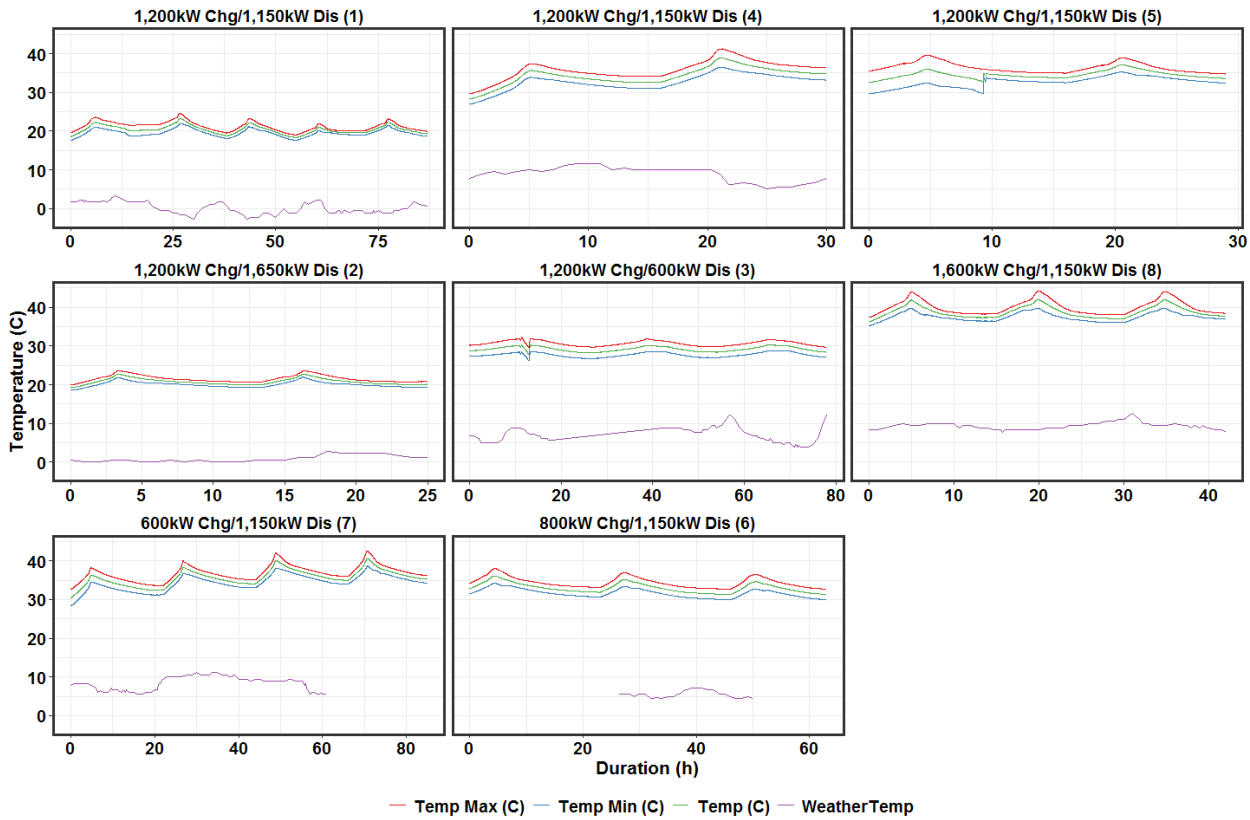

Figure 22. Battery Temperature Profile during Reference Performance Capacity Tests

3.2 Response Time/Ramp Rate Test

The test was done starting with discharge at 95% SOC, followed by discharge pulses at ~10% decrements to 40% SOC. This was followed by discharging to 12% SOC, and charge pulse at every ~10% SOC increment. The power levels were chosen to ensure the power stayed constant for the entire 15-minute duration of the pulse. Note that 15 minutes is the smallest time step for which signals can be sent. For charge, a 1,600 kW signal was sent in the 0 to 63% SOC range, followed by 1,400 kW and 1,200 kW at 70 and 75% SOC, respectively. The discharge requested power varied from 800 to 2,200 kW in the 40 to 95% SOC range.

The FBESS response to the signal is shown in Figure 23. At t = 0, the command was sent to the FBESS. The communication lag, or the time for the requested power to reach the FBESS, is <2 seconds, while the hardware responds within 1 second once the command reaches the FBESS. For nine runs, the sum of communication and hardware lag was less than 2 seconds, while for two runs, it was less than 3 seconds.

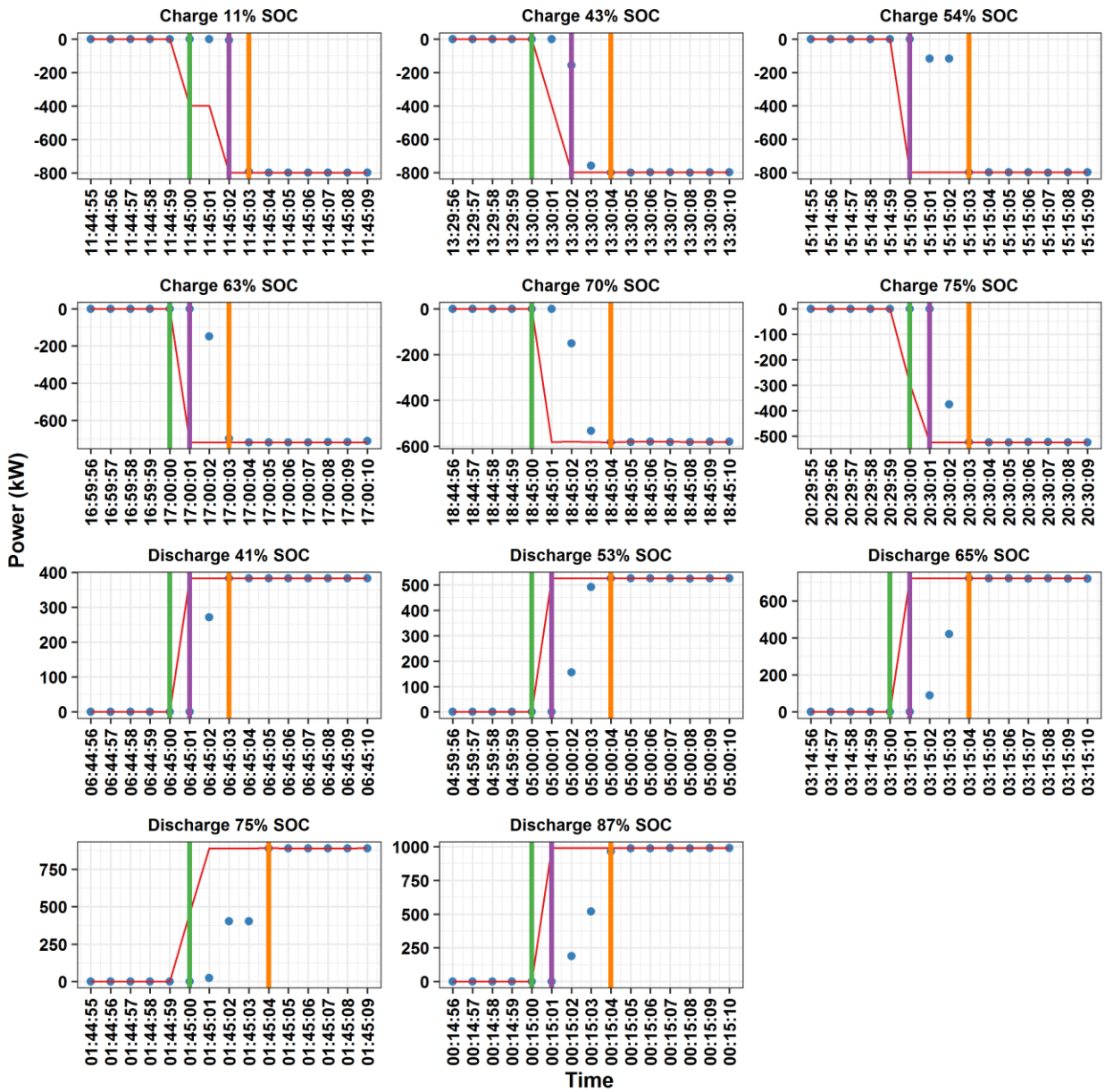

Figure 23. FBESS Response Along with Signal Request – Reference Performance Test

The response of the FBESS at the PCS is shown in Figure 24. The maximum charge power is reached in 2 to 3 seconds, corresponding to a ramp rate of 33 to 50% of the requested power per second. During discharge, the FBESS responded in the 2 to 4 second range, corresponding to a ramp rate of 425 to 660 kW/s or 25 to 50% of requested power per second.

The internal resistance was measured by dividing the 5-second change in DC voltage by the change in current. For this test, Strings 2 and 3 were active. The resistance was calculated by dividing the average voltage of the strings by the total current. To estimate the four-string equivalent resistance for FBESS, with the four strings connected in parallel at the 280 VAC level, this value was divided by 2. The calculated four-string charge resistance was 0.04 to 0.05 ohms for both charge and discharge across the SOC range investigated, with a slight increase at SOC <60%. The only exception was the high charge

internal resistance of 0.094 ohms at 12% SOC, possibly due to the fact that at low SOC, the coupled mass transfer-charge transfer resistance is large (Crawford et al. 2015). This was not confirmed for discharge pulses at low SOC because the lowest SOC for discharge was ~40%.

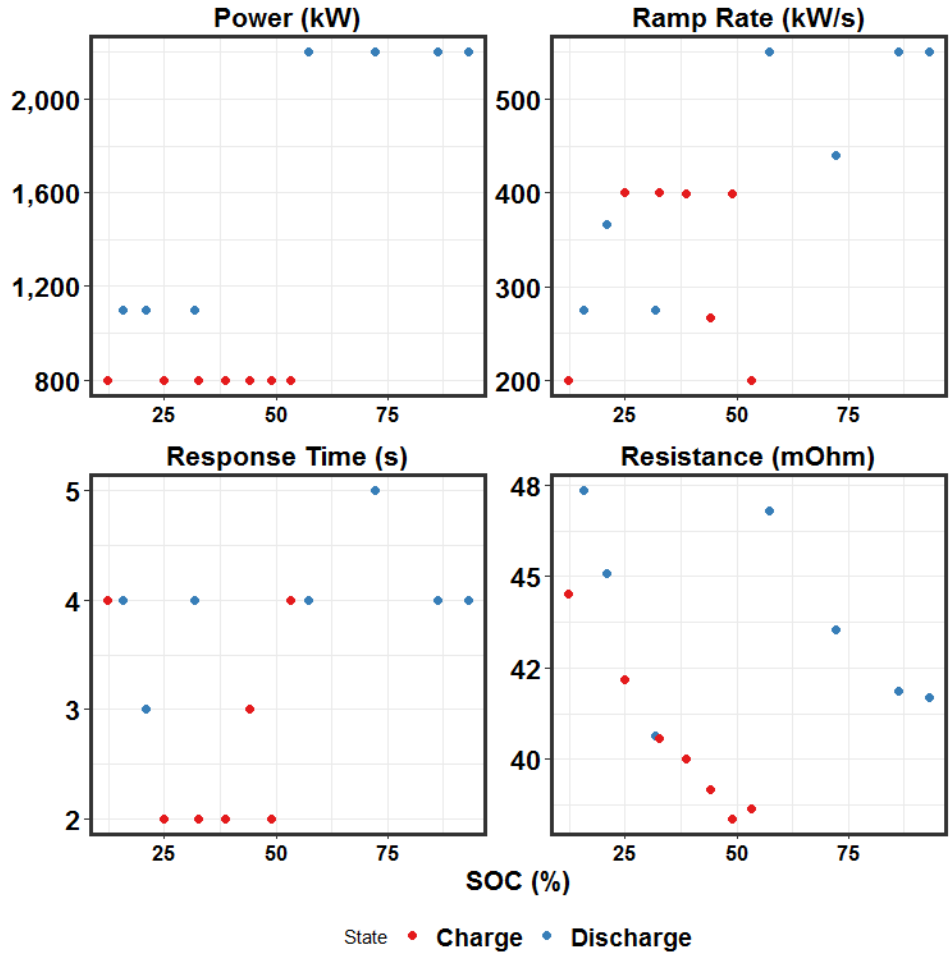

Figure 24. Response Time and Ramp Rate Reference Performance Test Results.

The in situ resistance for all strings (normalized to the four-string value) is shown in Figure 25. In general, the charge and discharge resistance increase slightly at SOC <40%. Overall, there is no trend with increasing test duration.

3.3 Frequency Regulation Test

The FBESS was subjected to the DOE-OE frequency regulation signal as part of the RPT. The starting SOC was set at 93% to ensure the FBESS can provide the necessary power throughout the test. Because signals could be changed only every 15 minutes, one power unit was set at -600 kW for charge and 1600 kW for discharge to ensure power levels could be maintained for the 15-minute duration. As expected, the SOC decreased with test duration. The results from this test is shown in Figure 26 and Table 6.

The duty cycle for Run 1 lasted 12 hours, while for Run 2 it was 24 hours.

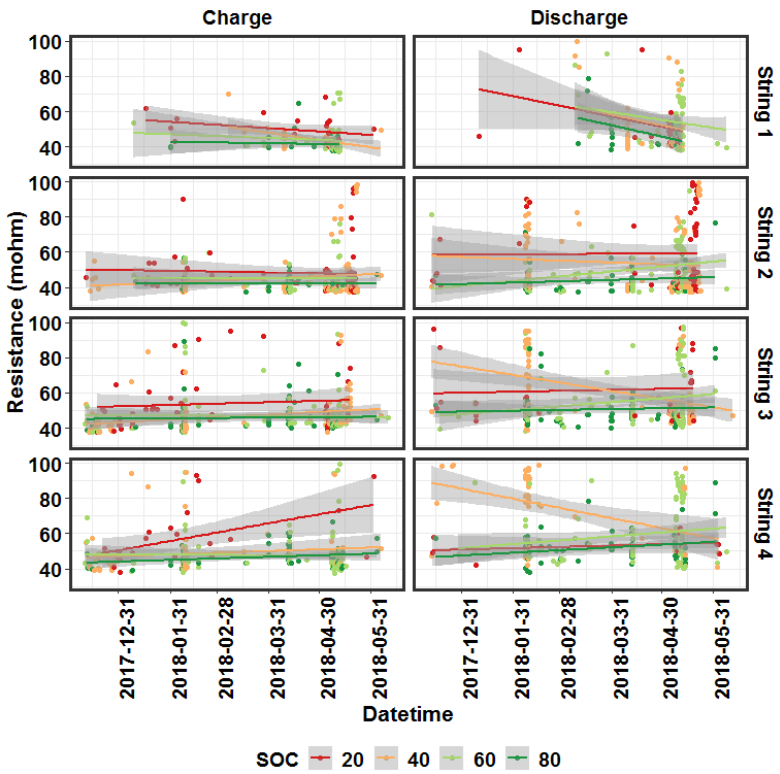

Figure 25. In Situ Charge and Discharge Resistance for Each String- Resistance Normalized to Four-String Basis

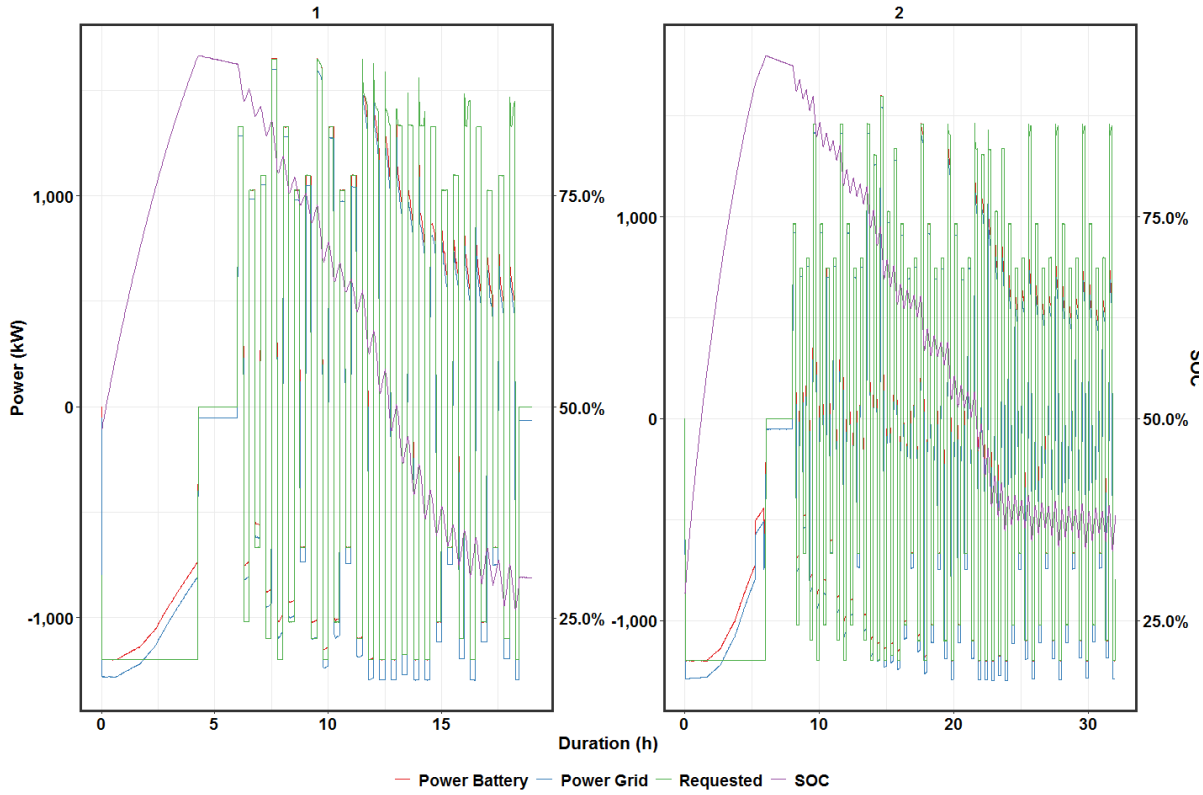

Figure 26. Results from Frequency Regulation DOE Protocol Tests

Table 6. Frequency Regulation Test Results

Date	2018-02-07	2018-02-08
Duration (h)	19	32
Strings Active	3	3
Avg Charge Power (kW)	-1430	-1393
Avg Discharge Power (kW)	1,290	1,079
SOC Range	26-92	28-95
Charge Energy (kWh)	16,969	25,619
Discharge Energy (kWh)	8,208	13,384
RTE	48.4	52.2
Charge Energy No Rest (kWh)	16,534	25,055
Discharge Energy No Rest (kWh)	8,208	13,384
RTE No Rest	48.5	52.2
Charge Energy No Auxiliary (kWh)	15,292	23,080
Discharge Energy No Auxiliary (kWh)	8,461	13,919
RTE No Auxiliary	55.3	60.3
Mean Charge Temperature (ºC)	35	35
Mean Discharge Temperature (ºC)	36	35
Mean Temperature (ºC)	36	35
Mean Ambient Temp (ºC)	NA	NA

The RTE ranged from 48 to 52%, with the RTE increasing to 55 to 60% when auxiliary consumption was excluded. Signal tracking was not evaluated because the reference signal changes only once every 15 minutes. Note that towards the second half of the duty cycle, the FBESS was not able to provide the requested discharge power, as the SOC decreased to the 50 to 55% range. The performance of all strings declined, but as shown in Figure 27, Strings 3 and 4 were weaker than String 2.

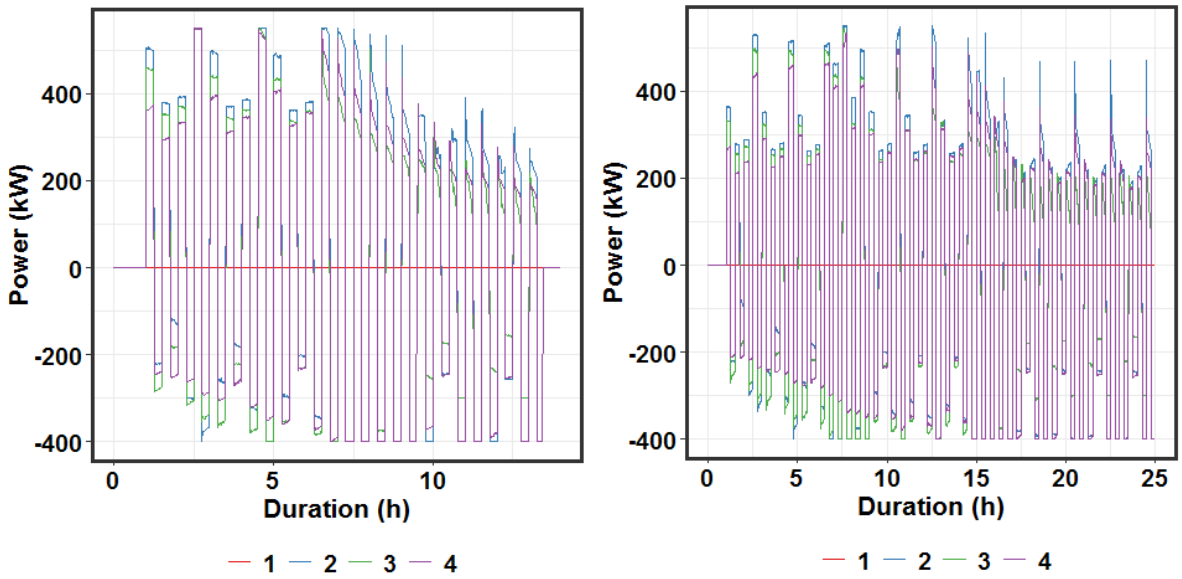

Figure 27. Results Showing Strings 3 and 4 are Weaker than String 4 during Frequency Regulation Test Run 1 (left) and Run 2 (right)

3.4 Use-Case 1: Energy Arbitrage

3.4.1 Duty Cycle Summary

The energy arbitrage duty cycle was modeled using PNNL's Battery Storage Evaluation Tool (BSET) by maximizing ESS revenue for a 1-week period using historic Mid-Columbia wholesale energy price data.

3.4.2 Test Results

All four strings were active for this test. The test was intended for a duration of 1 week or 168 hours. However, after 132 hours (5.5 days), String 1 dropped out because of a PCS fault. String 3 showed initial signs of weakness on 2018-05-08 19:10:00 when its discharge power was ~50% of the power through the other strings while its SOC remained higher during discharge. This was an indication that one of the battery modules was out of balance with the rest of the modules in String 3. Note that at the start of rest after discharge on 2018-05-10 11:20:00, String 3 was subjected to pulse charge power to keep its SOC in the 4 to 15% range. String 4 also appeared to weaken as evidenced by its typical SOC behavior before failure towards the end of discharge at 2018-05-09 21:00:00. The rate of SOC change decreased at this stage, accompanied by a decrease in discharge power, as one of the battery modules in this string approached the lower SOC limit (see Chapter 1). With each subsequent discharge, this effect was more pronounced. Hence in spite of the reasonably high charge and discharge power levels, the RTE was low at 48%. Due to rest duration being quite low at less than 1% of test duration, the RTE without rest was only marginally higher at 48.4%. Excluding auxiliary consumption, the RTE was 56.3%. These are very low RTE numbers, possibly related to weak stacks present in battery modules within Strings 3 and 4. The discharge power flow along with SOC profile from 2018-05-10 10:00:00 to 2018-05-10 12:45:00 is shown in Figure 28. String 1 and 2 are the strongest and pick up a greater share of the discharge power. String 3 is the weakest string, while String 4 appears stronger than String 3. During rest, String 3 is subject to charge pulses, while String 4 SOC decreases in the typical fashion that is a precursor to String 4 failure.

Results are shown in Figure 28 for the entire duty cycle and in Figure 29 and Table 7 for each day.

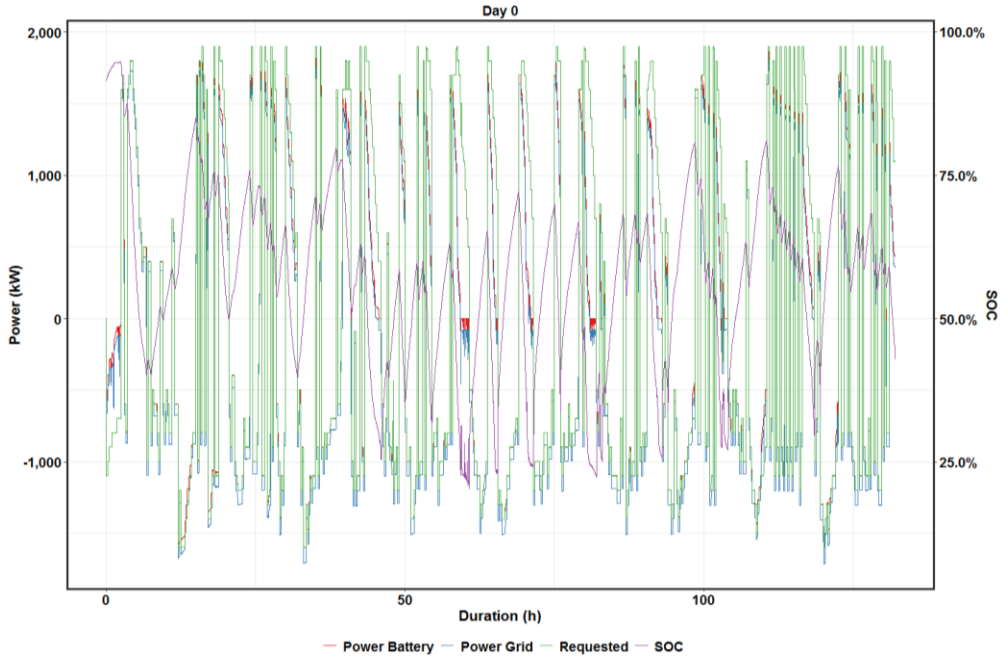

Figure 28. Energy Arbitrage Results

Table 7. Energy Arbitrage Test Results

Date	2018-05-08	2018-05-08	2018-05-09	2018-05-10	2018-05-11	2018-05-12
Duration (h)	132	24	24	24	24	24
Rest Fraction	0.00	0.00	0.01	0.00	0.00	0.00
Strings Active	4	4	4	4	4	4
Average Charge Power (kW)	-1026	-903	-1052	-1110	-1025	-993
Average Discharge Power (kW)	879	1,062	964	689	673	895
SOC Range	20-95	40-95	25-80	20-72	22-70	27-81
Charge Energy (kWh)	92,338	16,474	18,649	16,596	16,088	17,027
Discharge Energy (kWh)	44,280	9,082	9,484	7,010	7,225	8,025
RTE	48.0	55.1	50.9	42.2	44.9	47.1
Charge Energy No Rest (kWh)	91,351	16,403	18,531	16,317	15,856	16,833
Discharge Energy No Rest (kWh)	44,280	9,082	9,484	7,010	7,225	8,025
RTE No Rest	47.4	54.9	50.7	41.3	44.1	46.5
Charge Energy No Auxiliary (kWh)	83,263	14,906	16,980	14,935	14,402	15,316
Discharge Energy No Auxiliary (kWh)	46,906	9,594	10,111	7,450	7,705	8,475
RTE No Auxiliary	56.3	64.4	59.5	49.9	53.5	55.3
Mean Charge Temperature (ºC)	41	38	41	41	41	41
Mean Discharge Temperature (ºC)	42	39	41	43	42	42
Mean Temperature (ºC)	41	39	41	42	42	41
Mean Ambient Temperature (ºC)	NA	NA	NA	NA	NA	NA

The RTE at 55% is highest for day 1, and decreases from to 42% in day 3. Subsequent to that, because of an increasing average SOC of operation, the RTE increased to 45% in day 4 and 47% in day 5. As seen in Figure 30, the String 3 SOC drops to ~3% during rest on day 3 (May 10), which led to in high power consumption. String 4 also shows the onset of failure as its SOC decreased at a faster rate compared to the String 1 and 2 SOCs during rest. This is the reason the RTE with auxiliary power excluded remains low in the 50 to 55% range for days 3 to 5, in spite of average charge and discharge levels being at optimum levels of 1000 kW and 700 kW, respectively.

3.5 Use-Case 2: System Capacity

3.5.1 Duty Cycle Summary

System capacity or resource adequacy results from peak shaving services tied to system-wide peak load conditions. To determine the hours when energy storage would be needed to provide capacity services, hourly system-wide load data was obtained for 2015. Capacity triggers are defined differently for each utility. For SnoPUD, the capacity duty cycle assumed a 4-hour peak shaving requirement, which is a standard industry requirement and was confirmed as reasonable by SnoPUD staff. The capacity duty cycle is developed as a 7-day schedule of charging/discharging cycles with discharge periods from 1 to 4 hours. System capacity test results are shown in Figure 31 and Table 8.

The RTE ranged from 43 to 54% for all four runs. For the last run, the RTE was highest at 54%, corresponding to ~1,000 kW charge and discharge and rest fraction of 0.13. The third run had low charge power, high discharge power and a rest fraction of 0.36. These counteracting forces led to a moderately high RTE of 49%. The lowest RTE of 43% was obtained for the lowest discharge power of 915 kW, with rest fraction of 0.27. Removing the rest period increased RTE by about 2%, with the smallest increase corresponding to lowest rest fraction. Removing auxiliary consumption increased RTE by ~10% for all

runs. The highest RTE corresponded to average power of 1000 kW, with a slight dip at higher power levels. The lowest RTE was obtained at average power levels of 800 kW, where the temperature was lowest at 29°C.

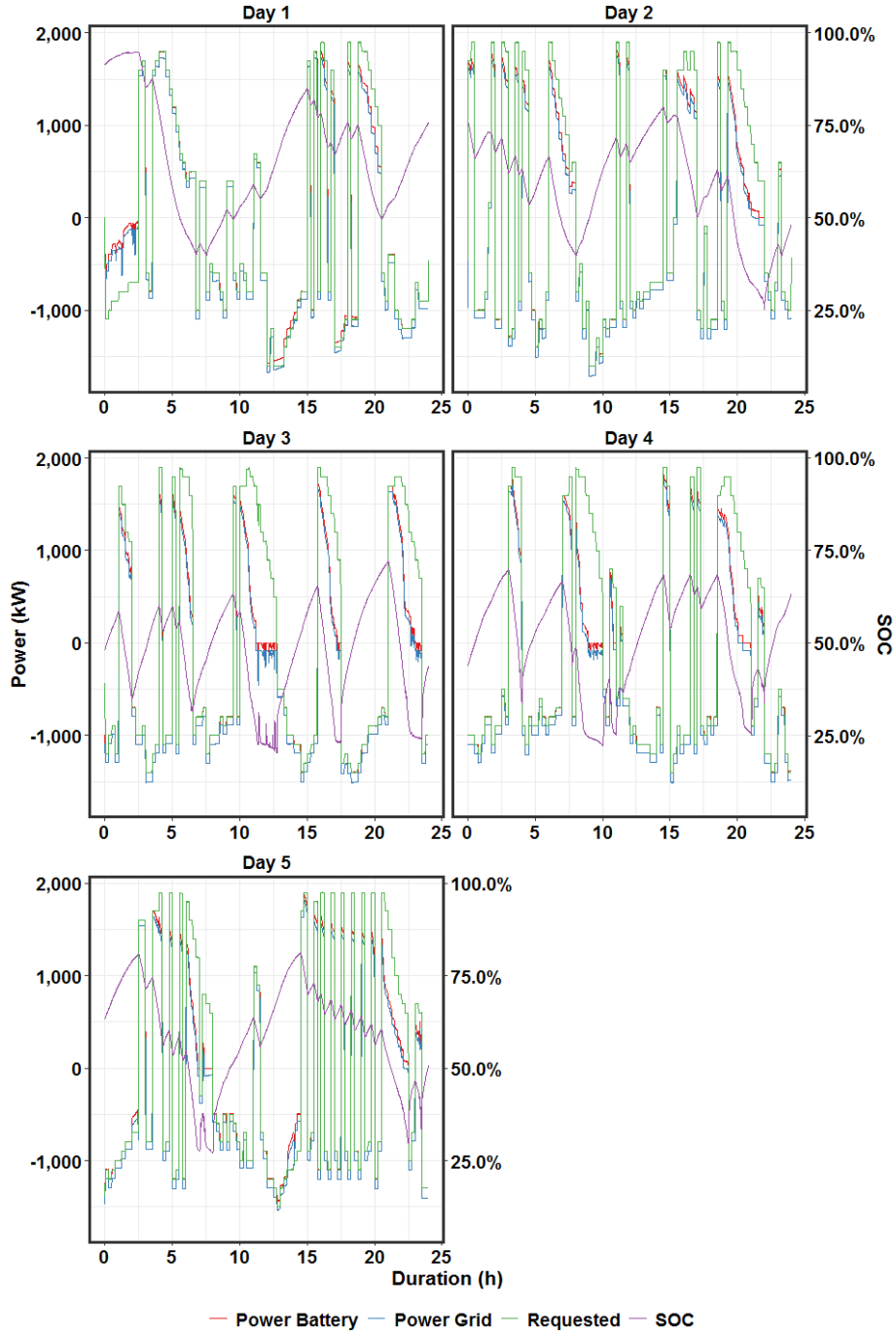

Figure 29. Energy Arbitrage Results for Each Day

For all runs, the FBESS provided the requested discharge power, while charge tapered towards the end of the runs to ensure the FBESS reached its upper SOC limit.

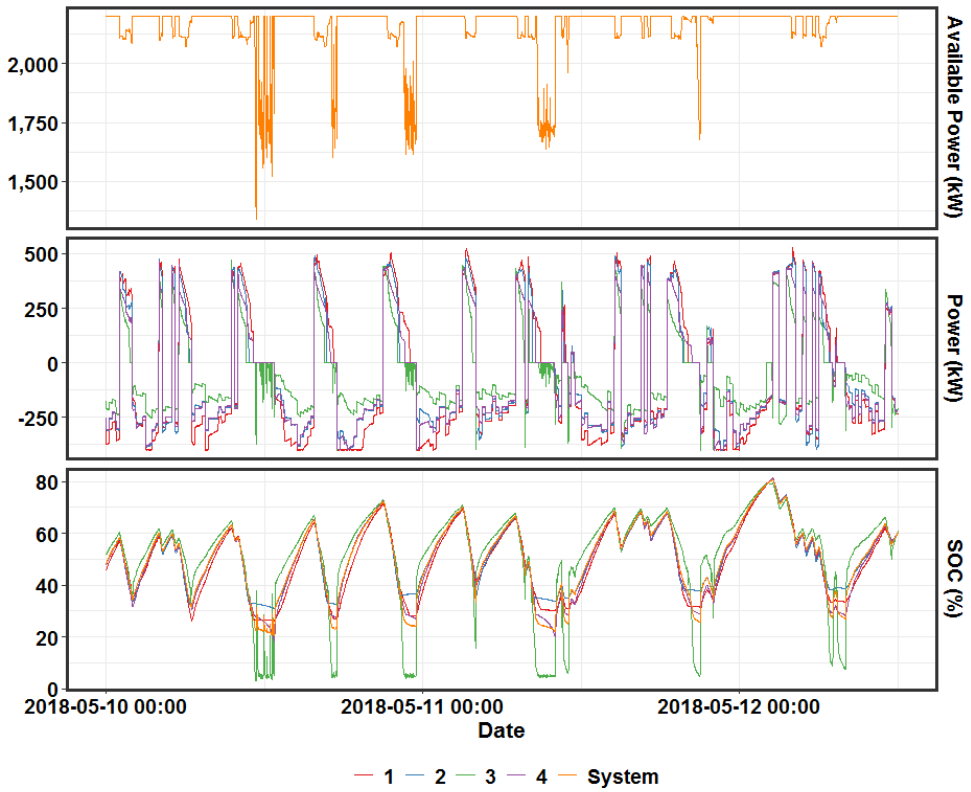

Figure 30. Weak Strings 3 and 4 during Arbitrage Test

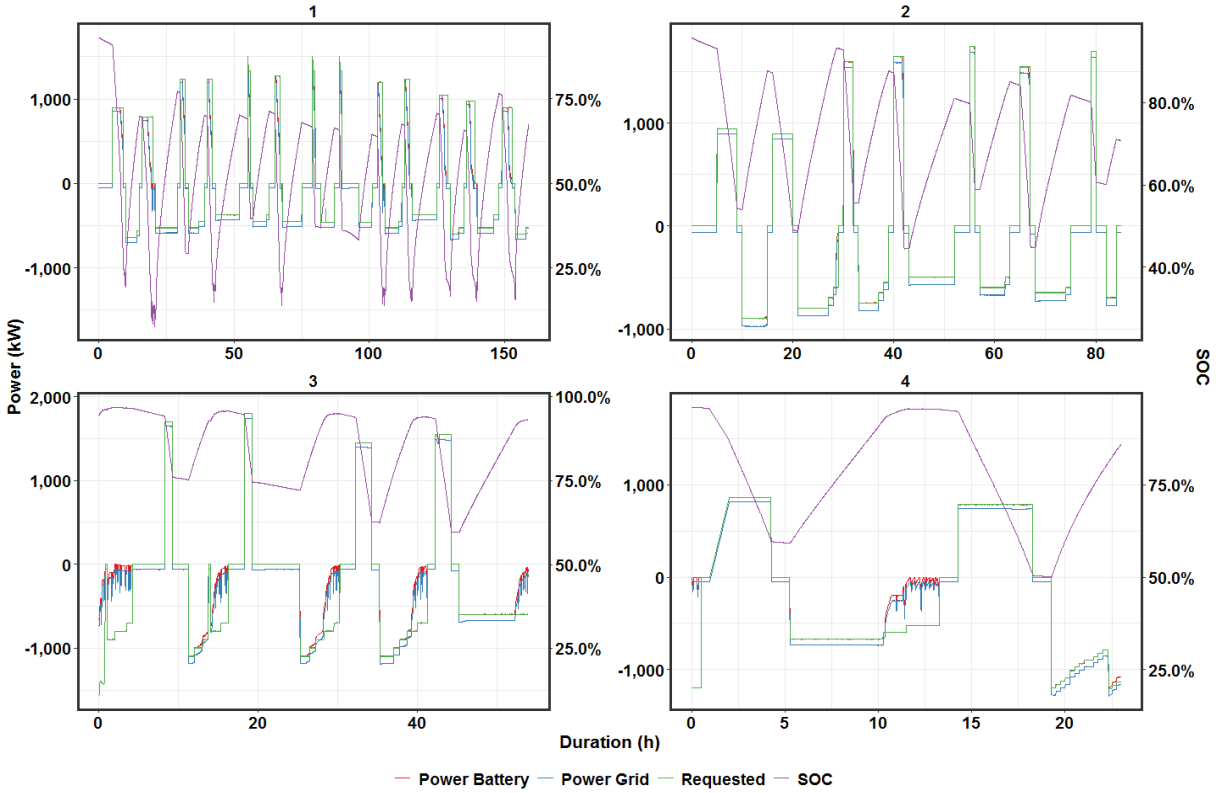

Figure 31. System Capacity Test Results

Table 8. System Capacity Test Results

Date	2018-02-24	2018-03-09	2018-03-17	2018-03-28
Duration (h)	159	86	54	22
Rest Fraction	0.27	0.31	0.36	0.13
Strings Active	3	4	4	3
Average Charge Power (kW)	-715	-734	-617	-973
Average Discharge Power (kW)	917	1207	1516	1024
SOC Range	8-93	44-96	60-97	50-96
Charge Energy (kWh)	67,332	37,181	18,672	12,644
Discharge Energy (kWh)	28,770	19,392	9,124	6,882
RTE	42.7	52.2	48.9	54.4
Charge Energy No Rest (kWh)	64,168	35,521	17,450	12,441
Discharge Energy No Rest (kWh)	28,770	19,392	9,124	6,882
RTE No Rest	44.6	54.4	52.3	55.3
Charge Energy No Auxiliary (kWh)	57,027	31,958	15,285	11,313
Discharge Energy No Auxiliary (kWh)	30,454	20,210	9,473	7,281
RTE No Auxiliary	53.4	63.2	62.0	64.4
Mean Charge Temperature (ºC)	29	34	37	32
Mean Discharge Temperature (ºC)	29	32	38	32
Mean Temperature (ºC)	29	34	37	32

3.6 Use-Case 3: Regulation

3.6.1 Duty Cycle Summary

The duty cycle for this test was developed by scaling the DOE-OE frequency regulation signal such that 1 power unit corresponded to 1600 kW, the maximum continuous charge rate. The starting SOC was set at 95% to ensure the FBESS can provide the necessary power throughout the test. Because signals could be changed only every 15 minutes, the 4-second resolution signal had to be transformed. The discharge and charge energy were integrated every 30 minutes. To calculate the power signals, the discharge and charge energy were divided by 15 minutes so that every 30 minutes we had a 15-minute discharge followed by a 15-minute charge, with the same energy throughput as the original signal. As expected, the SOC decreased with test duration.

3.6.2 Test Results

The average charge and discharge power levels were low at 550 and 380 kW, respectively. Since there was no rest period during testing, the RTE was 50% in spite of the low power levels. As expected, RTE rose by 18% when auxiliary consumption was excluded. In spite of the average power levels being low, the mean temperature during testing was 35°C, probably contributing to the higher than expected RTE. Since signals could be sent only every 15 minutes, the FBESS signal tracking is deceptively high.

Regulation test results are shown in Figure 32 and Table 9.

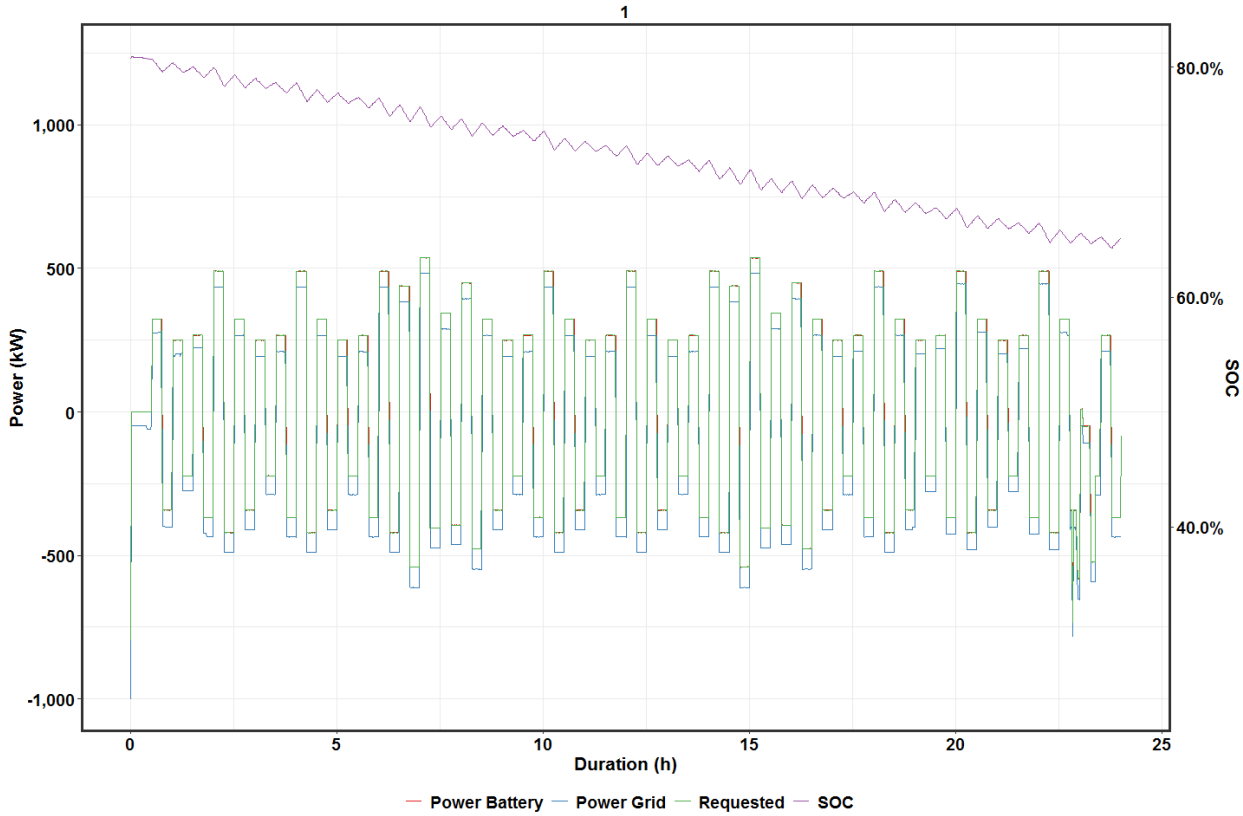

Figure 32. Regulation Test Results

Table 9. Regulation Results

Date	2018-04-12
Duration (h)	24
Strings Active	3
Average Charge Power (kW)	-552
Average Discharge Power (kW)	381
SOC Range	64-81
Charge Energy (kWh)	9,108
Discharge Energy (kWh)	4,549
RTE	49.9
Charge Energy No Rest (kWh)	8,910
Discharge Energy No Rest (kWh)	4,549
RTE No Rest	49.5
Charge Energy No Auxiliary (kWh)	7,714
Discharge Energy No Auxiliary (kWh)	5,228
RTE No Auxiliary	67.8
Mean Charge Temperature (ºC)	35
Mean Discharge Temperature (ºC)	35
Mean Temperature (ºC)	35
Mean Ambient Temperature (ºC)	NA

3.7 Use-Case 4: Real-World Flexibility

3.7.1 Duty Cycle Summary

This service is related to capacity firming of variable generation resources, such as wind or solar farms. The idea is to control ESS power such that the wind or solar farm output could be used as a "firm" generation capacity for a given period of time. The level at which the output will be firmed up and for how long would depend on many aspects, including system conditions and market or the hosting utility's requirements. ESS will import power (charge) from the wind/solar farm if there is over-generation with respect to a given firm level and will export power (discharge) if there is under-generation with the same reference firm level.

3.7.2 Test Results

Two runs of 48 hours each were performed. The average charge power for both runs were nearly the same at ~340 kW, while the average discharge power for Run 2, at 306 kW, was twice that for Run 1. This resulted in a lower minimum SOC for Run 2 at 40%, compared to 78% for Run 1. The Run 1 duty cycle was more volatile, with higher peak power levels for charge and discharge, and extended periods of low power levels. Run 2 power levels were less volatile, with peak discharge levels 50% of Run 1. As seen earlier, PCS one-way efficiency decreased with decreasing power levels, especially during discharge. At the average power level of 153 kW, the one-way PCS efficiency is 82%, while at the average power level of 306 kW, the one-way PCS efficiency is 90%. Also, the absolute value requested power for Run 1 is between 0 and 50 kW for several hours. As seen earlier the PCS one-way efficiency 30% at 50 kW, and rapidly approaches zero as power decreases. The RTE for Run 1 is lower, probably due to PCS efficiency being lower at low power levels. Note that the DC-DC RTE for Run 1 was actually greater than Run 2, in line with our findings that DC RTE increases as power levels decrease.

Real-world flexibility test results are shown in Figure 33 and Table 10.

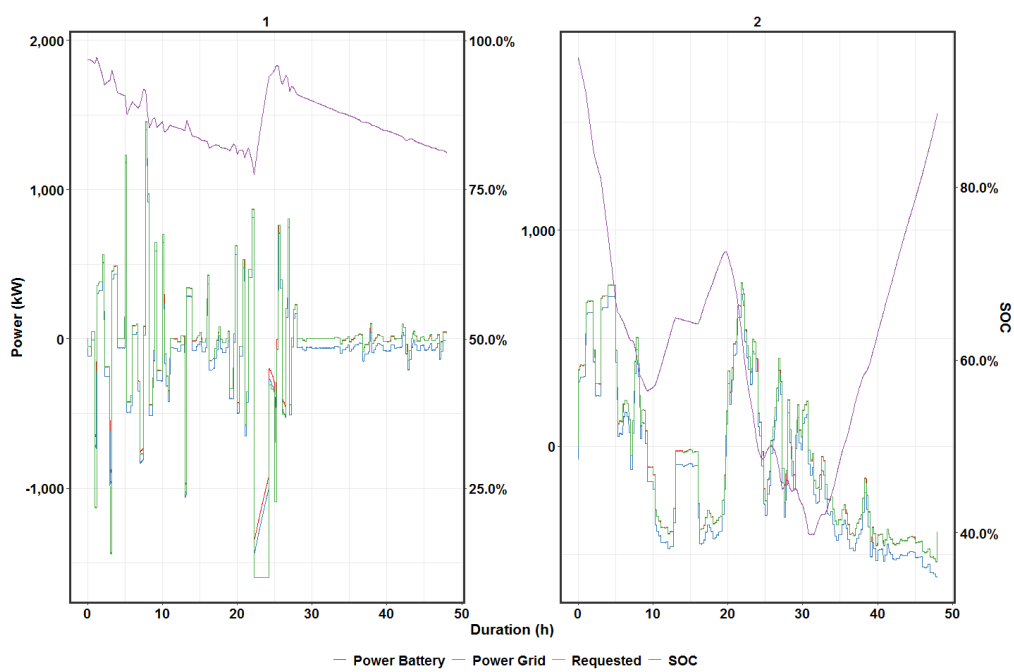

Figure 33. Real-World Flexibility Test Results

Table 10. Real-World Flexibility Test Results

Date	2018-03-31	2018-04-05
Duration (h)	48	48
Rest Fraction	0.12	0.00
Strings Active	4	4
Average Charge Power (kW)	325	356
Average Discharge Power (kW)	153	306
SOC Range	78-97	40-95
Charge Energy (kWh)	10,461	11,890
Discharge Energy (kWh)	3,468	5,371
RTE	33.1	45.2
Charge Energy No Rest (kWh)	9,359	11,869
Discharge Energy No Rest (kWh)	3,468	5,371
RTE No Rest	32.2	45.1
Charge Energy No Auxiliary (kWh)	7,576	9,681
Discharge Energy No Auxiliary (kWh)	4,139	6,351
RTE No Auxiliary	54.6	65.6
Mean Charge Temperature (ºC)	36	36
Mean Discharge Temperature (ºC)	36	36
Mean Temperature (ºC)	36	36
Mean Ambient Temperature (ºC)	NA	NA

3.8 Use-Case 5: Load Shaping

3.8.1 Duty Cycle Summary

The load shaping duty cycle for SnoPUD is developed in BSET by minimizing the balancing payment to the Bonneville Power Administration. The balancing payment is composed of varying levels of charges depending on the gap between scheduled and actual load demand and energy price. Minimizing the balancing payment while maintaining the SOC between 10 and 90% produces an optimum charge/discharge schedule. A 1-month balancing duty cycle using December 2015 data was developed.

3.8.2 Test Results

Two runs were performed to get the desired 168 hours of operation. Load shaping test results are shown in Figure 34 and Table 11.

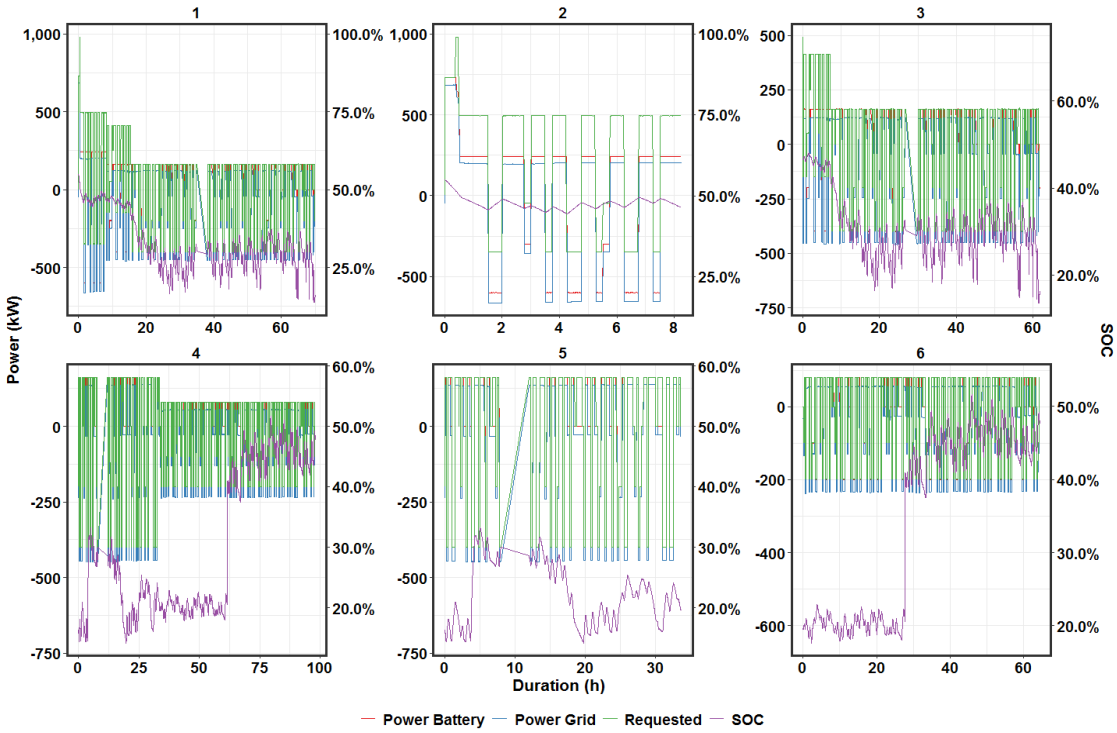

Figure 34. Load Shaping Test Results

Table 11. Load Shaping Test Results

Date	2018-05-17	2018-05-17	2018-05-17	2018-05-20	2018-05-20	2018-05-21
Duration (h)	70	8	62	98	34	64
Rest Fraction	0.03	0.00	0.03	0.05	0.08	0.04
Strings Active	2	2	2	1	1	1
Average Charge Power (kW)	-860	-1,195	-816	-1,044	-1,571	-821
Average Discharge Power (kW)	195	472	153	213	363	143
SOC Range	14-55	44-55	14-48	14-52	14-33	18-52
Charge Energy (kWh)	24,634	4,335	20,299	36,594	16,263	20,333
Discharge Energy (kWh)	9,398	2,675	6,730	14,468	7,171	7,297
RTE	38.2	61.7	33.2	39.5	44.1	35.9
Charge Energy No Rest (kWh)	20,554	4,271	16,283	33,449	14,991	18,458
Discharge Energy No Rest (kWh)	9,398	2,675	6,730	14,468	7,171	7,297
RTE No Rest	39.9	61.2	34.3	37.6	43.0	33.2
Charge Energy No Auxiliary (kWh)	17,937	3,899	14,038	28,672	13,304	15,368
Discharge Energy No Auxiliary (kWh)	11,704	3,077	8,634	18,531	8,368	10,163
RTE No Auxiliary	65.2	78.9	61.5	64.6	62.9	66.1
Mean Charge Temperature (ºC)	37	39	36	31	32	30
Mean Discharge Temperature (ºC)	37	39	37	31	32	30
Mean Temperature (ºC)	37	39	37	31	32	30
Mean Ambient Temperature (ºC)	NA	NA	NA	NA	NA	NA

3.9 Use-Case 6: Power Factor Correction

3.9.1 Duty Cycle Summary

To perform in any Volt/VAR-related application, the FBESS inverters will have to dispatch a certain amount of VAR (reactive power) to achieve a VAR-dependent target. Therefore, as a simplistic approach, this use-case test is conducted by deploying the FBESS inverters to correct the power factor at the bank meter to unity.

3.9.2 Test Results

The power factor at the bank meter was controlled to 1 by varying the FBESS VAR output. The commands were sent by DERO based on its algorithm. Note that some real power also flowed during this power factor correction period, probably to maintain a minimum power factor level of 0.25 at the FBESS. Assuming negative reactive power is capacitive, periods of capacitive power corresponded to discharge mode for the FBESS. For the first half of the subsequent charge, reactive power was positive, while it was negative during the second half of charge. This appears to indicate the FBESS discharge or charges based on an algorithm independent of the power factor algorithm. Based on FBESS SOC trends, the algorithm for charge or discharge appears to be designed to keep the FBESS SOC in the 20 to 90% range. The power factor at the bank meter was ~0.96 before and after the test and was >0.99 for 79% of test duration. The FBESS does power factor correction as intended.

Power factor correction test results are shown in Figure 35 and Table **12**.

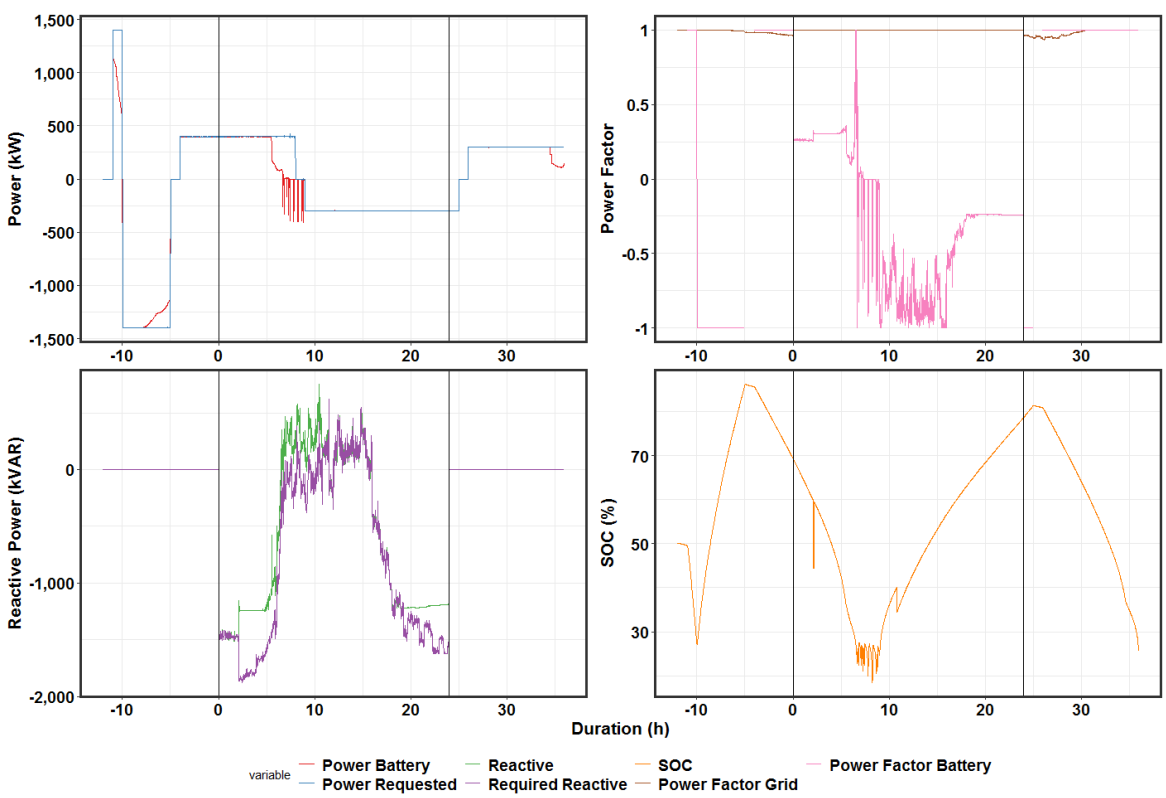

Figure 35. Power Factor Correction Test Results

Table 12. Power Factor Correction Results

Date	2018-04-19
Duration (h)	24
Rest Fraction	0.03
Strings Active	3
Average Charge Power (kW)	-484
Average Discharge Power (kW)	282
SOC Range	18-79
Charge Energy (kWh)	7577
Discharge Energy (kWh)	3202
RTE	42.3
Charge Energy No Rest (kWh)	6963
Discharge Energy No Rest (kWh)	3202
RTE No Rest	43.8
Charge Energy No Auxiliary (kWh)	5595
Discharge Energy No Auxiliary (kWh)	3866
RTE No Auxiliary	69.1
Mean Charge Temperature (ºC)	37
Mean Discharge Temperature (ºC)	37
Mean Temperature (ºC)	37
Mean Ambient Temperature (ºC)	NA

3.10 Use-Case 7: Optimal Utilization of Energy Storage

The objective of this test is to evaluate ESS performance when a set of services from all other use-cases is co-optimized. MESA 1 did not complete use case 7. This test was not conducted because the FBESS was not available for testing. PNNL will complete the SNO-controls integration work highlighted in Figure 36 by evaluating the performance of Doosan's DERO.

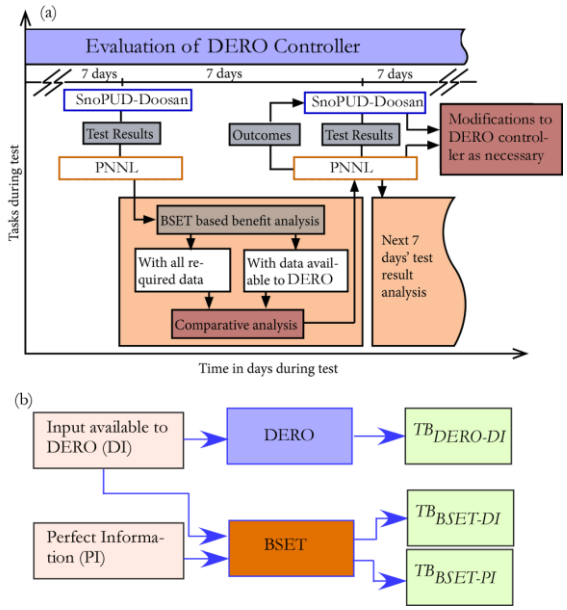

Figure 36. DERO Performance Evaluation Methodology. (a) Test arrangement and task outline. (b) DERO and BSET input and output.

4.0 Lessons Learned

This section provides an at-a-glance view of important lessons learned on the technical aspects of MESA 2 FBESS based on the experiences gained during the testing process and the test results. Conclusions drawn from the overall testing effort and the importance of the test results are provided in Chapter 6.

4.1 Lessons Learned from Test Results

1. The FBESS discharge power was constant down to various SOC levels based on discharge power. The charge power did not affect the discharge energy, which is as expected. Discharge energy peaked at 1,100 kW discharge power. This was the optimal point at which electrochemical losses and auxiliary consumption was minimum. When auxiliary consumption was not considered, the peak occurred at lower power levels. While data could not be obtained at low enough power levels, it appears peak energy is obtained at discharge power levels of 300 kW, below which PCS losses come into play.
2. The RTE peaked at 1,100 kW for discharge and 1,200 kW for charge. As expected, excluding auxiliary consumption led to higher RTEs at low discharge power levels. Limited tests show that at power levels <150 kW, the RTE is lower, possibly due to low PCS efficiency.
3. The discharge energy ranged from 3,435 to 5,275 kWh. If auxiliary consumption was excluded, the range was 3,615 to 6,095 kWh.
4. The upper limit of calculated discharge energy at the PCS, normalizing the measured energy by 100% DOD, was 6,630 kWh, which is much less than the system rating of 8000 kWh. The corresponding number inclusive of auxiliary losses was 5,735 kWh. Both of these numbers corresponded to 550 kW discharge, 1,200 kW charge, and an SOC range of 6 to 98%.
5. When auxiliary consumption during the 1- to 1.75-hour rest periods were excluded, the RTE rose by 2 to 4%. When the auxiliary consumption was excluded throughout the test, the RTE increased by 8 to 18%, with larger increases at lower rates. When the charge power was halved from 1,200 kW, the increase in RTE while excluding auxiliary consumption was only 13%. This is probably due to greater taper durations designed for charge to ensure the FBESS SOC reaches the intended maximum SOC.
6. The cumulative RTE for strings varied from 40% to 63%. Strings 3 and 4 had the lowest RTEs, while String 2 had the highest RTE.
7. Cumulative RTEs for Strings 3 and 4 stayed low throughout. The RTEs for Strings 1 and 3 decreased over the testing period. Note that Strings 3 and 4 had weak stacks from the start of testing, whereas String 1 had its first imbalance on 2018-03-06, while String 2 had its first imbalance on 2018-05-07 (excluding one imbalance at the start). This appears to indicate that the Strings 3 and 4 had weak modules from the start, while String 1 and String 2 stacks got progressively weaker as the test progressed. Having maximum SOC and minimum SOC tags for each string would have helped in understanding how the BMS directs power across the strings.
8. The available power tag did not recognize strings that dropped off during discharge due to low SOC. Even during rest after discharge, the available power did not adjust down to reflect the weak strings. It is only when SOC reached 0% or when the string could not accept a subsequent charge command that the available power was adjusted downward. This results in overestimation of the available power.

9. During rest, when a string was pulse charged to keep its SOC above a critical level, the available power decreased by the magnitude of charge power. It is not clear why the BMS does this. One possible explanation is if the FBESS is sent a charge command, that string can only absorb its rated power minus that of the charge power to which it is subject. Also, because the string SOC is low, the rule of thumb appears to be that the string discharge power is its rated power minus the magnitude of the charge power.
10. The Electric Power Research Institute Energy Storage Integration Council meeting held November 16, 2017, identified SOC calibration procedure, seasonal testing for auxiliary load, SOC loss rate due to reactive power injection, and state-of-health definition and tests as key gaps that merit further studies. This project addressed all of these gaps.
11. BMS related issues included:
    - Distribution of power among strings as a function of their SOC deviation from the average of all strings.
    - Pulse charging strings during rest when the SOC reaches a critical low limit of 2 to 5%.
    - For String 4, most of the time the SOC drop is too steep at the end for pulse charging to be initiated, and the string SOC is set to 0% when a module SOC reaches -100%.
    - The presence of a variable speed drive suggests the BMS adjusts flow rate based on power level and SOC.
    - Available strings were reduced much later than when they dropped out during discharge.
12. The FBESS controlled the power factor quite accurately within 1% of the target power factor.
13. The internal resistance was lowest at ≤20% SOC for charge and discharge. Charge and discharge resistances typically were highest for 20% SOC. The exception was during discharge for Strings 3 and 4 for which 40% SOC corresponded to highest internal resistance, followed by 20% SOC. This was because of weak battery modules in these strings causing premature end to discharge at relatively high SOC levels of 25 to 50% at a moderate discharge power level of 550 kW.
14. During discharge, a string power drops to zero at a high SOC of 50%. The SOC of each string is the average of SOC for the four battery modules within the string. The BMS stops discharge when the SOC in any battery module reaches 0%. It would have been useful to have the maximum and minimum SOCs for each module so modeling could be done at the module level to reliably predict individual string performance. The end user also would be able use this additional information to adjust the battery operating parameters. At a minimum, having the maximum and minimum SOC values for each string would provide the end user advance information prior to unanticipated string failures due to module mismatch within the string.

4.2 Lessons Learned in Design of Data Transfer

1. The data transfer set up was quite smooth. Data was transferred from the MESA 2 supervisory control and data acquisition system to the server of the PNNL contractor. Using a MySQL connection, data were downloaded onto a PNNL computer and a PNNL shared drive, where all data reside. Options for transferring all the data to a PNNL storage site are being explored. The DC voltage and current information was not requested by PNNL due to a miscommunication on what was available. UET subsequently provided this information.

4.3 Lessons Learned in Design of Test Set Up

1. Detailed line diagrams were provided by SnoPUD. The following lessons were learned:
   - It became clear that the bank meter power flow is not relevant because power flows for multiple feeders are registered in the bank meter.
   - Detailed descriptions for various breakers, switches and contactors were available. S-32-E1A shows 1000-V 1200-A DC contactors connecting the four battery modules in series with each other. The DC contactors are normally open, and hence should be shown as connected in parallel to each string.
2. Power factor was controlled at the bank meter.
3. The bank meter measures power flow across multiple feeders, including the feeder where the FBESS is located.
4. Each String can be placed in local mode and balanced by UET.
5. Because of the 15-minute minimum gap between commands, it was important to be able to predict the SOC change of the FBESS accurately. Due to weak stacks present in the modules within each string, it was a challenge to accurately predict SOC trends because of strings dropping out during a test.
6. There is no active heating. Thermal management for this FBESS is limited to cooling, which becomes operational only during continuous operation at >35°C or at >40°C as measured by the temperature sensors. There is one temperature sensor for each battery container electrolyte that monitors temperature in the pipe for a total of 16 sensors for the FBESS.
7. The difference between maximum and minimum temperature was less than 5°C, indicating an effective thermal management system.
8. The availability of power flow and SOC information for each String allowed development of an algorithm to predict power distribution among strings as a function of SOC deviation of each String from the mean SOC for all strings.

4.4 Lessons Learned from Site-Related Issues

1. Because of strings dropping out during testing, the requested power was adjusted to reflect the active strings.
2. It would have been useful to get tags that show the number of active strings, and the strings that are active.
3. To avoid confusion, the test start times and relevant details were shared across the relevant SnoPUD, PNNL, UET, and Doosan staff.
4. Updates of the number of active strings and the SOC of each string were provided at the end of each day
5. When a string dropped out, UET placed it on local mode and did the necessary maintenance/repairs. The ongoing test was completed before UET brought the string online, thus ensuring that testing was not disrupted. This is an example of the importance of close coordination among UET, PNNL, and MESA 2 personnel.
6. Each UET site visit was coordinated with the safety team at SnoPUD. This shows the importance of close coordination not just among technical staff, but also the host safety personnel for operation in an energized substation.

7. Because multiple parties needed to know the status of the FBESS, UET sent prompt communications to the team on the status of repairs and when the strings were brought back online. On some occasions, UET provided detailed descriptions of the problems.
8. The Doosan SOC estimator did not appear to take into consideration the number of active strings.

5.0 Novel Findings

5.1 State-of-Charge Model

To generate the most meaningful tests, a model was developed to predict how the SOC of the battery varied over time. This model consisted of two components—one to predict the maximum power the battery could provide at a given SOC and one to predict how the SOC changed at a given power (provided this power is within the predicted power ranges). This is because in order to predict the SOC change effectively, we need to know if the system can actually provide the requested power.

To predict the available power, the power was analyzed with respect to SOC during periods when power was tapering. The results are shown in Figure 37.

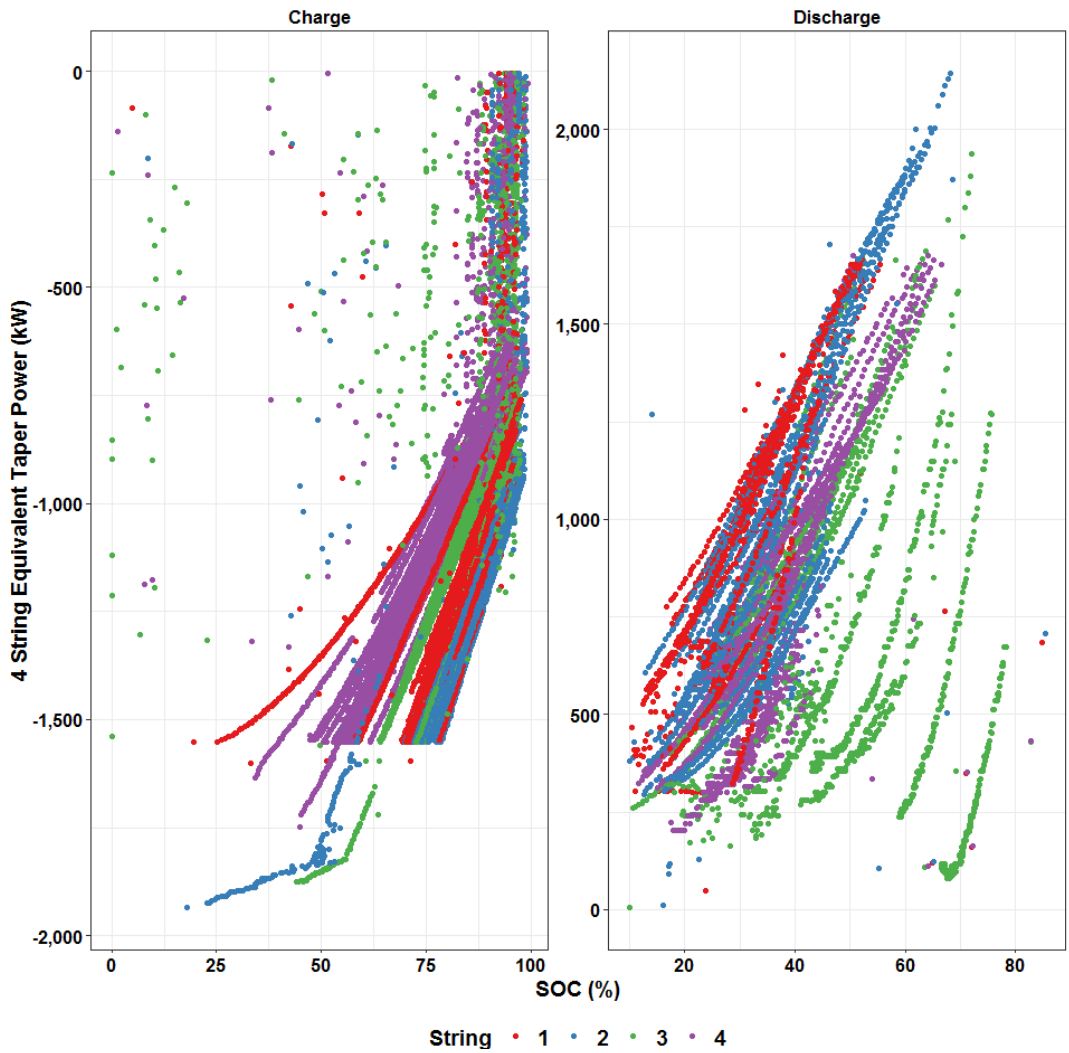

Figure 37. Taper Power as a Function of SOC during Charge and Discharge

A linear relationship for power as a function of SOC was developed for discharge and charge. In practice, a more conservative model was used to account for the large spread in power levels, with the same string at the same SOC giving different maximum powers during different tests.

To predict how the SOC changed vs. time, a multilinear regression was done of change in SOC vs. the time integral of the following equation:

$$\Delta SOC = \int \left(C_0 + C_1 \frac{P}{SOC} + C_2 P + C_3 \frac{P}{SOC^2} + C_4 P\, SOC + C_5 P^3 \right) dt$$

Taking the time derivative of both sides, the following relationship was obtained:

$$\frac{dSOC}{dt} = C_0 + C_1 \frac{P}{SOC} + C_2 P + C_3 \frac{P}{SOC^2} + C_4 P\, SOC + C_5 P^3$$

A trial and error approach was used to select terms that were most predictive. In future work, a more robust method will be used to select the terms.

A demonstration of this model for the baseline tests is provided in Figure 38, with red lines representing the actual SOC and blue lines the predicted SOC from our model. A dotted line is used to represent regions where the power tapers. In general, the model does not perform well while in the taper region.

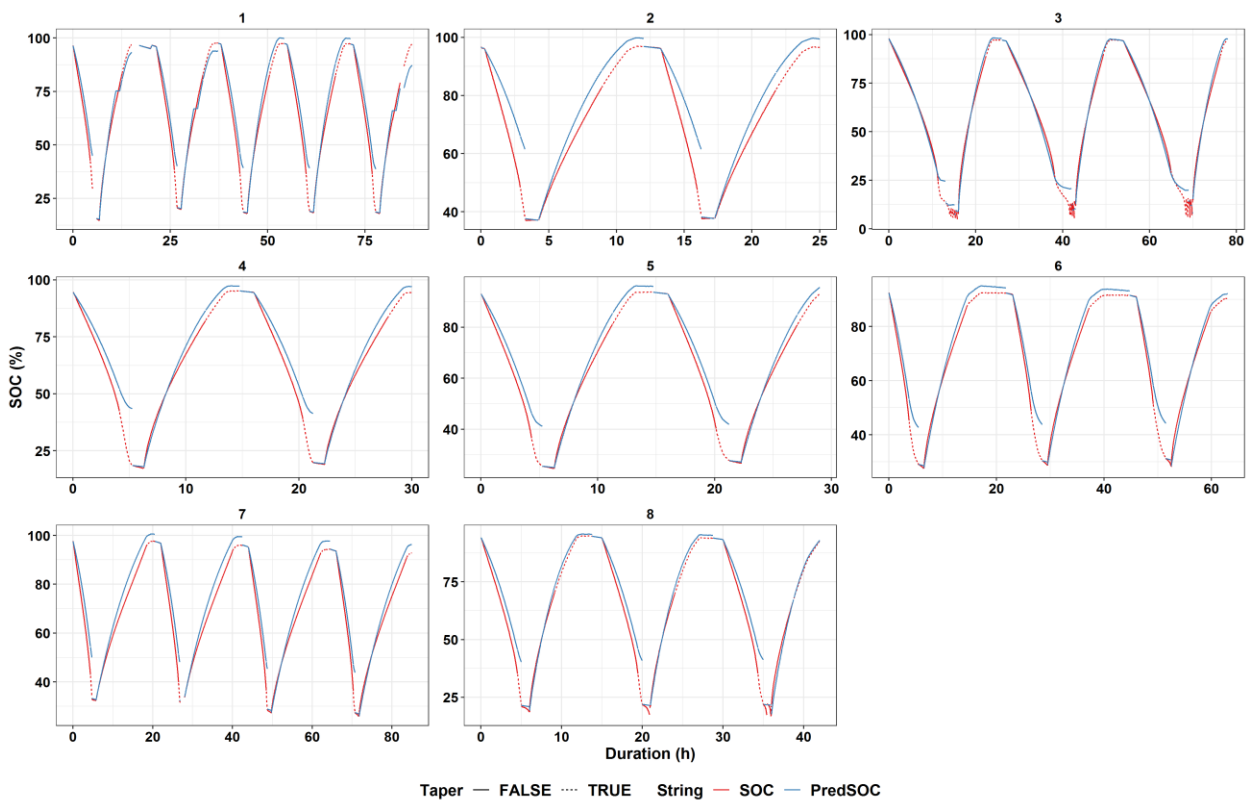

Figure 38. Validation of FBESS Performance Model

The FBESS temperature increased during discharge and decreased during charge, with no change during rest as seen in Figure 39. We regressed the rate of change of temperature vs. power and difference between FBESS and ambient temperature, as shown in Table 13, with an adjusted R^2 of 0.96. The positive coefficient for power shows an endothermic effect for negative power (or charge). The ohmic heating effect is represented by the coefficient of the P^2 term. The entropic term dominates for this high energy to power battery, which is consistent with the findings of Viswanathan et al. (2010). Note that at 1,600 kW, the E/P is 8,800 kWh/1,600 kW, or 5.5, while at 500 kW, the E/P is 17.6.

When the difference between the temperature of the FBESS and ambient temperature increases, a lower temperature increase occurs, either due to greater heat loss to ambient or to active cooling being initiated.

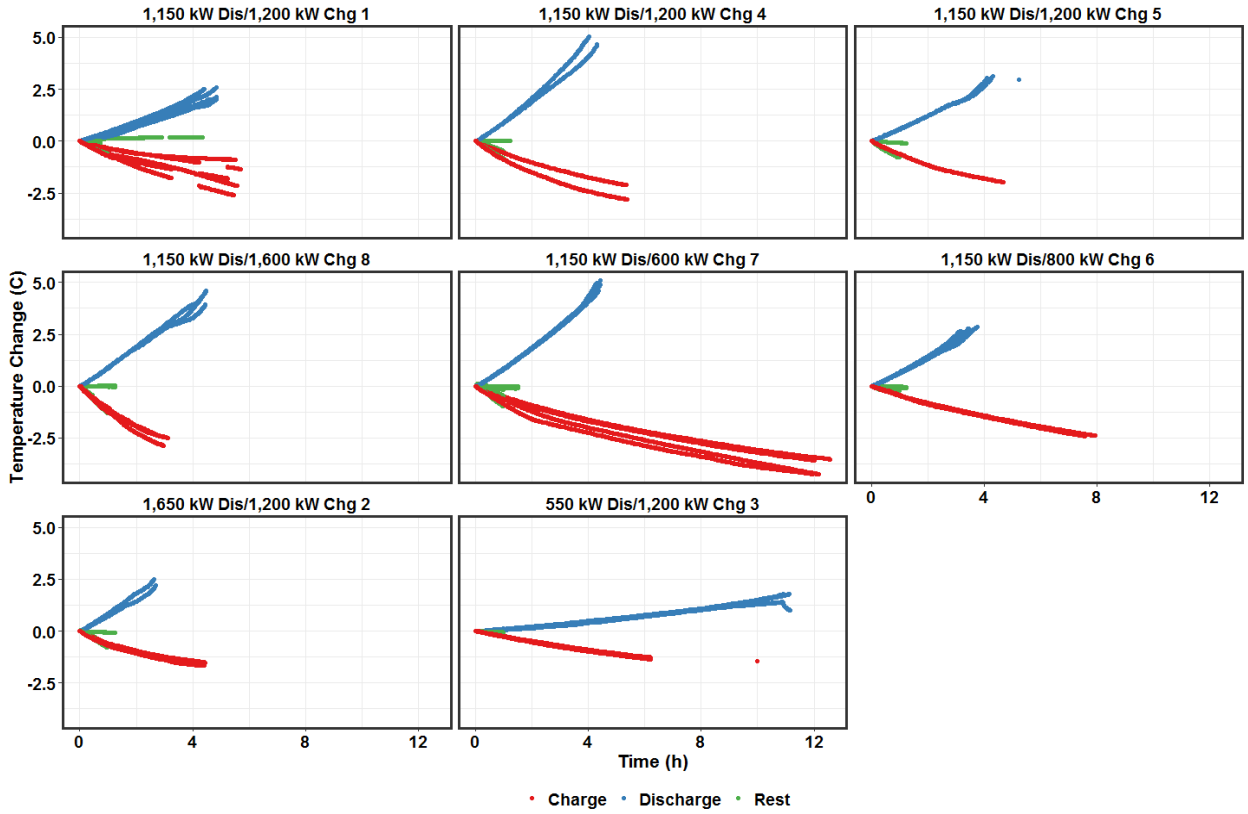

Figure 39. Temperature Change for the Various Baseline Capacity Tests for Charge, Rest and Discharge.

Table 13. Regression Results for Rate of Temperature Change as a Function of Power, Power2, and the Difference between FBESS and Ambient Temperature.

Parameter	Coefficient	Std. Error	Units
Power (kW)	0.000646	1.02e-06	C/kWh
Power Squared (kW^2)	1.93e-07	1.71e-09	C/(kW^2-h)
Delta Temperature (ºC)	-0.00163	3.54e-05	C/(C-h)

6.0 Conclusions

The 2.2-MW, 8-MWh advanced FBESS at the Everett substation is installed to provide energy shifting, grid flexibility, and improved distribution system efficiency. As part of Washington CEF 1, a $4.4 million grid modernization grant was awarded to SnoPUD MESA 2 to support the FBESS project and to provide technical support to evaluate the effectiveness and economics of the FBESS project and energy storage applications in general. Because FBESSs are quite diverse in their characteristics, it was important to characterize their performance and stability over time using a DOE-OE standardized test procedure for energy storage. Normalizing FBESS performance to this standardized baseline also facilitates evaluation of FBESS against other electro-chemistries evaluated for similar use cases.

This study investigated the technical performance of the Everett substation FBESS. Baseline tests were intended to assess the general technical capability of the FBESS (e.g., stored energy capacity, ramp rate performance, ability to track variable charge/discharge commands, DC battery internal resistance, etc.) while the use case tests were used to examine the performance of the FBESS while engaged in a specific service (e.g., arbitrage, capacity, regulation services, load following, and load shaping services). Parameters that are important for understanding FBESS performance when subjected to actual field operation for economic purposes (e.g., RTE, auxiliary consumption, command tracking performance, temperature variations, parasitic power loss during power electronics switching during rest, SOC excursions, etc.) were examined. These metrics were used to quantify performance of the FBESS in several use cases in comparison with baseline performance.

The analyses of FBESS performance confirm that the technical characteristics the Everett FBESS (e.g. capacity) and performance (e.g., response rate) are generally compatible with the range of use cases investigated in this project. However, the availability factor (i.e., hours available for operation/total hours) during the field-testing period was low and the FBESS was ultimately taken out of operation before field testing could be completed. Because of failure of individual battery strings during testing, the delivered power and energy during testing were less than scheduled. On several occasions, testing had to be done at partial power output with less than four strings.

The FBESS did not deliver the 8,000-kWh rated energy at any power levels investigated, with the highest energy measured being approximately 6,300 kWh at 92% DOD, without accounting for auxiliary load.

The RTE at the grid was 54 to 63%, while at the PCS level, it was 68 to 75%. This is in line with the Performance Specifications Table as reported by Schenkman and Borneo (2015).

Listed below are multiple parameters that should be considered for optimum operation of the FBESS:

- Effect of auxiliary consumption
- Effect of PCS losses
- Effect of charge-discharge power levels
- SOC drop during rest due to DC discharge of battery
- Energy availability as a function of power levels at the PCS level and at the grid
- Reliability of strings and ability to detect the onset of string failure
- Effect of ambient temperature, and operation mode on FBESS performance
- FBESS reliability and how to improve it.

This detailed findings described in this report will be beneficial to SnoPUD in understanding the performance of the current Everett substation FBESS and in designing appropriate operational strategies. In addition, the results and lessons presented herein would be beneficial in general for any task or effort that needs technical assessment on similar types of FBESSs based on field deployment results.

Some specific conclusions are:

- The system rated energy of 8,000 kWh at 1 MW was not verified. The maximum energy achieved was 5,250 kWh obtained at 1,100 kW in the 36 to 97% SOC range.
- Excluding auxiliary consumption, a maximum energy of 6,100 kWh was obtained at 550 kW in the 28 to 98% SOC range.
- Including taper, the highest energy obtained was 6,300 kWh when auxiliary consumption was excluded in the 5 to 97% SOC range, while including auxiliary consumption corresponded to discharge energy of 5,670 kWh in the 18 to 97% SOC range. Normalizing these numbers at 100% DOD gave discharge energies of 6,845 and 7,180 kWh, respectively, which still are lower than the rated 8,000 kWh.
- The FBESS RTE for baseline reference performance capacity tests was 54 to 63%, increasing to 68 to 75% when auxiliary consumption was excluded.
- The RTE for baseline reference performance frequency regulation test was in the 48 to 52% range, increasing to 55 to 60% when auxiliary consumption was excluded.
- The gain in RTE while excluding auxiliary consumption was greater at lower power levels. Lowering discharge power levels resulted in greater RTE gain.
- For constant power charge, the RTE peaks at 1,100 kW discharge. When auxiliary consumption is excluded, the RTE increases with decreasing discharge power down to 550 kW.
  - Studies were not carried out to estimate RTE at lower power levels. It is expected that the RTE without auxiliary consumption would peak around 300 kW, below which the PCS efficiency drops rapidly. There is a hint of flattening of the RTE at the low discharge power level of 550 kW.
  - The DC-DC RTE trend was similar to RTE without auxiliary consumption. As expected, the DC-DC RTE increases with decreasing power levels, whereas the AC-AC RTE drops at low power levels due to PCS losses. It should be noted that below a certain power level, self-discharge mechanisms such as electrolyte crossover may dominate, reversing this increasing DC-DC RTE trend with decreasing power levels.
- For constant power discharge of 1,150 kW, RTE decreased at <1,200 kW charge, and was constant at >1,200 kW charge, showing the greater impact of auxiliary consumption at lower power levels, and the balancing of auxiliary consumption and electrochemical losses at >1200 kW charge. Excluding auxiliary losses, the RTE peaked at 1,200 kW charge. Note that PCS losses are lower for charge across all power levels. Hence, PCS losses do not dominate up to the 600 kW charge power levels used in RPTs. However, because of taper during charge, the FBESS spends more time at power levels lower than 600 kW, resulting in higher PCS losses. At charge power levels greater than 1,200 kW, electrochemical losses dominate.
  - This is supported by the DC RTE for fixed rate discharge, where RTE increases as expected with decreasing charge power levels. The increase in RTE is not as steep as for discharge at various power levels, due to greater current during discharge at fixed power and SOC lending itself a higher RTE increase as discharge power decreases.

- Charging was endothermic, while discharging was exothermic. In spite of this, auxiliary consumption for fixed power level was higher for charge, indicating charging may require higher flow rates.
  - The increase in RTE when excluding auxiliary consumption was lower than for charge as seen earlier, probably due to higher PCS losses in the taper region of charge.
- The ramp rate for charge and discharge was in the 400 to 800 kW/second range, corresponding to response times in the 2 to 4 second range.
  - At low a SOC of 12%, the charge ramp rate was low, possibly due to low operating voltage. At a high SOC of 75%, the ramp rate was even lower, possibly because the BMS limits ramp rates above a certain SOC. The charge ramp rate peaked in the 40 to 60% SOC range.
  - At high SOC of 87% during discharge, the ramp rate was maximum at 660 kW/s. The ramp rate decreased with decreasing SOC, and was 425 kW/second at 40% SOC. The low ramp rate during charge at this SOC may be due to BMS limiting ramp rate based on the high internal resistance at this SOC.
- The internal resistance was in a tight range of 45 to 50 milliohms across the SOC range investigated, with an outlier at 12% SOC corresponding to 95 milliohms.
  - In situ resistance for each string was in line with the measured FBESS resistance from RPTs.
  - Charge and discharge resistance were highest for 20% SOC for all strings.
    - The exception was during discharge for Strings 3 and 4, where 40% SOC corresponded to the highest internal resistance, followed by 20% SOC. This was because of weak battery modules in these strings causing premature end to discharge at relatively high SOC levels of 25 to 50% at moderate discharge power levels of 550 kW.
- The RTE varied from 33 to 54% for the various use cases. High rest percent and low power levels lowered the RTE due to auxiliary consumption. Excluding auxiliary consumption, the RTE increased to ~300 kW average power, below which PCS efficiency dropped, lowering RTE. The increase in RTE when excluding auxiliary consumption was highest for low power levels and high rest periods.
- During rest, the PCS is in switching mode for 5% of the time. The DC discharge current was non-zero during the time PCS does not switch during rest, and as high as 20 A per string and approached 0 A when PCS was switching. This resulted in a rate of decrease of SOC of 0.5% per hour.
- Thermal management is based on cooling by circulating glycol using a heat exchanger in the cathode flow path, coupled with a blower to remove heat from the heat exchanger when the FBESS temperature is higher than a set-point of 35°C for extended operation per UET Technical Specifications (Schenkman and Borneo 2015) and if it reaches 40°C per a UET engineer (Weber 2018). As expected, auxiliary consumption increased as FBESS temperature increased. At low temperatures (<20°C), auxiliary consumption was ~12 kW per string, which is in line with the values communicated by an UET engineer.[6]
- Available power as indicated by the BMS was not reliable. After a string dropped off during discharge, it required the string SOC to reach 0% or a subsequent charge command to be issued for available power to be reliably reduced by the appropriate value.
- Strings 1, 2, and 3 were subject to pulse charges during rest to keep the SOC above a critically low value, while String 4, on a majority of occasions, simply went to 0% SOC, without charge pulses to keep its SOC within the desired range.

[6] This information was present in a word document created by Viswanathan of PNNL "UET and Avista system notes.docx" last edited July 19, 2017.

  - These behaviors allow determination of onset of failure, allowing an operator to make suitable arrangements in advance of failure.
  - During these charge pulses, the available power was reduced by the magnitude of the pulse. This appears to be a way for the BMS to reliably track available power during these special occasions when pulse charge is needed to keep the SOC within the desired range.
- PCS losses were less during charge than during discharge. The PCS losses for each string were different. Strings with the highest losses during discharge had the lowest losses during charge. The maximum PCS efficiency during charge was in line with its electrical specification of 98.4% maximum efficiency, but it was only ~96% during discharge.
- It was difficult to determine a trend in state-of-health degradation because each string had faulty modules that failed periodically.
- The total test duration was 173 days, out of which 78 days, or 45%, were lost due to various reasons. Of these lost days, 50 were due to string-related issues such as stack SOC mismatch and leaks. Pump-related issues contributed to 10 lost days or 6%, while communications, maintenance, human error and miscellaneous contributed to 18 lost days or 10%. String-related issues contributed to 64% of the 78 days lost. There were 38 work stoppages, of which 63% were related to strings.

7.0 References

Crawford AJ, E Thomsen, D Reed, D Stephenson, V Sprenkle, J Liu, and VV Viswanathan. 2016. Development and validation of chemistry agnostic flow battery cost performance model and application to nonaqueous electrolyte systems, *International Journal of Energy Research* 40(12):1611-1623. DOI:10.1002/er.3526

Doosan GridTech Inc (Dooson). 2016a. "Products: Doosan GridTech Software™." Seattle, Washington. http://www.doosangridtech.com/products/. Accessed April 9, 2019.

Doosan GridTech Inc (Dooson). 2016b. "Applications: Doosan GridTech Distributed Energy Resource Optimizer™ (DG-DERO™)." Seattle, Washington. http://www.doosangridtech.com/products/distributed-energy/applications/. Accessed April 9, 2019.

Energy Storage Association (ESA). "Redox Flow Batteries." Undated. Available at http://energystorage.org/energy-storage/technologies/redox-flow-batteries. Accessed January 23, 2019.

Miller A (Ed.). Undated. "SunSpec Energy Storage Models." Document 12032, Draft Version 4, Available at http://mesastandards.org/wp-content/uploads/2017/09/SunSpec-Alliance-Specification-Energy-Storage-ModelsD4rev0.25.pdf.

Modular Energy Storage Architecture (MESA). 2016. *MESA Open Standards for Energy Storage – Draft*. Available at http://mesastandards.org/wp-content/uploads/2016/11/MESA-ESS-Specification-November-2016-Draft-2.pdf. Accessed on December 27, 2016.

Schenkman BL and DR Borneo. 2015. "Sandia Third-Party Witness Test of UniEnergy Technologies 1 MW/3.2 MWh Uni.System™." SAND2016-6187R, Sandia National Laboratories, Albuquerque, New Mexico. https://www.sandia.gov/ess-ssl/publications/SAND2015-6187R.pdf. Accessed April 9, 2019.

Sun C. 2015. Information provided by Chauncey Sun of Uni Energy Technologies by email or by telephone conversation with VV Viswanathan of PNNL in late 2015, captured in a word document "UET and Avista system notes.docx" prepared by Viswanathan, last edited 07/19/2017.

Snohomish County Public Utility District (SnoPUD). Undated. "Snohomish PUD MESA 2 Vanadium Flow Battery." Everett. Washington. www.commerce.wa.gov/wp-content/uploads/2018/08/Energy-MESA2-FactSheet_082418.docx. Accessed January 24, 2019.

UniEnergy Technologies (UET). Undated. "Uni.System:™ Grid-Scale Energy Storage Solution." http://uetechnologies.com/images/product/UET_UniSystem_Product_Sheet_reduced.pdf. Accessed April 9, 2019.

Viswanathan VV, D Choi, D Wang, S Towne, RE Williford, J-G Zhang, J Liu, and Z Yang. 2010. "Effect of entropy of lithium intercalation in cathodes and anodes on Li-ion battery thermal management." *Journal of Power Sources* 195(11)3720-3729. Available at https://www.sciencedirect.com/science/article/pii/S0378775309021119. Accessed on April 9, 2019.

Viswanathan VV, DR Conover, AJ Crawford, S Ferreira, and D Schoenwald. 2014. "Protocol for Uniformly Measuring and Expressing the Performance of Energy Storage Systems." PNNL-22010 Rev. 1, Pacific Northwest National Laboratory, Richland, Washington. Available at https://www.sandia.gov/ess-ssl/docs/ESS_Protocol_Rev1_with_microgrids.pdf\. Accessed April 9, 2019.

WeatherUnderground. https://www.wunderground.com/personal-weather-station/dashboard?ID=KWADEMIN7. Accessed April 9, 2019.

Weber, Logan. Message to Viswanathan of PNNL February 2, 2018. Email.

Appendix A

Supplemental Information

A.1 Baseline Results – No Taper

Table A.1. Baseline Results Excluding Discharge and Charge Taper

Test	Cycle	Date	Duration (h)	Strings Active	Avg Discharge Power (kW)	Avg Charge Power (kW)	SOC Range	Charge Energy (kWh)	Discharge Energy (kWh)	RTE	Charge Energy No Rest (kWh)	RTE No Rest	Charge Energy No Aux (kWh)	Discharge Energy No Aux (kWh)	RTE No Aux	Mean Temp (C)	Mean Amb Temp (C)	DC Charge Energy (kWh)	DC Discharge Energy (kWh)	RTE DC
	1	2017-12-22	21.0	2	1150	1200	43-82	5931	3406	57.4	5368	63.5	5002	3613	72.2	20.6	1.8	2444	1875	76.7
1	2	2017-12-22	17.0	2	1150	1200	40-82	5735	3566	62.2	5601	63.7	5214	3786	72.6	20.9	-0.4	2540	1957	77.0
1	3	2017-12-23	17.0	2	1150	1200	37-82	6039	3738	61.9	5900	63.4	5492	3976	72.4	20.0	-1.4	2676	2052	76.7
1	4	2017-12-24	17.0	2	1150	1200	36-82	6033	3757	62.3	5898	63.7	5490	3996	72.8	19.7	0.0	2675	2059	77.0
1	5	2017-12-25	15.0	2	1150	1200	36-79	5614	3501	62.4	5527	63.3	5146	3728	72.4	20.6	-0.3	2508	1924	76.7
1	Cumulative	NA	87.0	2	NA	NA	NA	29352	17968	61.2	28294	63.5	26344	19099	72.5	NA	NA	12843	9867	76.8
1	Mean	NA	17.4	2	1150	1200	38-81	5870	3594	61.2	5659	63.5	5269	3820	72.5	20.4	-0.1	2569	1973	76.8
2	1	2017-12-25	13.0	2	1650	1200	48-81	4772	2747	57.6	4595	59.8	4276	2877	67.3	20.8	0.2	2084	1482	71.1
2	2	2017-12-26	12.0	2	1650	1200	48-81	4771	2795	58.6	4682	59.7	4356	2934	67.4	20.8	1.6	2122	1511	71.2
2	Cumulative	NA	25.0	2	NA	NA	NA	9543	5542	58.1	9277	59.7	8632	5811	67.3	NA	NA	4206	2993	71.2
2	Mean	NA	12.5	2	1650	1200	48-81	4772	2771	58.1	4638	59.8	4316	2906	67.3	20.8	0.9	2103	1496	71.2
3	1	2018-01-11	27.0	2	550	1200	28-87	7454	4289	57.5	7372	58.2	6731	4962	73.7	29.2	6.5	3304	2653	80.3
3	2	2018-01-12	27.0	2	550	1200	28-88	7726	4455	57.7	7537	59.1	6876	5166	75.1	29.1	8.1	3377	2766	81.9
3	3	2018-01-13	24.0	2	550	1200	30-88	7456	4390	58.9	7456	58.9	6798	5089	74.9	29.3	6.9	3338	2725	81.6
3	Cumulative	NA	78.0	2	NA	NA	NA	22636	13134	58.0	22365	58.7	20405	15217	74.6	NA	NA	10019	8144	81.3
3	Mean	NA	26.0	2	550	1200	29-88	7545	4378	58.0	7455	58.7	6802	5072	74.6	29.2	7.2	3340	2715	81.3
4	1	2018-01-17	16.0	4	1150	1200	44-81	5117	3027	59.2	4972	60.9	4630	3173	68.5	32.9	10.1	4543	3316	73.0
4	2	2018-01-17	14.0	4	1150	1200	40-82	5586	3455	61.9	5512	62.7	5131	3632	70.8	35.9	7.5	5035	3801	75.5
4	Cumulative	NA	30.0	4	NA	NA	NA	10703	6482	60.6	10484	61.8	9761	6805	69.7	NA	NA	9578	7117	74.3
4	Mean	NA	15.0	4	1150	1200	42-81	5352	3241	60.5	5242	61.8	4880	3402	69.7	34.4	8.8	4789	3558	74.2
5	1	2018-01-19	16.0	3	1150	1200	37-80	5659	3389	59.9	5493	61.7	5073	3574	70.5	34.2	7.5	3734	2802	75.0
5	2	2018-01-19	13.0	3	1150	1200	40-79	5170	3118	60.3	5087	61.3	4695	3291	70.1	35.0	6.9	3457	2584	74.7
5	Cumulative	NA	29.0	3	NA	NA	NA	10829	6507	60.1	10580	61.5	9768	6865	70.3	NA	NA	7191	5386	74.9
5	Mean	NA	14.5	3	1150	1200	38-80	5414	3254	60.1	5290	61.5	4884	3432	70.3	34.6	7.2	3596	2693	74.8
6	1	2018-01-20	23.0	3	1150	800	45-87	5962	3559	59.7	5802	61.3	5222	3750	71.8	33.5	6.2	3826	2946	77.0
6	2	2018-01-21	23.0	3	1150	800	49-86	5371	3180	59.2	5212	61.0	4690	3348	71.4	32.8	5.7	3436	2632	76.6
6	3	2018-01-22	17.0	3	1150	800	51-85	4754	2835	59.6	4679	60.6	4212	2985	70.9	32.8	5.8	3084	2347	76.1
6	Cumulative	NA	63.0	3	NA	NA	NA	16087	9574	59.5	15693	61.0	14124	10083	71.4	NA	NA	10346	7925	76.6
6	Mean	NA	21.0	3	1150	800	48-86	5362	3191	59.5	5231	61.0	4708	3361	71.4	33.0	5.9	3449	2642	76.6
7	1	2018-01-27	22.0	4	1150	600	43-96	7680	4558	59.3	7524	60.6	6688	4777	71.4	33.6	6.9	6476	4993	77.1
7	2	2018-01-28	22.0	4	1150	600	41-94	7541	4540	60.2	7449	60.9	6619	4761	71.9	35.2	10.2	6413	4979	77.6
7	3	2018-01-29	22.0	4	1150	600	38-92	7629	4516	59.2	7464	60.5	6628	4741	71.5	36.7	7.6	6422	4961	77.3
7	4	2018-01-30	19.0	4	1150	600	37-91	7475	4427	59.2	7399	59.8	6570	4645	70.7	37.1	7.2	6366	4859	76.3
7	Cumulative	NA	85.0	4	NA	NA	NA	30325	18041	59.5	29836	60.5	26505	18924	71.4	NA	NA	25677	19792	77.1
7	Mean	NA	21.2	4	1150	600	40-93	7581	4510	59.5	7459	60.5	6626	4731	71.4	35.7	8.0	6419	4948	77.1
8	1	2018-02-03	15.0	4	1150	1600	36-70	4383	2542	58.0	4224	60.2	3964	2688	67.8	38.5	9.3	3891	2811	72.2
8	2	2018-02-03	15.0	4	1150	1600	35-69	4184	2408	57.6	4032	59.7	3778	2559	67.7	38.7	9.2	3710	2676	72.1
8	3	2018-02-04	12.0	4	1150	1600	36-67	3664	2125	58.0	3664	58.0	3432	2256	65.7	39.0	9.7	3370	2359	70.0
8	Cumulative	NA	42.0	4	NA	NA	NA	12231	7075	57.8	11920	59.4	11174	7503	67.1	NA	NA	10971	7846	71.5
8	Mean	NA	14.0	4	1150	1600	36-69	4077	2358	57.9	3973	59.3	3725	2501	67.1	38.7	9.4	3657	2615	71.4

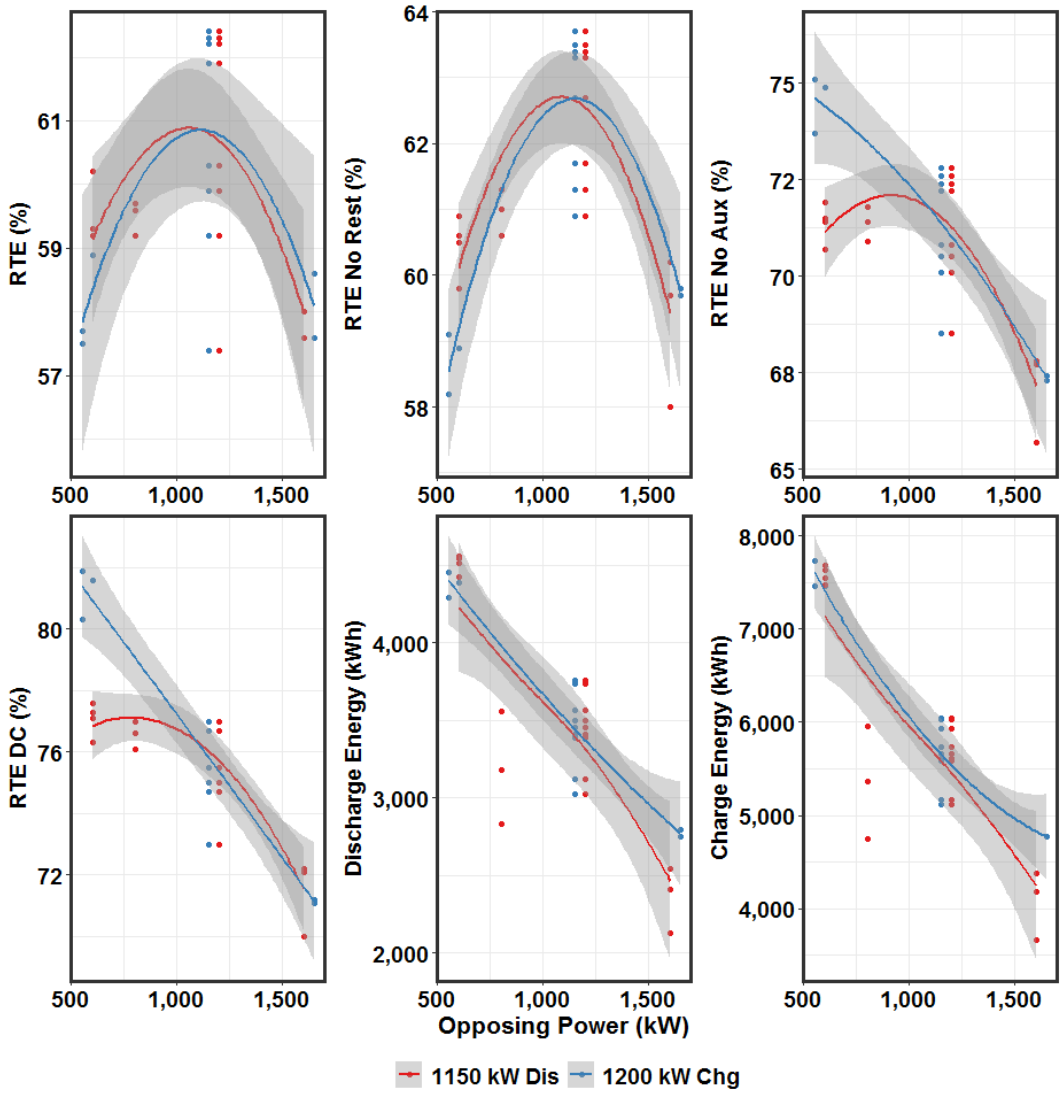

Figure A.1. Baseline Results Excluding Charge and Discharge Taper

A.2 Baseline Results – with Taper

Table A.2. Baseline Results Including Charge and Discharge Taper

Test	Cycle	Date	Duration (h)	Strings Active	Avg Discharge Power (kW)	Avg Charge Power (kW)	SOC Range	Charge Energy (kWh)	Discharge Energy (kWh)	RTE	Charge Energy No Rest (kWh)	RTE No Rest	Charge Energy No Aux (kWh)	Discharge Energy No Aux (kWh)	RTE No Aux	Mean Temp (C)	Mean Amb Temp (C)	DC Charge Energy (kWh)	DC Discharge Energy (kWh)	RTE DC
1	1	2017-12-22	21.0	2	1150	1200	15-97	10031	5223	52.1	9468	55.2	8772	5549	63.3	20.6	1.8	4282	2878	67.2
1	2	2017-12-22	17.0	2	1150	1200	20-98	9328	5470	58.6	9194	59.5	8522	5831	68.4	20.9	-0.4	4150	3012	72.6
1	3	2017-12-23	17.0	2	1150	1200	18-98	9652	5653	58.6	9513	59.4	8798	6057	68.8	20.0	-1.4	4283	3126	73.0
1	4	2017-12-24	17.0	2	1150	1200	18-97	9597	5672	59.1	9462	59.9	8751	6076	69.4	19.7	0.0	4260	3132	73.5
1	5	2017-12-25	15.0	2	1150	1200	18-97	9462	5634	59.5	9375	60.1	8668	6044	69.7	20.6	-0.3	4220	3121	74.0
1	Cumulative	NA	87.0	2	NA	NA	NA	48070	27652	57.5	47012	58.8	43511	29557	67.9	NA	NA	21195	15269	72.0
1	Mean	NA	17.4	2	1150	1200	18-97	9614	5530	57.6	9402	58.8	8702	5911	67.9	20.4	-0.1	4239	3054	72.1
2	1	2017-12-25	13.0	2	1650	1200	37-97	8189	4561	55.7	8012	56.9	7408	4784	64.6	20.8	0.2	3607	2462	68.3
2	2	2017-12-26	12.0	2	1650	1200	38-97	8099	4583	56.6	8010	57.2	7393	4812	65.1	20.8	1.6	3597	2476	68.8
2	Cumulative	NA	25.0	2	NA	NA	NA	16288	9144	56.1	16022	57.1	14801	9596	64.8	NA	NA	7204	4938	68.5
2	Mean	NA	12.5	2	1650	1200	37-97	8144	4572	56.2	8011	57.0	7400	4798	64.8	20.8	0.9	3602	2469	68.5
3	1	2018-01-11	27.0	2	550	1200	6-98	11328	5044	44.5	11246	44.9	10072	6191	61.5	29.2	6.5	4916	3355	68.2
3	2	2018-01-12	27.0	2	550	1200	5-97	9677	5142	53.1	9488	54.2	8623	6298	73.0	29.1	8.1	4231	3415	80.7
3	3	2018-01-13	24.0	2	550	1200	6-97	10850	5190	47.8	10850	47.8	9828	6345	64.6	29.3	6.9	4822	3441	71.4
3	Cumulative	NA	78.0	2	NA	NA	NA	31855	15376	48.3	31584	48.7	28523	18834	66.0	NA	NA	13969	10211	73.1
3	Mean	NA	26.0	2	550	1200	6-97	10618	5125	48.5	10528	49.0	9508	6278	66.4	29.2	7.2	4656	3404	73.4
4	1	2018-01-17	16.0	4	1150	1200	17-95	9053	5047	55.7	8909	56.7	8269	5328	64.4	32.9	10.1	8109	5571	68.7
4	2	2018-01-17	14.0	4	1150	1200	19-95	8988	5211	58.0	8914	58.5	8240	5511	66.9	35.9	7.5	8074	5771	71.5
4	Cumulative	NA	30.0	4	NA	NA	NA	18041	10258	56.9	17823	57.6	16509	10839	65.7	NA	NA	16183	11342	70.1
4	Mean	NA	15.0	4	1150	1200	18-95	9020	5129	56.9	8912	57.6	8254	5420	65.7	34.4	8.8	8092	5671	70.1
5	1	2018-01-19	16.0	3	1150	1200	25-94	8460	4973	58.8	8294	60.0	7630	5297	69.4	34.2	7.5	5615	4165	74.2
5	2	2018-01-19	13.0	3	1150	1200	27-93	8196	4902	59.8	8113	60.4	7457	5235	70.2	35.0	6.9	5484	4124	75.2
5	Cumulative	NA	29.0	3	NA	NA	NA	16656	9875	59.3	16407	60.2	15087	10532	69.8	NA	NA	11099	8289	74.7
5	Mean	NA	14.5	3	1150	1200	26-93	8328	4938	59.3	8204	60.2	7544	5266	69.8	34.6	7.2	5550	4144	74.7
6	1	2018-01-20	23.0	3	1150	800	28-93	8790	4689	53.3	8630	54.3	7391	5036	68.1	33.5	6.2	5312	3976	74.8
6	2	2018-01-21	23.0	3	1150	800	29-92	8525	4520	53.0	8366	54.0	7129	4861	68.2	32.8	5.7	5116	3843	75.1
6	3	2018-01-22	17.0	3	1150	800	28-91	7614	4316	56.7	7539	57.2	6643	4658	70.1	32.8	5.8	4831	3688	76.3
6	Cumulative	NA	63.0	3	NA	NA	NA	24929	13525	54.3	24535	55.1	21163	14555	68.8	NA	NA	15259	11507	75.4
6	Mean	NA	21.0	3	1150	800	28-92	8310	4508	54.3	8178	55.2	7054	4852	68.8	33.0	5.9	5086	3836	75.4
7	1	2018-01-27	22.0	4	1150	600	32-98	9108	5098	56.0	8952	56.9	7880	5346	67.8	33.6	6.9	7600	5584	73.5
7	2	2018-01-28	22.0	4	1150	600	33-97	9609	5125	53.3	9517	53.9	8353	5377	64.4	35.2	10.2	8054	5618	69.8
7	3	2018-01-29	22.0	4	1150	600	27-95	8971	5096	56.8	8806	57.9	7711	5356	69.5	36.7	7.6	7431	5604	75.4
7	4	2018-01-30	19.0	4	1150	600	26-94	8525	4929	57.8	8449	58.3	7451	5188	69.6	37.1	7.2	7205	5430	75.4
7	Cumulative	NA	85.0	4	NA	NA	NA	36213	20248	55.9	35724	56.7	31395	21267	67.7	NA	NA	30290	22236	73.4
7	Mean	NA	21.2	4	1150	600	30-96	9053	5062	56.0	8931	56.8	7849	5317	67.8	35.7	8.0	7572	5559	73.5
8	1	2018-02-03	15.0	4	1150	1600	18-95	9029	5273	58.4	8871	59.4	8286	5570	67.2	38.5	9.3	8131	5822	71.6
8	2	2018-02-03	15.0	4	1150	1600	17-94	9253	5155	55.7	9100	56.6	8402	5468	65.1	38.7	9.2	8211	5721	69.7
8	3	2018-02-04	12.0	4	1150	1600	17-93	8709	5012	57.5	8709	57.5	8024	5321	66.3	39.0	9.7	7811	5571	71.3
8	Cumulative	NA	42.0	4	NA	NA	NA	26991	15440	57.2	26680	57.9	24712	16359	66.2	NA	NA	24153	17114	70.9
8	Mean	NA	14.0	4	1150	1600	18-94	8997	5147	57.2	8893	57.8	8237	5453	66.2	38.7	9.4	8051	5705	70.9

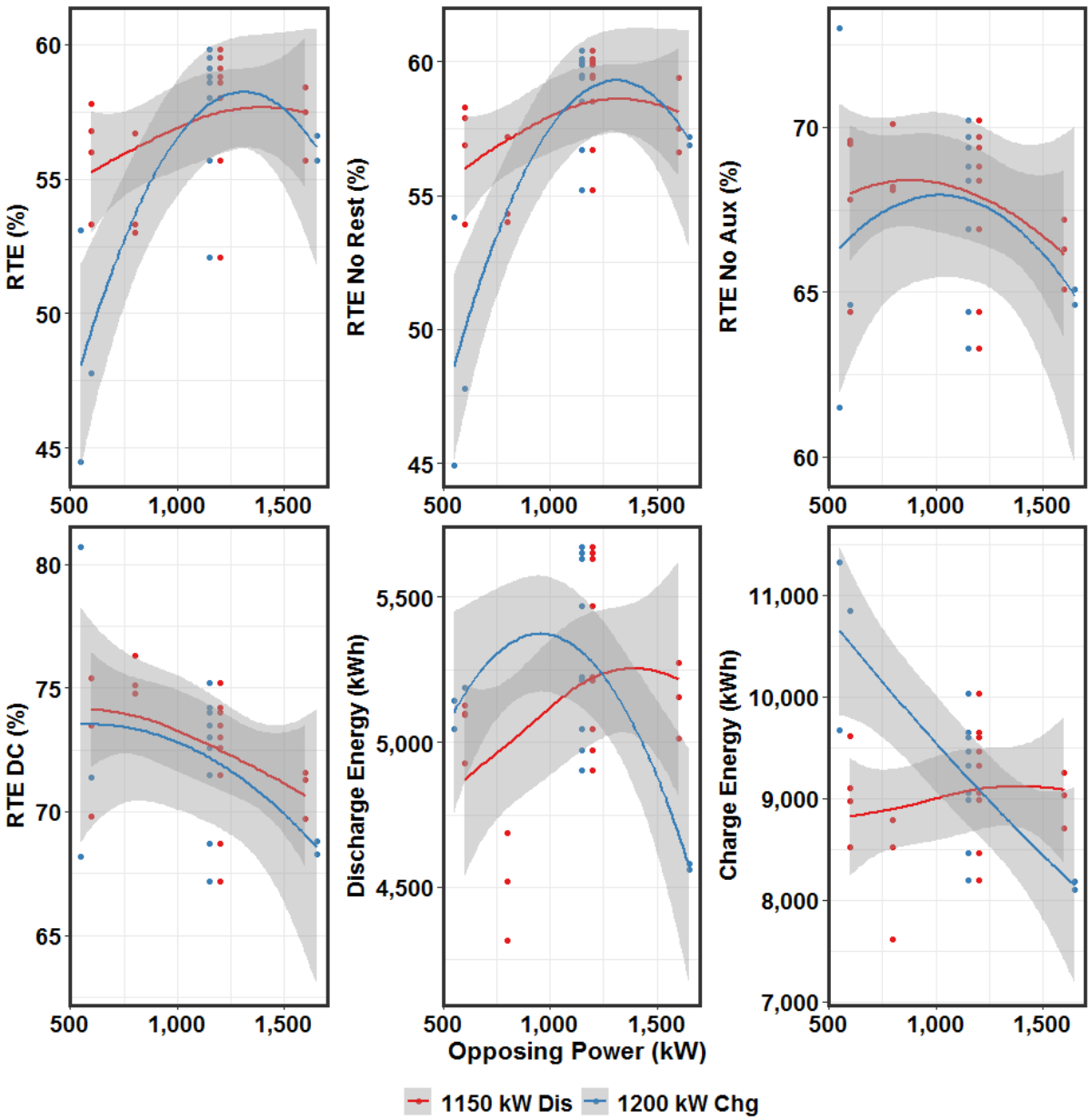

Figure A.2. Baseline Results Including Charge and Discharge Taper

A.3 String 1 Baseline Results

Table A.3. String 1 Baseline Results

Date	2018-01-17	2018-01-27	2018-02-03
Duration (h)	30	85	42
Strings Active	4	4	4
Average Charge Power (kW)	293	144	399
Average Discharge Power (kW)	280	294	296
SOC Range	17-96	25-98	19-94
Cycles	2	4	3
Charge Energy No Auxiliary (kWh)	2,060	2,039	2,155
Discharge Energy No Auxiliary (kWh)	1,309	1,374	1,434
RTE No Auxiliary	63.5	67.4	66.5
Mean Charge Temperature (ºC)	30	34	38
Mean Discharge Temperature (ºC)	28	33	39
Mean Temperature (ºC)	29	34	39
Mean Amb Temperature (ºC)	NA	NA	NA

A.4 String 2 Baseline Results

Table A.4. String 2 Baseline Results

Date	2018-01-11	2018-01-17	2018-01-19	2018-01-20	2018-01-27	2018-02-03
Duration (h)	78	30	29	63	85	42
Strings Active	4	4	4	4	4	4
Average Charge Power (kW)	297	280	293	162	140	399
Average Discharge Power (kW)	128	308	297	284	309	311
SOC Range	5-99	15-97	21-96	22-96	25-99	19-96
Cycles	3	2	2	3	4	3
Charge Energy No Auxiliary (kWh)	2,376	2,263	2,171	2,152	2,034	2,222
Discharge Energy No Auxiliary (kWh)	1,719	1,544	1,551	1,559	1,452	1,522
RTE No Auxiliary	72.3	68.3	71.4	72.5	71.4	68.5
Mean Charge Temperature (ºC)	29	37	37	36	36	38
Mean Discharge Temperature (ºC)	28	37	39	38	35	39
Mean Temperature (ºC)	28	38	38	37	36	39
Mean Ambient Temperature (ºC)	NA	NA	NA	NA	NA	NA

A.5 String 3 Baseline Results

Table A.5. String 3 Baseline Results

Date	2017-12-22	2017-12-25	2018-01-11	2018-01-17	2018-01-19	2018-01-20	2018-01-27	2018-02-03
Duration (h)	87	25	78	30	29	63	85	42
Strings Active	4	4	4	4	4	4	4	4
Average Charge Power (kW)	292	296	298	301	301	177	139	398
Average Discharge Power (kW)	277	402	148	281	269	257	279	260
SOC Range	17-96	36-96	1-97	16-94	22-95	24-95	25-98	2-97
Cycles	5	2	3	2	2	3	4	3
Charge Energy No Auxiliary (kWh)	1,878	1,853	2,050	2,025	1,985	1,915	1,891	1,958
Discharge Energy No Auxiliary (kWh)	1,419	1,187	1,452	1,327	1,341	1,268	1,279	1,240
RTE No Auxiliary	75.6	64.1	70.8	65.5	67.6	66.2	67.7	63.3
Mean Charge Temperature (ºC)	36	38	36	37	38	37	37	38
Mean Discharge Temperature (ºC)	37	38	37	37	39	38	37	40
Mean Temperature (ºC)	36	38	37	37	38	37	37	39
Mean Ambient Temperature (ºC)	NA	NA	NA	NA	NA	NA	NA	NA

A.6 String 4 Baseline Results

Table A.6. String 4 Baseline Results

Date	2017-12-22	2017-12-25	2018-01-17	2018-01-19	2018-01-20	2018-01-27	2018-02-03
Duration (h)	87	25	30	29	63	85	42
Strings Active	4	4	4	4	4	4	4
Average Charge Power (kW)	306	302	325	305	259	176	399
Average Discharge Power (kW)	297	420	278	295	321	266	275
SOC Range	12-99	38-98	16-94	31-90	36-88	26-96	21-94
Cycles	5	2	2	2	3	4	3
Charge Energy No Auxiliary (kWh)	2,106	1,910	2,002	1,601	1,296	1,853	1,960
Discharge Energy No Auxiliary (kWh)	1,548	1,240	1,264	1,086	821	1,226	1,282
RTE No Auxiliary	73.5	64.9	63.2	67.8	63.3	66.1	65.4
Mean Charge Temperature (ºC)	37	37	33	36	35	36	38
Mean Discharge Temperature (ºC)	37	38	32	37	36	37	39
Mean Temperature (ºC)	37	37	33	37	35	37	38
Mean Ambient Temperature (ºC)	NA	NA	NA	NA	NA	NA	NA

A.7 FBESS Technical Specifications

Table A.7. Technical Specifications

UNLIMITED CYCLES

NO CAPACITY FADE

NO THERMAL RUNAWAY

100% USE OF CHARGE

FACTORY INTEGRATION

MODULAR ASSEMBLY

BUILT-IN SECONDARY CONTAINMENT

FACTORY TESTING

RAPID PERMITTING

PLUG & PLAY

RATED TO TRANSPORT AND SEISMIC CODES

ZERO-COST DISPOSAL

100% RECYCLABLE

© 2016, UniEnergy Technologies, LLC

UNI.SYSTEM™ (AC) PERFORMANCE DATA			
Peak Power	600 kW_{AC}		
Maximum Energy	2.2 MWh_{AC}		
Discharge time	2h	4h	8h
Power	600 kW_{AC}	500 kW_{AC}	275 kW_{AC}
AC (Roundtrip) Efficiency	≈70%		
Voltage	12.47kV +/- 10%		
Current THD (IEEE 519)	<5%THD		
Response Time	<100ms		
Reactive Power	+/- 450kVAR		
Humidity	95%RH noncondensing		
Footprint	820 ft^2 (76m^2)		
Envelope	41'[W] x 20'[D] x 9.5'[H] (12.5m[W]x6.1m[D]x2.9m[H])		
Total Weight	375,000 lbs (170,000 kg)		
Cycle and Design Life	Unlimited cycles over the 20 year life		
Ambient Temp.	-40°F to 122°F (-40°C to 50°C)		
Self Discharge	Max 2% of stored enegy		

A.8 Site Drawings

A.8.1 Relaying and Metering Diagram for Everett Substation

As seen in Figure A.3, Bank 2 consists of Units 12 through 18, of which Unit 17 exchanges power with the FBESS. Hence the bank meter information is not relevant to this analysis.

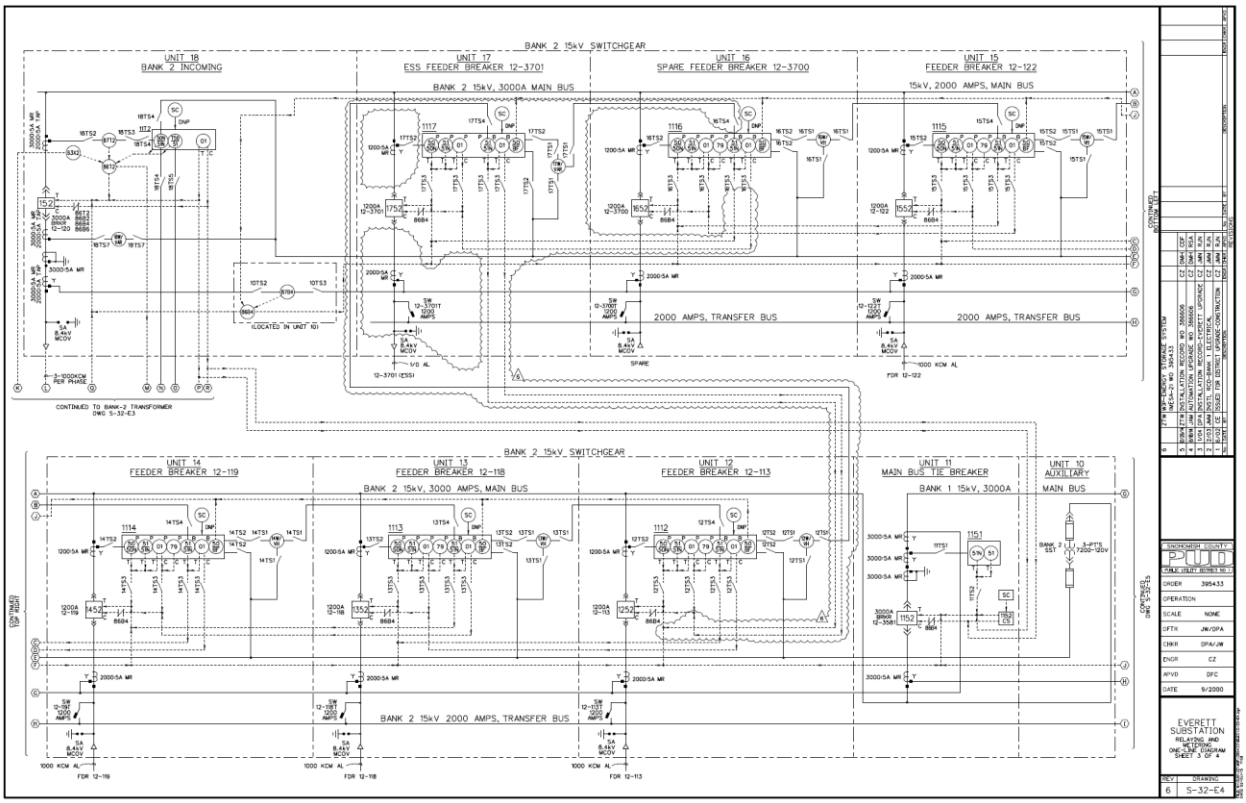

Figure A.3. Relaying and Metering Diagram for Everett Substation S-32-E4

The 12-3701 feeder meter at the 12-kV level, denoted by ES2_0332, measures power exchange with the FBESS. This exchanges power with transformers T1, T2, T3, and T4 in Figure A.4.

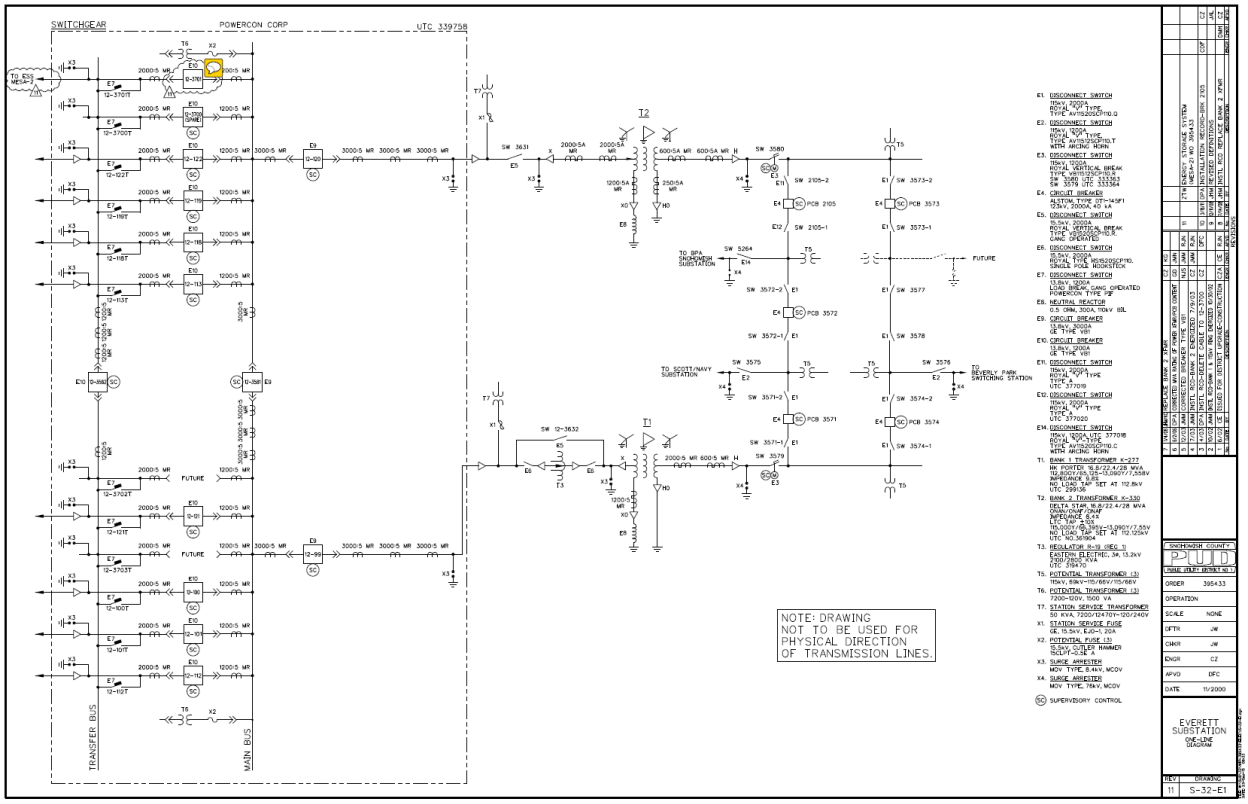

Figure A.4. One-Line Diagram for Everett Substation S-32-E1

Each string exchanges power with the grid through transformers T1−T4.

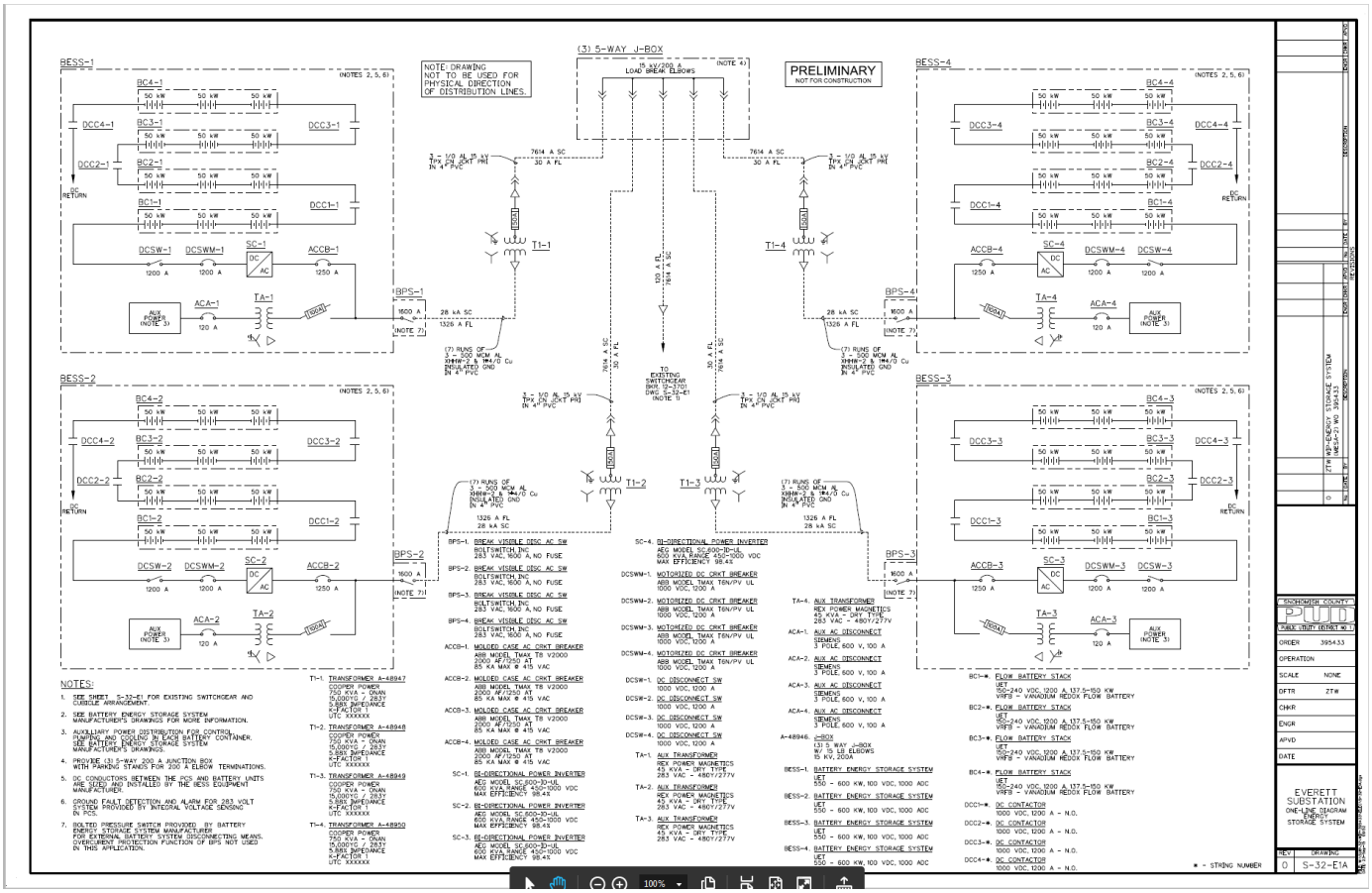

Figure A.5. One-Line Diagram for Energy Storage System S-32-E1A

Each string consists of four stack assemblies BC1, BC2, BC3 and BC4. Each auxiliary load ─ PCS control, lighting, BMS control, and ventilation ─ is powered by one leg of the 480-V AC side of TA-X. DCC1, 2, 3, and 4 are contactors rated at 1000 V DC connecting each stack assembly in series. In Figure A.5, DCSW and DCSWM are DC disconnect and motorized DC circuit breakers, respectively.

According to the MESA 2 one-line diagram shown below in Figure A.5 and three-line diagram shown in Figure A.6, there are four DC contactors rated at 1000 VDC and 100 A per module, all in series with each other. Hence these contactors have to be in normally closed state to allow power flow between containers. However, the full one-line diagram, not shown, labels these DC contactors as normally open (N.O.). This is probably incorrect, since no power flow would be possible if these contactors are in N.O. position. If any container fails, the string is taken out of service. For the Avista battery system, these DC contactors are similarly mislabeled as N.O. In addition, there is a 100V 1200 A DC contactor in parallel to the three series-connected stacks. These have been correctly labeled as N.O. When one container containing the 3-stack module fails, the series connected contactor opens while the parallel connected contactor closes to allow power flow by bypassing the failed string.

The Three-Line diagram shown in Figure A.6 shows the various auxiliary loads for each string

- Pumps, Instruments, I/O
- PCS control
- Lighting
- BMS control & vent
- Spare

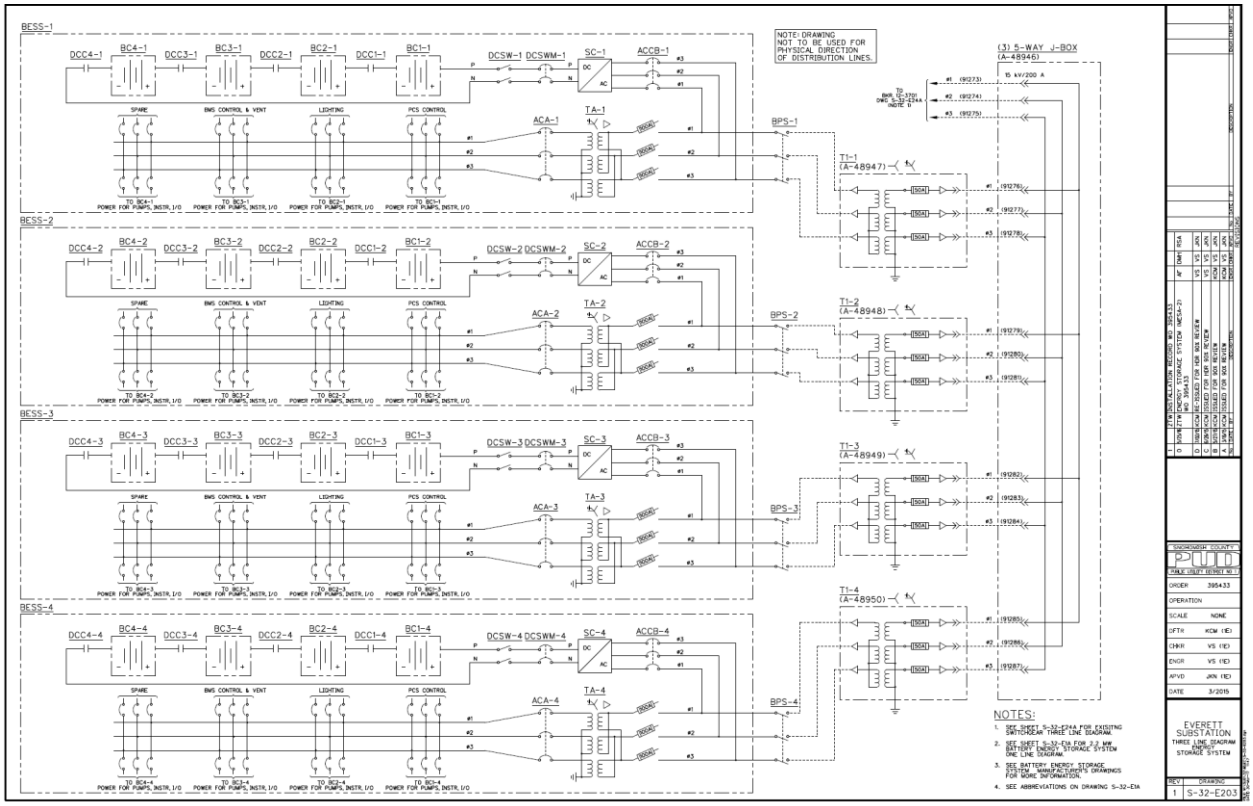

Figure A.6. Three-Line Diagram for Energy Storage System S-32-E203

A.9 Summary of UET Maintenance Findings

1 Contents

2 Purpose 4

2.1 UET Personnel 4

3 Response Summary 4

3.1 Leak Alarm 1/5/2017 12:53pm 4

3.2 Time of Events 4

3.3 Leak Alarm 1/5/2017 4:43pm 5

3.4 Time of Events: 5

4 Corrective Actions 6

4.1 Part Replacement 6

4.2 String Matching 6

5 UET System Management 6

2 Purpose

The following report details the scheduled activities, emergency response, and root cause for the 1/5/2017 leak alarms that occurred in String 2 Battery 3. This report first outlines the 12:53pm leak alarm then the 4:43pm alarm within the same battery.

2.1 UET Personnel

- Nick Schroeder – Lead Field Technician
- Greg Arnolds – Field Technician
- John Fitzsimmons – Field Technician
- Matt Kotch – Field Technician

3 Response Summary

3.1 Leak Alarm 1/5/2017 12:53pm

While UET was conducting scheduled maintenance, the site loss power around 12:53pm. Upon review of the data historian, String 2 Battery 3 was found to have an anolyte leak sensor engaged. UET immediately responded to the affected battery, and found less than half a gallon of electrolyte to have been released within the containment basin of the pump assembly. The affected pump tub was recently replaced on 1/3/2017. UET promptly removed all electrolyte within the pump basin, and determined that the pipe flange above the pump assembly to be sufficiently tightened, but not properly seated prior to operation. There is no previous history of flange connections becoming misaligned during normal operation. Two UET technicians properly seated the flange plates to the internal gasket, and then tested the system for operation. The flow test determined the connections to be sufficient for operating requirements and the UET team proceeded to handoff the system for PNNL testing at 3:00pm.

Date/Description	Time
1/5/2017: Match all strings for PNNL Testing	7:00 am -12:50 pm

---

UniEnergy Technologies

Version 1.0

1/5/2017: Leak Sensor Trip in String 2 Battery 3	12:53 pm
1/5/2017: Loss Site Power	12:53 pm
1/5/2017: UET Emergency Response	12:53 pm – 1:30 pm
1/5/2017: Re-energize Site	1:30 pm – 2:30 pm
1/5/2017: Finish Matching all Strings	2:30 pm – 3:00 pm
1/5/2017: Customer Handoff	3:05 pm

3.3 Leak Alarm 1/5/2017 4:43pm

At 4:43pm, UET received notification that String 2 Battery 3 had a leak sensor engaged within the same pump assembly. UET responders arrived on site at 5:30pm and immediately conducted a safety brief which concluded at 5:45pm. Following the safety brief, three UET members inspected String 2 Battery 3 and found no sign of a leak in the skid or tar compartments. After further investigation, it was found that the leak sensor's electrical connection to have been exposed to electrolyte from the event earlier in the day. The team then took this leak sensor out of operation to bring the string back online. It is important to note, that there is a total of three leak sensors in the tank compartment of each battery, UE removed one from service, and verified that the other two sensors were operational prior to system testing. By 9:00pm, String 2 was re-energized and a functional flow test was conducted to ensure all fluid connections were correctly fastene By 9:15pm, all strings were handed over for scheduling.

3.4 Time of Events:

Date/Description	Time
1/5/2017: Received Leak Notification	4:43 pm
1/5/2017: UET Responders Arrived Onsite	5:30 pm
1/5/2017: Safety Brief	5:30 pm – 5:45 pm
1/5/2017: Initial Inspection	5:45 pm – 6:30 pm
1/5/2017: System Troubleshooting	6:30 pm – 8:45 pm

1/5/2017: System Test	8:45 pm – 9:00 pm
1/5/2017: Customer Handoff	9:00 pm – 9:15 pm

4 Corrective Actions

4.1 Part Replacement

UET recommends that the leak sensor and wiring harness to be replaced at the next available maintenance period. The system is able to run safely, and parts are on hand for corrective actions. The duration of this replacement is estimated to take 2 hours.

4.2 String Matching

Prior to Customer handoff, UET is recommending a SOC match across all strings at the MESA 2 site. This will allow for a swift handoff to SnoPUD for PNNL testing to begin. The duration of this evolution is estimated to take 2 hours.

1 Contents

2 Purpose 3

2.1 UET Personnel 3

3 Response Summary 3

3.1 Leak Alarm 1/9/2017 7:13PM 3

3.2 Time of Events 3

4 UET System Management 4

3.1 Leak Alarm 1/9/2017 7:13PM

UET was notified at 7:13PM of a container leak alarm in String 4 Battery 1. UET responders arrived on site at 8:30PM and conducted a safety brief which concluded at 8:45PM. Immediately following, String 4 Battery 1 was inspected for any signs of an electrolyte leak. No electrolyte was found in the skid or tank compartment of the battery system. Upon further investigation, the team found 3" to 4" of water within the tank compartment of the suspect battery. This has been a reoccurring phenomenon within this battery. Immediate actions were taken, which included relocating the leak sensor t on top of the tanks and a thorough inspection for container. There was no sign of water entering the container. By 9:45pm the battery was determined to be safe and the Safety Watch and Relay proceeded with energizing the site. Both UET members left the site by 10:00 pm after system was handed back over for control.

3.2 Time of Events

Schedule Outline:

Date/Description	Time
1/9/2018: Arrived on Site	8:30 pm
1/9/2018: Safety Brief	8:30 pm – 8:45 pm
1/9/2018: Initial Inspection	8:45 pm – 9:00 pm
1/9/2018: Immediate Actions	9:00 pm – 9:30 pm

1/9/2018: Re-energize Site	9:30 -10:00 pm
1/9/2018: UET Departure	10:00 pm

3.3 1/11/2018 Findings:

During a return maintenance trip, UET found a large concentration of water building up on the roof of String 4 Battery 1. The water was located on the hinge side of the hatch and appeared to be cresting the top of the hatch lid. This could be the potential location of the water ingress. Short-term solutions will include an external weather strip, internal gasket additions, and bolting down the hatch after each use. Long term solutions are being reviewed internally and updates will be sent accordingly. It is important to note, this is the only container experiencing water intrusion.

Water Intrusion on String 4 Battery 1

1 Contents

2 Purpose 3

2.1 UET Personnel 3

3 Inspection Summary 3

3.1 Container Inspection 1/11/2018 7:00am to 1:00pm 3

4 Short-Term Solutions 3

5 Proposed Schedule 3

6 Example Photos 4

6.1 Example Photo(s) #1: 4

6.2 Example Photo #2 5

7 UET System Management 6

2 Purpose

During an onsite inspection, UET technicians noted a possible cause for the recent water intrusion on String 4 Battery 1. The following information provides details on the root cause, short term solutions, and timeline.

2.1 UET Personnel

- Greg Arnolds – Field Technician
- Nick Schroeder – Field Technician

3 Inspection Summary

3.1 Container Inspection 1/11/2018 7:00am to 1:00pm

During the follow-up inspection for the most recent leak events on String 4 Battery 1, two technicians found a large concentration of water building up on the hinge side of the roof hatch (see example photo #1). The estimated depth of the water was 3". The team then proceeded to verify if the water was entering the container and small amounts of liquid were found on the inner frame of the access port (see example photo #2). The team removed as much water as possible, however given the current environment, water was expected to continue to buildup.

4 Short-Term Solutions

During the next available maintenance period, UET plans to add an extra gasket to the underside of the roof hatch and bolt down the hatch lid. This will mitigate the risk of further water intrusion and allow the system to be ready for PNNL testing.

5 Proposed Schedule

(Next Available Maintenance Day)

Task Description	Date	Duration
Install roof hatch gasket	TBD	2 hrs
Bolt down roof hatch	TBD	15 mins

The areas circled in yellow outline the affected hatch and hinge points. The blue outline represents the location of which the water was reported.

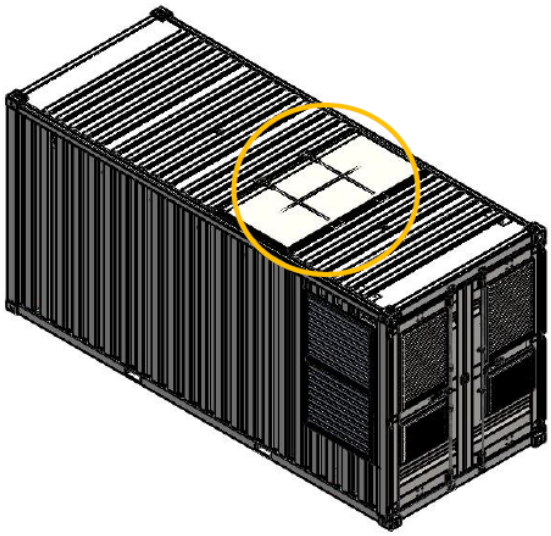

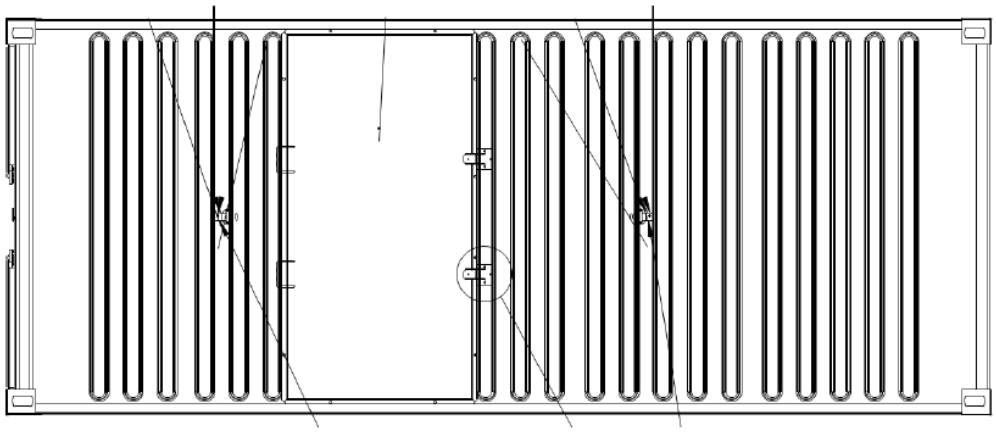

The below photo represents the access space below the hatch. The highlighted perimeter around the access space marks the location for the additional gasket material.

UET UniEnergy Technologies

Version 1.0

A.10 Algorithm for Power Distribution Assuming Maximum and Minimum SOC for Each String is Available

If Max SOC and Min SOC tags were available, the following analysis would have been instructive.

1. Plot Max SOC – Min SOC vs. time for all strings.
2. Plot discharge power distribution as f(min SOC deviation from average min SOC) for all strings – lower the min SOC, lower the discharge power.
3. Plot charge power distribution as f(max SOC deviation from average max SOC) for all strings.
4. Plot discharge and charge power distribution as f(delta SOC max – min SOC) for all strings.

Hypothesis

1. Discharge power decreases with increasing negative deviation of minimum SOC from average minimum SOC.
2. Charge power decreases as with increasing positive deviation of maximum SOC from average maximum SOC.
3. Discharge or charge power decreases as maximum – minimum SOC increases.

The other BMS features are as follows, based on communication with UET (Weber 2018) and our hypothesis.

1. Once a module SOC reaches a lower limit of 0% (1.25 V/cell), it stops discharge. That is why discharge abruptly ends when SOC is as high as 50% as has happened for String 4.
2. Once a module SOC reaches -100% SOC (1V/cell), it sets the string SOC to 0% and disconnects the string and decreases available power. Before this, if there is a Charge command, it disables the string and does not accept charge if any module SOC is less than some unknown negative value.
3. For strings that pulse during rest from 2 to 25% SOC, the criterion for stopping discharge is the same. During a subsequent charge, so far, we have not observed such strings to drop out. This appears to indicate that the minimum SOC for the modules within these strings is not less than the above unknown negative value.
4. During charge, there does not appear to be a similar shutdown feature. At least, in the limited data obtained, this has not been observed. The power simply tapers as a string SOC approaches its upper limit. Note that as delta SOC increases, the SOC at which string power tapers decreases—the weak modules are at low SOC while the healthy modules have reached the higher SOC limit. Since they are connected in series, the string power tapers at SOC levels that are lower than that for strings with uniform modules. At a fixed power during charge, as SOC increases, current decreases, hence the rate of charge of SOC decreases, thus giving plenty of time for the BMS to adjust power downward for strings with mismatched modules. This is not the case for discharge, where the current increases at fixed power discharge, resulting in faster tare of change of SOC. This results in termination of discharge for these strings.

Pacific Northwest
NATIONAL LABORATORY

www.pnnl.gov

902 Battelle Boulevard
P.O. Box 999
Richland, WA 99352
1-888-375-PNNL (7665)

U.S. DEPARTMENT OF
ENERGY